

APPROACHES IN OSTEOARTHRITIS THERAPY: FROM BIOMATERIALS TO
IMMUNOLOGY

by
Heather Jacobs Faust

A dissertation submitted to Johns Hopkins University in conformity with the requirements for the
degree of Doctor of Philosophy

Baltimore, Maryland
August 2018

© 2018 Heather Faust
All Rights Reserved

Abstract

Many biomaterials are being researched for applications in tissue regeneration, but so far, none have led to successful disease modification of osteoarthritis (OA). This dissertation details the application of several biomaterials, including ECM and a peptide-polymer, for OA treatment. The first segment details the use of porcine urinary bladder matrix in a post-traumatic mouse model of OA. The second segment details the use and optimization of a hyaluronic acid binding peptide in a post-traumatic mouse model of OA. These studies focus on the potential OA disease modifying activity of applying these therapies intra-articularly to the joint. This work resulted in improved OA disease outcome in a post traumatic mouse model of OA. However, this work led us to question the nature of the immune system in the OA microenvironment to help better understand the state of the knee joint, which will help inform future therapies. The final segment of the dissertation details the study of immune cells in the OA microenvironment during the course of post-traumatic OA progression. This work elucidated alterations in cytokines and immune cell populations that have not previously been studied in OA. These cells and cytokines are new potential targets for OA therapy.

Thesis Readers

Jennifer Elisseeff, Ph.D.

Department of Biomedical Engineering, Johns Hopkins University

Lynne Jones M.D. Ph.D.

Orthopaedic Surgery, Johns Hopkins University School of Medicine

Acknowledgements

To my advisor, Jennifer Elisseeff. Thank you for allowing me to grow as an independent scientist and explore the areas that caught my interest. I leave my PhD feeling like I really ventured deep into the heart of OA.

To my thesis committee members, particularly my committee chair Lynne Jones, thank you for all your advice over the last few years. Your advice has been invaluable.

To my lab mates for your endless support and friendship. I especially want to thank Ani for your guidance and hard work when I was just getting started in the lab. To Kaitlyn for your help teaching me flow cytometry amongst many other things. To Matt, thank you for always answering my questions, no matter how many I asked. I also want to thank Hong and Chris for helping me with so, so, many harvests.

To my husband, Travis. I love you so much. I would not have been able to make it through graduate school without you. I can always depend on you for anything- including lab advice.

To my family, Mom, Dad, and Zack: Thank you for always supporting my dreams, and for helping inspire me to pursue science. I will never forget our dinner conversations involving math and physics.

Table of Contents

Abstract	ii
Acknowledgements	iii
List of Abbreviations	vi
List of Tables	vii
List of Figures	viii
Chapter 1: Introduction.....	1
Abstract.....	2
Cartilage and Cartilage Repair	2
Tissue Engineering for Cartilage Regeneration	5
Cartilage surface modification	6
Cell types for cartilage repair.....	7
Bioscaffolds in cartilage repair	7
Biological factors.....	12
Translation of cartilage tissue engineering.....	14
Current and Future Trends in Cartilage Engineering.....	18
Approaches in osteoarthritis therapy: from biomaterials to immunology	20
Chapter 2: Application of extracellular matrix in osteoarthritis	23
Abstract	24
Introduction.....	25
Methods.....	28
Results.....	33
Discussion.....	37
Acknowledgements	41
Chapter 3: Optimization and application of HA binding peptide-polymers in osteoarthritis	50
Abstract	51
1. Introduction	52
2. Methods	55
3. Results	62
4. Discussion	68
5. Conclusion.....	71
Competing interests.....	72
Acknowledgements	72
Figures.....	73
Chapter 4: Th17 and senescent cells in osteoarthritis	88
Abstract.....	89
Introduction	90
Methods.....	93

Results.....	98
Immune cells and IL-17 are altered post ACLT	98
Clearance of SnCs reduces Th17 related cytokines	101
Local and systemic immune response correlate with the local joints immune changes	102
IL17 expression correlates with senescent cells development.....	103
Discussion	104
Conclusion.....	106
Figures	107
Chapter 5: Conclusions and Future directions	116
Permission Letters to Reprint or Use Copyrighted Material	129

List of Abbreviations

ACL	Anterior cruciate ligament
ACLT	Anterior cruciate ligament transection
CCL	chemokine (C-C motif) ligand
CCR	chemokine (C-C motif) receptor
CD	cluster of differentiation
DAMP	damage-associated molecular pattern
ECM	extracellular matrix
FN	fibronectin
HA	hyaluronic acid
IFN γ	interferon gamma
IL	interleukin
iNOS	inducible nitric oxide synthase
OA	osteoarthritis
PCL	poly(capro-lactone)
PEG	poly(ethylene glycol)
ROS	reactive oxygen species
TGF β	transforming growth factor beta
TLR	toll-like receptor
TNF α	tumor necrosis factor alpha
UBM	urinary bladder matrix

List of Tables

Supplementary Table 1. Peptide sequences	77
--	----

List of Figures

Chapter 1 Figures.....	22
Figure 1. Revised approach to tissue engineering triad.....	22
Chapter 2 Figures.....	42
Figure 2.1 UBM treated mice show reduced OA progression.....	42
Figure 2.2 UBM injection decreases expression of inflammatory markers.....	43
Figure 2.3 UBM injection decreases expression of inflammatory markers.....	44
Figure 2.4 Collagen 2 α 1 Staining.....	45
Figure 2.5 UBM treatment reduces pain.....	46
Figure 2.6 UBM decreased inflammatory markers in human primary chondrocytes.....	47
S. Figure 2.1 UBM can reduce chondrocyte toxicity in the presence of IL-1 β	48
S. Figure 2.2 UBM particle size distribution.....	49
Chapter 3 Figures.....	73
Figure 1. HABP hyaluronic acid binding characterization.....	73
Figure 2. Localization of optimized peptide-polymer <i>in vivo</i>	74
Figure 3. HABP2-8-arm PEG-COLBP reduces OA progression.....	75
Figure 4. HABP2-8arm peg-COLBP reduces OA progression in aged mice.....	76
S. Fig. 1 Peptide-polymer reduces cartilage degeneration without HA supplementation.....	78
S. Figure 2. Peptide alone can modulate inflammatory cytokine expression.....	79
S. Figure 3. QCMD frequency and dissipation plots demonstrating COLBP binding to collagen80	
S. Figure 4. Assessment of HABP2 binding to HA with ITC.....	81
S. Figure 5. Example U-SPECT images after intra-articular injection of ¹¹¹ In labeled PEG- COLBP.....	82
S. Figure 6. HABP2-8-arm PEG-COLBP localizes to degenerated cartilage, synovium, and subchondral bone.....	83

S. Figure 7. HABP2-8-arm PEG-COLBP localizes to degenerated cartilage, synovium, and subchondral bone. 1-hour post injection.	84
S. Figure 8. HABP2-8-arm PEG-COLBP localizes to degenerated cartilage, synovium, and subchondral bone. 24 hours post injection.	84
S. Figure 9. HABP2-8-arm PEG-COLBP reduces OA progression.....	85
S. Figure 11. Polymer-peptides halts OA progression	87
Chapter 4 Figures.....	107
Figure 1. IL-17 is altered post ACLT.....	107
Figure 2. Clearance of SnCs attenuates the development of OA and reduces the Th17 related expressions in joints.	109
Figure 3. Local and systemic immune response correlate with the local joints immune changes in aged and young mice.....	110
Figure 4. IL17 expression parallels senescent cells development, and IL17RAKO mice attenuates the development of pain.....	111
Figure 5. Senescent cells induce Th17 polarization.....	112
S. Figure 1. ACLT induces macrophage infiltration.....	113
S. Fig. 2. Inguinal lymph node gene expression	114
S. Fig. 3. ACLT alters the local lymphoid tissues.....	114
S. Fig. 4. Therapeutic intervention results in modulation of gene expression in the Inguinal LNs	115

Chapter 1: Introduction

This introduction has been reprinted with permission from Elsevier

This chapter was published in Principles of Regenerative Medicine 3rd Edition, by Anthony Atala, Robert Lanza, Tony Mikos. Cartilage Tissue Engineering, Copyright Elsevier (2018)

Abstract

Tissue engineering aims to repair injured and diseased tissue to restore function. Cartilage is an integral component of the joint and the degeneration of the articular cartilage leads to osteoarthritis. Traditional approaches for engineering cartilage to treat osteoarthritis (OA) employ cells, scaffolds, and biological signals or growth factors, alone or in combination. Cartilage has been engineered both *in vitro* and directly *in vivo*. This research has resulted in numerous therapies in development and clinical testing, as well as some clinically approved products for treating cartilage defects in OA patients. However, clinical efficacy in a broad patient population remains a challenge. Defining the impact of a diseased or inflammatory environment, such as occurs with OA, on cartilage tissue engineering is an area of growing interest that will lead to approaches to further increase the efficacy these new therapies. This chapter will also discuss future perspectives in the field, highlighting new research on the role of immune environment in tissue regeneration and the potential impact on cartilage.

Key Words: Cartilage, engineering, scaffold, immune system, osteoarthritis

Cartilage and Cartilage Repair

Cartilage is a connective tissue that functions to provide form, strength, and support. There are three types of cartilage distinguished by their molecular components in the

extracellular matrix (ECM), their anatomical location, and their function. Hyaline (articular) cartilage has a white glassy appearance and is found primarily in articulating joints. Its ECM is mainly composed of water, hyaluronate, proteoglycans, and type II collagen. Hyaline cartilage functions to provide stable movement with minimal friction. It has high viscoelasticity and demonstrates an excellent ability to provide resistance to compression and cushion the impact caused by physical load during movement (1). Elastic cartilage is distinguished by the presence of elastin in the ECM. Elastic cartilage provides a structural function, represented by the support it provides in the external ear. Lastly, fibrocartilage has a higher proportion of type I collagen in its ECM. Fibrocartilage is found in the meniscus, intervertebral disc and at the distal region of tendons and ligaments in apposition to bone, providing tensile strength and countering compression and shear forces (2).

All of the three types of cartilage feature a sparse cellularity, limited blood supply, and lack of neural innervations. These cartilages have intrinsically poor reparative capabilities due to their purported inability to form a clot to attract the necessary fibroblasts and start subsequent tissue synthesis for repair (3). Once defects, even very small ones, are initiated in cartilage, the degradation process is progressive (4). One of the irreversible consequences of the destruction of articular cartilage is arthritis, a leading cause of disability. Osteoarthritis (OA), the most common type of arthritis, is characterized by articular cartilage loss and degeneration, subchondral bone thickening, osteophyte formation, and joint inflammation (5). OA is widespread globally in 60–70% of people older than 65 years of age (6-8). Over 21 million people are suffering from this disease in the USA, and 10% of cases are estimated to be caused by previous trauma to the weight-bearing joints, which is classified as post-traumatic osteoarthritis (PTOA) (9). PTOA develops not only in elderly people, but also in young people suffering the results of previous

trauma. Once a cartilage defect is present, cartilage matrix continues to be lost while the surrounding tissues become more inflamed and contribute to further cartilage matrix destruction (10). This causes significant pain, disability, and morbidities, strongly affecting an individual's capacity to live a full and active life.

Current surgical treatment options available for focal cartilage repair include microfracture and osteochondral autografting. Microfracture may be considered a current standard for cartilage repair and is a low cost and minimally invasive procedure (11, 12). This technique employs subchondral drilling to initiate cartilage repair by inducing bleeding, enabling mesenchymal progenitor cells from the bone marrow to migrate into the lesion site. After this procedure, the repair tissue appears to be a cartilage-like substitute but is primarily composed of fibrocartilage. Unfortunately, the repair fibrocartilage has inferior quality and longevity compared to the native hyaline cartilage, thus only delaying cartilage degeneration for a few years (12). Osteochondral autografting or mosaoplasty is a technique of autotransplantation in which osteochondral plugs are harvested from non-weight-bearing or low-weight-bearing regions of the joint and implanted into defects that have been prepared and sized. In clinical testing, survival of the transplanted hyaline cartilage has been reported in 85% of patients, with a 91% good to excellent clinical outcome reported by patients followed for 3–6 years (13, 14). Additionally, follow up 10 years after surgery demonstrated improved clinical outcomes compared to microfracture (15). However, the cartilage autografts suffer from many problems including limited donor tissue availability, donor site injury, scarring, and pain, prompting the development of an innovative bioengineered therapy called autologous chondrocyte implantation (ACI), which will be discussed later in this chapter (16, 17).

Allograft tissue transplants address the donor tissue availability challenge and are a fast growing therapy.

Tissue Engineering for Cartilage Regeneration

To overcome the treatment obstacles of the available surgical options for cartilage repair, the reconstruction of cartilage using tissue engineering techniques has attracted tremendous attention. Tissue engineering is a multidisciplinary field that applies the principles of engineering, life sciences, cell and molecular biology to the development of biological substitutes that restore, maintain, and improve tissue function (18). The historical approach to cartilage engineering is to select and optimize the following components to be used individually or in combination to regenerate organs or tissues: (1) reparative cells that can form a functional matrix, (2) an appropriate scaffold for transplantation and support, and (3) bioreactive molecules, such as cytokines and growth factors, that will support and choreograph formation of the desired tissue (19). Biological cues and key biological factors that promote tissue repair in the local *in vivo* tissue environment continue to be discovered and developed, propelling the field forward. For example, the innate and adaptive immune systems are newly appreciated factors for successful tissue engineering. The immune system participates in many facets of tissue repair via scavenging dead cells and debris, inducing vascularization of injured tissue, and recruiting progenitor cells to tissue (20-22). More specifically, Badylak discovered that macrophage phenotype is important in muscle remodeling, and that macrophage phenotype is influenced by ECM scaffolds implanted into a muscle wound (23). Sadler found that CD4⁺ Th2 cells were necessary for pro-regenerative macrophage polarization and subsequent muscle regeneration after a treatment with ECM scaffolds, concluding

that the adaptive immune system as well as the innate immune system are important for functional tissue regeneration with a scaffold (24). Although little is known about how either innate or adaptive immune cells may be involved in cartilage regeneration, it is likely to be a future focus for the field (Figure 1).

Cartilage surface modification

Engineering therapies aimed to prevent cartilage deterioration after injury are valuable considering that cartilage is extremely difficult to repair. As lubrication of the cartilage surface is extremely important for its proper movement without friction and mechanical degradation, viscosupplementation is a common procedure. Viscosupplementation replenishes the molecules in the synovial fluid that naturally lubricate the cartilage surface, most commonly hyaluronic acid. One strategy is to enhance viscosupplementation with synthetic molecules such as a hyaluronic acid binding peptide to further enhance the retention of hyaluronic acid at the joint surface (25, 26). Synovial fluid can also be enhanced with synthetic charged polymers and synthetics with large molecular brush structures (27). Synthetic lubricin, synthetic mimics of lubricin, and recombinant lubricin have also been created to replenish lubricin lost at the beginning of cartilage degeneration before major structural cartilage changes have occurred (28). These lubricin mimics bind hyaluronic acid to the cartilage surface, increasing boundary layer lubrication. Synthetic scaffolds for directing cartilage tissue repair will be covered in the scaffold section.

Cell types for cartilage repair

Different cell sources are available to provide reparative tissue including differentiated cells, mesenchymal stem cells (MSCs), and embryonic progenitor cells. Chondrocytes and MSCs are the two most investigated cell sources for cartilage tissue engineering. Here, I will focus on MSCs. MSCs are attractive cells for repairing cartilage because in addition to their ability to differentiate into chondrocytes, MSCs have immunomodulatory properties. MSCs can migrate to sites of inflammation, and can modulate lymphocyte cell function through several growth factors and cytokines including TGF- β 1, nitric oxide, and IL-10 (29). This immunomodulation is especially important when considering the destructive environment in which a cartilage construct is likely to be implanted. MSC therapies for OA are currently undergoing clinical trials, but not many long-term results are currently available. Therapies being tested include injection of MSCs isolated from different sources, MSC injection with additional biological factors, and injection of ex vivo expanded MSCs (30). A clinical trial of bone marrow derived MSC injections showed improved WOMAC scoring over one-year post treatment, indicating decreased pain and increased function. Additionally, X-ray and MRI findings indicated that MSC treatment may halt the progression of cartilage loss (31). However, a common problem with MSC therapy is the poor delivery and retention of MSCs at the cartilage defect site. There are preclinical models aimed at optimizing MSC delivery, however most clinical trials inject MSCs free of scaffold (30).

Bioscaffolds in cartilage repair

Tissue engineering scaffolds are designed to provide a 3D environment to support and direct cellular processes in their migration, proliferation, and differentiation toward functional tissue. Scaffolds can be applied with cells, however applying scaffold without

cells is becoming more attractive because cell therapy is costlier. The selection of bioscaffolds for cartilage engineering requires complex mechanical properties that can support cellular functions, biocompatibility, capability of waste and nutrient transport, and sufficient structural integrity for joint reconstruction. Both natural and synthetic materials have been applied as cartilage tissue engineering scaffolds in a variety of forms, including fibrous structures, porous sponges, woven or non-woven meshes, and hydrogels.

Natural Scaffolds

Collagen

Collagen is the primary structural protein found in both bone and cartilage (32, 33). As such, collagen-based scaffolds are theoretically capable of supporting chondrocyte attachment and function. They are also biocompatible and biodegradable. Collagen scaffolds have been used in a wide variety of forms such as gels, membranes, and sponges into which cells and/or bioactive factors may be introduced (34, 35). Pieper et al. utilized a cross-linked porous type II collagen sponge to support the proliferation and differentiation of chondrocytes under cell culture condition up to 14 days (34).

Yokoyama et al. cultured MSCs in a collagen gel matrix in a chondrogenic medium supplemented with bone morphogenetic protein-2 (BMP-2), transforming growth factor- β 3 (TGF- β 3), and dexamethasone (36). The constructs were characterized by a downregulation of type I collagen, and upregulation of type II collagen and the cartilage-related proteoglycans aggrecan, biglycan, and decorin. The maximum size of cartilaginous tissue produced was 7 mm in diameter and 0.5 mm in thickness, still too small for partial-thickness cartilage repair. These cell-based studies indicate some of the

disadvantages of collagen scaffolds. Collagen gels allow for uniform mixing of cells and matrix, and for extensive molding and shaping of tissue, but tend to be fragile until new matrix is laid down. Solid collagen scaffolds such as membranes or sponges exhibit greater initial mechanical strength, but at the cost of less flexibility in shaping and a greater risk of non-uniform cell seeding. Collagen remains a useful scaffold with which to study 3D cell culture, but the disadvantages noted above weigh against its use in clinical applications.

Hyaluronic acid

Hyaluronic acid (HA) is a polysaccharide that is naturally found both in the ECM of articular cartilage and in synovial fluid and is responsible for the high lubricity of the cartilage surface. It is composed of alternating residues of *N*-acetyl-D-glucosamine and D-glucuronic acid. As with collagen, interest focused on HA as a potential scaffold for cartilage engineering is due to its intimate association with chondrocytes *in vivo*. Intra-articular HA injection has been used to treat symptoms of osteoarthritis with very large world markets and sales, and enhances cartilage lubrication and exerts many biologic effects on cells. HA has been shown to have a stimulatory effect on chondrocyte production of type II collagen and proteoglycan (37). HA also has many immunomodulatory properties. HA below < 50kDa it is considered low molecular weight (LMW), inflammatory HA, and at 10^3 - 10^4 kDa and greater it is anti-inflammatory (38). HA interacts with many cell receptors including RHAMM, CD44, and the immune related receptors TLR2 and 4, giving it the ability to impact inflammation and cell migration-both important aspects of wound healing (39). It is also thought that LMW HA

may provide a danger signal to immune cells to attract them to the site of tissue degeneration to aid in tissue debris clearance, which can damage tissue when occurring chronically (40). These properties make HA a highly dynamic and important molecule to include in scaffold designs, especially considering that HA makes up a significant part of the chondrocyte pericellular matrix (41) Clinical trials using HA to treat OA have found variable results in the efficacy of HA to reduce OA progression. More research on how variation in different HA products such as molecular weight and cross-linking affects clinical outcome is needed to optimize HA therapeutic effect (42).

Extracellular Matrix as a biomaterial

The ECM, which contains growth factors and structural components including collagens, proteoglycans, and elastins, has been used with great success in treating muscle and chronic non-healing wounds. Despite this, few studies have been done implementing ECM into cartilage defects, in part because of a concern for using xenogeneic materials as well as the relatively variable processing of ECM- there are no strict guidelines on what amount of cellular material should remain after decellularization (43, 44). However, a few groups have implemented xenogeneic materials into cartilage defects (45). One group used rabbit perichondrium in an articular cartilage defect in a sheep knee. After 12 weeks, new cartilage was formed and there was no immunologic reaction in the synovium (43). Another group implemented ECM particles *in vivo* to reduce OA progression in a rat model of OA (46). Treatment with human amnion decellularized membrane resulted in attenuated cartilage degradation, as well as increased levels in MCP-1, which recruits monocytes. This suggests that ECM can reduce OA progression, potentially through modulation of immune cells (47). Some groups have cultured cells to create “cell-derived ECM scaffolds” to avoid the use of xenogeneic

ECM, however the scale process still needs to be increased (48). Due to the limited availability of “cell-derived ECM scaffolds,” the use of xenogeneic ECM should be explored further (44).

Synthetic Scaffolds

Bioscaffolds derived from natural materials are generally considered more favorable in terms of the biological response they can elicit from cells compared to synthetic scaffolds (49). However, biological materials can be difficult to generate in large quantities with acceptable consistency, and often exhibit poor mechanical characteristics (35). Synthetic materials are generally less expensive than biologics and are created *de novo* and provide more precise control over the structural properties, mechanical properties, and rates of resorption with a great deal of batch-to-batch consistency (50).

The most common synthetic polymers and traditional tissue engineering scaffolds are polyglycolic acid (PGA), polylactic acid (PLA), polyethylene oxide (PEO), and various derivatives and copolymers based on these entities including poly-di-lactic-co-glycolic acid (PLGA) (35). In general, these materials exhibit many beneficial properties for the production of engineered tissue: a high surface area to volume ratio if processed correctly, sufficient porosity to allow for nutrient and waste diffusion, the potential for surface modification, and the ability to control their degradation rate via selection and modification of their chemical composition (51). In particular, the ability to specifically control the rate of degradation is important for scaffold survival *in vivo*. First, the scaffold must provide sufficient mechanical strength when first implanted but should optimally degrade at the same rate as new tissue generation. If degradation is too rapid, then there is a risk of cell loss, scaffold failure, and inflammation and death of surrounding tissue due

to rapid release of acidic breakdown products (52, 53). Conversely, an overly slow rate of scaffold degradation would likely impede tissue incorporation. The question remains: how do we determine the replacement rate of the cartilage tissue? This depends on a number of factors including the scaffold itself, but more importantly, the age of the patient and the level of inflammation in the joint. Articular cartilage changes with age, including increased collagen crosslinking, decreased synthesis of type 2 collagen and aggrecan, and reduced tensile strength (54). Additionally, senescent cells contribute to the poor reparative abilities of aging cartilage. Senescent cells do not divide but instead cause chronic inflammation in the aging tissue (55). Chondrocytes can also become senescent, slowing down the rate of scaffold replacement with new cartilage, further impacting the rate of new tissue growth.

Biological factors

Growth factors, cytokines, protein gradients, cell-cell interactions, and ECM-cell interactions control cellular differentiation, migration, adhesion, and gene expression. How growth factors control cartilage development, maintenance, and changes during diseased states has been investigated intensively. The primary growth factor families that control cartilage homeostasis are the TGF- β superfamily, BMPs within the TGF- β superfamily, insulin-like growth factors (IGFs) and fibroblast growth factors (FGFs). The role of each of these factors in cartilage growth and homeostasis, as well as effects on stem cells, is varied and diverse. To briefly summarize, TGF- β and IGF generally exert anabolic effects on chondrocytes including inducing increased type II collagen and GAG synthesis, maintaining chondrocyte phenotype, and promoting chondrocyte proliferation, whereas FGF suppresses proteoglycan synthesis and encourages chondrocytes to take a fibroblast morphology (56). Despite TGF- β signaling generally maintaining chondrocyte phenotype and encouraging chondrocyte growth, TGF- β signaling is altered in OA, resulting in

deleterious effects (57). Most growth factor-only related approaches to preventing cartilage loss involve modulating either anabolism or catabolism of the cartilage tissue and/or inhibiting pro-inflammatory cytokine signaling. Examples include intra-articular injection of TGF- β , interleukin-1 β (IL-1 β) inhibitors, and MMP13 inhibitors (58, 59). However, the diverse roles of growth factors cause difficulty in attempting to implement them in cartilage engineering. Some anabolic growth factors may cause osteophytes in OA, or do not induce a response in older cells, or may not be enough to combat the degradatory enzymes present in a diseased joint (60). There are also additional signaling molecules, integrins, which are molecules that span the cell membrane and connect the cell cytoskeleton to the extracellular matrix (ECM). This allows the cell environment-including material stiffness and mechanical forces- to influence cell morphology, migration, and signal transmission (61).

Growth factors can also be broadly administered to a cartilage defect via platelet rich plasma (PRP), an autologous blood product containing platelet-derived growth factors. PRP contains TGF- β 1, IGF-1, VEGF, and PDGF (platelet derived growth factor). PRP can be made with or without leukocytes. The mechanism of how PRP coordinates an anti-inflammatory, proliferative, or remodeling response in cartilage is still unknown, but is thought to be due to stimulating cell proliferation, migration, and matrix synthesis (62, 63). Despite lack of FDA approval, the components that form PRP are approved, and PRP has been used in cartilage defects clinically, in many cases in combination with microfracture or scaffolds (64). There are many proposed mechanism of action for PRP, including that the growth factors secreted by platelets are be responsible for at least part of the cartilage repair and pain relief, however, more research is needed to further define PRP's mechanism of action (65). Once a mechanism is defined, it will be easier to optimize PRP for treatment of osteoarthritis.

Translation of cartilage tissue engineering

Preclinical Translation

There are many important aspects to consider in designing preclinical (“in vivo”) studies for translating engineered scaffolds/cell/peptide therapies including the clinical indication, animal, and disease model. The type of therapy will also dictate study design and approach. For example, initial studies for cell-seeded scaffolds often start with simple subcutaneous implantation to examine their ability to generate cartilaginous tissue *in vivo*. If these studies show that the *in vivo* environment and tissue scaffold is not hostile to the development of cartilage and osteochondral tissues, the therapy is then tested in the target tissue to determine therapeutic efficacy.

The choice of animal model as well as the application of the material is crucial to successfully moving therapies to the clinic. For example, if an engineered cartilage construct is intended to fill articular cartilage defects, it is likely that the person receiving the cartilage construct will have osteoarthritis or some chronic inflammation. So, not only is the promotion of new cartilage formation and lack of rejection by the animal important, but as the presence of disease will have many implications on the success of the therapy, preclinical testing of materials needs to take the disease state into account. In the case of OA, there are several mouse as well as rat and guinea pig models of OA requiring either mechanical loading of the knee joint, transecting the ACL or meniscus, or injecting MIA (monoiodoacetate) to induce cartilage damage (66).

Animal models still have room to improve. Many therapies, such as iNOS inhibitors and COX inhibitors, were shown to decrease cartilage lesions and osteophytes in separate OA animal models, but did not show clinical efficacy in humans (67). This problem may

be due in part to the fact that most preclinical testing is performed early in OA disease progression, however people treated clinically are in late stage OA. Additionally, animals used experimentally are generally young adults as opposed to the majority of OA patients, who are aging adults over 60 (67). Studies evaluating the biological differences in OA between young and old animals are needed to help advance the utility of animal models in screening therapies.

Clinical Translation

There are many different cartilage bioengineering therapies currently in clinical testing, with most therapies consisting of either scaffold alone or scaffold plus cells (MSCs or chondrocytes), mesenchymal stem cell only therapies, PRP injections, and viscosupplementation (68). Autologous chondrocyte implantation (ACI) is meant for localized cartilage injuries and applies the patient's own expanded chondrocytes in solution to the defect under a surgically closed periosteal flap (16, 17). This allows the autologous articular chondrocytes to synthesize new cartilaginous matrix in the defect site. ACI is clinically approved (Carticel), but the clinical outcomes of the standard ACI methods have disadvantages including donor site morbidity, risk of leakage of transplanted chondrocytes, complexity of the surgical procedure (69), uneven distribution of the cell suspension in the transplanted site (70), periosteal hypertrophy (71), and dedifferentiation of the chondrocyte phenotype during *in vitro* monolayer culture (72, 73). These problems prompted matrix-induced ACI (MACI), second-generation ACI to be developed. MACI involves applying cell-seeded constructs instead of cell suspensions for cartilage repair. Vericel MACI therapy has recently been approved clinically in the US by the FDA and is the first autologous cellularized scaffold approved in the US for the repair of cartilage defects. This MACI technique uses an implant with a bio-

resorbable Type I / III collagen membrane with approximately 1,000,000 cells per square centimeter. This therapy has been found to improve KOOS score (Knee Injury and Osteoarthritis Outcome Score) more significantly than microfracture but have similar histological repair outcomes in phase three clinical testing (74).

Variations of the MACI approach include a technology in which the *in vitro* chondrocyte expansion was performed using a 3D scaffold made from modified HA (75). The scaffold was then implanted into cartilage defects via a mini-arthrotomy or an arthroscopic approach. Their cohort includes 141 patients followed for 2–5 years. Their results appear impressive, with improvement in subjective symptoms reported in over 90% of patients. Second-look arthroscopy was performed in 55 patients, and the cartilage repair was graded as normal or near-normal in over 95% of these patients. Biopsies were taken in 22 of these 55 patients, which revealed a hyaline appearance in 12 out of 22, with the remainder having a mixed or fibrocartilaginous appearance. Currently, Histogenics has the most advanced engineered cartilage therapy in the US. This MACI therapy, NeoCart, expands chondrocytes, after which they are seeded on a collagen scaffold that is matured in a bioreactor before implantation in a cartilage defect. Now in Phase III clinical testing in the US, results thus far demonstrate reduced pain, increased function, and imaging-confirmed defect filling with NeoCart treatment (76).

Biomaterials alone are also being implanted in conjunction with microfracture or other autologous cell/tissue sources for focal cartilage repair to provide a simplified off-the-shelf therapeutic. Various approaches have been developed to incorporate biomaterials with microfracture, e.g. using polymer scaffold combined with minced cartilage from a biopsy (77, 78), implanting collagen membranes microfracture (79), and applying

chitosan mixed with blood after microfracture (80, 81). These biomaterial-guided tissue repair methods may be more economical and provide an off-the-shelf therapy that is more efficacious than surgical intervention alone.

Achieving integration of engineered tissue with host cartilage is still a troublesome problem for cartilage reconstruction, especially for long-term cartilage repair (82). Cartilage integration failure was very common and probably caused by a variety of factors, including limited chondrocyte mobility in the cartilage extracellular matrix, chondrocyte cell death at the wound edge, chondrocyte dedifferentiation in the engineered tissue, the type of biomaterial scaffold, and the origin and the stage of the cells used for cartilage tissue engineering. Corresponding solutions have been reported to enhance the construct including cartilage integration by pretreating the cartilage interface enzymatically to break down collagenous matrix (83, 84), inhibiting the chondrocyte death at the lesion edge (85), and using immature constructs instead of mature constructs (83). Recently, we developed a mechanically strong biological glue to bridge native cartilage with biomaterial scaffolds (86). This glue is based on chondroitin sulfate (CS), one of the major components of the cartilage ECM, functionalized with methacrylate and aldehyde groups to react chemically with the biomaterials and cartilage proteins. Using this glue, full integration was achieved in full-thickness chondral defects following marrow stimulation. Recent studies suggest that PRP can improve cartilage integration of explants (87, 88), suggesting that immunomodulation plays an important role in successful explant integration.

Current and Future Trends in Cartilage Engineering

The tissue engineering techniques discussed above show great potential advantages over conventional surgical options and are being applied to clinical practice intensively (89). The ultimate aim of articular cartilage tissue engineering is to design an engineered tissue that can regenerate to hyaline cartilage with normal knee functions and integrate fully with the surrounding native cartilage. To date, no engineered tissue construct fulfills this criterion, and as such there is considerable ongoing work in various aspects of cartilage tissue engineering research from cell type, bioscaffold, biological factor, bioreactor, to tissue translation. It would be nearly impossible to summarize the vast body of this research in a single chapter, so the range of studies outlined above is necessarily only a brief summary of the past and current literature on selected topics.

The recurring theme throughout much of the current literature is that the engineered tissue has the histological appearance and biochemical makeup of cartilage of varying stages of maturation. However, it has been reported that mechanically most of these constructs are inferior to native cartilage. As the basic techniques of chondrocyte, osteoblast, and MSC culture are elucidated, the focus shifts toward improving the mechanical properties of engineered tissues. One concern is that, in order to achieve complete reconstruction of cartilage defects, the transplanted tissue can initially have mechanical strength inferior to native cartilage temporally to allow the tissue to mature and integrate to the surrounding cartilage ultimately under the *in vivo* environment. It should be considered that a large gap still exists between the *in vivo* studies and *in vitro* testing and optimization for the clinical translation of engineered cartilage. The *in vitro* methods should be standardized to provide clear results to develop successful clinical

applications for cartilage tissue engineering (90). There are several important basic questions that remain to be answered. What are the optimal types, amounts, and timing of the growth factor milieu? Perhaps PRP will help answer this question after further characterization. Will small molecular drugs work effectively for cartilage tissue engineering since many biological factors are complex and exhibit delivery problems? *In vitro* models provide the isolated environment necessary to clearly define genetic programming and signaling pathways that are involved in chondrocyte maintenance, however fail to compensate for all the dysregulated signaling pathways *in vivo* which will ultimately dictate the success or failure of a bioengineered therapy. More pre-clinical models of cartilage defects need to be utilized to determine the impact of the host environment on bioengineered therapies.

An overlooked aspect to cartilage engineering is the use of cytokines and manipulation of the immune cells that produce them. The immune system has typically been viewed only as being responsible for material rejection and tissue destruction, with immune suppression considered ideal. However, in light of recent work showing the importance of the innate and adaptive immune system in tissue repair, future work will most likely focus on modulating the immune system, not simply suppressing it.

NSAIDs and corticosteroids continue to be used despite studies that have shown some adverse effects regarding articular cartilage metabolism. Part of this is due to the fact that these treatments help to manage patient pain, however medications for pain relief are often un-effective in the management of arthritis pain. We need to develop better alternatives, particularly ones that do not broadly suppress the immune system like corticosteroids do. Harnessing macrophages and T cells for tissue regeneration would be

a logical strategy, considering that they already have many functions in tissue remodeling. Additionally, as T cell therapies are already used in other diseases such as cancer immunotherapy, they could be adapted for use in cartilage regeneration to guide macrophage polarization and direct the tissue repair process.

Of course, there are many more questions and challenges that remain before the promise of tissue engineering is fully realized. The contributions of scientists in fields as diverse as cell/molecular biology, materials science, chemistry, and mathematics will be required in order to answer these questions.

Approaches in osteoarthritis therapy: from biomaterials to immunology

This dissertation details the application of several biomaterials, including ECM and a peptide-polymer, for OA treatment. The first segment details the use of porcine urinary bladder matrix in a post-traumatic mouse model of OA. The second segment details the use and optimization of a hyaluronic acid binding peptide in a post-traumatic mouse model of OA. These studies focus on the potential OA disease modifying activity of applying these therapies intra-articularly to the joint. The final segment of the dissertation details the study of immune cells in post-traumatic OA progression. This work was undertaken to better understand the role of these immune cells, particularly of Th17 cells, in OA progression. As suggested in this introductory chapter, the immune state of tissue can impact the regenerative abilities of biomaterials. Therefore, it is important to better understand exactly how these immune cells are altered in OA before we can tailor our biomaterial-based therapies to reduce disease progression.

Tissues that play a role in OA progression besides cartilage are the synovium and subchondral bone marrow. It is important to take these tissues into account while trying

to repair cartilage because they contribute cells and cytokines which impact cartilage. It is known that there is often synovial inflammation in OA that can contribute to joint damage (91). Several immune cell types have been found in the synovium via immunohistochemistry in animal models of OA, including CD4⁺ T cells, CD8⁺ T cells, macrophages, and dendritic cells (92-95). In humans, T cells, B cells, NK cells, and dendritic cells have been identified in synovium via immunohistochemistry (95, 96). Despite these observations, no real initiative has been taken to further study the role these cells may have in the progression of OA, or how their modulation may lessen disease progression.

Additionally, the subchondral bone is an important joint component that is remodeled during the course of OA, either before or concurrently with cartilage destruction (97). The subchondral bone marrow contains many cell types including stromal cells and stem cells for hematopoiesis, and lymphocytes including T cells and B cells originate from the bone marrow (98). It is also known that when the subchondral bone in OA is remodeled, this is accompanied by macrophage infiltration and osteoclast formation (99, 100). One group performed flow cytometry and identify inflammatory cells in the OA subchondral bone marrow (101). Despite the identification and apparent involvement of these cells in OA, the state of these subchondral bone marrow immune cells has not been investigated further in OA progression. In chapter 4, we will go further into detail on cells of the immune system and what is known about their role in arthritis as well as present our findings on altered immune cell populations in the mouse ACL transection model of post traumatic OA.

Chapter 1 Figures

Figure 1. Revised approach to tissue engineering triad.

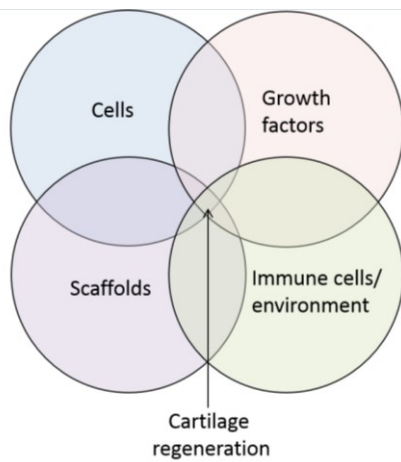


Figure 1. Cells, growth factors, and immune cells/immune environment contribute to engineered cartilage regeneration. The immune system contributes inflammatory and anti-inflammatory signals, as well as antigen specific and non-specific recognition of the engineered scaffold, which may dictate engineered tissue success.

Chapter 2: Application of extracellular matrix in osteoarthritis

Intra-articular Injection of Urinary Bladder Matrix Reduces Osteoarthritis Development

This article has been reprinted with permission from Springer Nature

License Number 4350940686473*

*Reprinted by permission from [Springer Nature]: [Springer][American Association of Pharmaceutical Scientists][Intra-articular Injection of Urinary Bladder Matrix Reduces Osteoarthritis Development, Heather N. Jacobs, Sona Rathod, Matthew T. Wolf, Jennifer H. Elisseeff] [2017]

Heather N. Jacobs^{1*}, Sona Rathod¹, Matthew T. Wolf¹, and Jennifer H. Elisseeff¹.

¹Translational Tissue Engineering Center, Wilmer Eye Institute and Department of Biomedical Engineering, Johns Hopkins University, Baltimore, MD 21287, USA.

*Corresponding author. Tel.: 410-614-6837; fax: 410-614-6840

Abstract

Micronized porcine urinary bladder matrix (UBM) is an extracellular matrix biomaterial that has immunomodulatory and pro-regenerative properties. The objective of this study was to assess the ability of UBM to alter disease progression in a mouse model of post-traumatic osteoarthritis (OA). Ten-week-old wild type C57BL/6 male mice underwent anterior cruciate ligament transection (ACLT) to induce OA. Two weeks after ACLT, UBM (50 mg/ml) or saline was injected into the mouse joint. At 4 and 8 weeks post-ACLT, cartilage integrity was assessed using OARSI scoring of histology, pain was evaluated, and joints were harvested for quantitative RT-PCR analysis of cartilage-specific and inflammatory gene expression. UBM-treated animals showed improved cartilage integrity at 4 and 8 weeks and reduced pain at 4 weeks compared to saline-injected mice. Animals injected with UBM expressed higher levels of genes encoding structural cartilage proteins, such as collagen2 α 1 and aggrecan, as well as anti-inflammatory cytokines, including interleukins 10 and 4. UBM decreased cartilage

degeneration in the murine ACLT model of OA, which may be due to reduced inflammation in the joint and maintenance of high expression levels of proteoglycans.

Introduction

Osteoarthritis (OA) is a prevalent degenerative musculoskeletal disease that results in both biological and mechanical dysfunction of the cartilage tissue that lines the surface of articulating joints. Between 2010 and 2012 alone, 52.5 million adults were diagnosed with OA in the U.S. (102). OA is characterized by a progressive loss of cartilage tissue, dysfunctional remodeling of the underlying bone, inflammation of the synovial membrane, and abnormalities in lubrication of the articular joint. Current therapies for OA are minimal and often palliative. Palliative options include non-steroidal anti-inflammatory drugs (NSAIDs) and corticosteroid injections to control pain; however, these pharmaceuticals do not slow or reverse disease progression. The primary therapeutic treatment for OA is end-stage joint replacement, such as total-knee replacement surgery. These surgeries are invasive, and as severity of OA is increasing in younger patients, the comparably short lifetime of knee joint replacements present a challenge (103). The ultimate goal for OA treatment is to find a disease-modifying osteoarthritis drug (DMOAD) that can promote tissue regeneration, reduce or stop the progression of OA, and ultimately promote regeneration of the lost tissue. There is a small number of promising DMOAD pharmaceuticals currently in clinical development that aim to modulate either anabolism or catabolism of the cartilage tissue, or inhibit pro-inflammatory cytokine signaling. These therapies include intra-articular injection of an interleukin-1 β (IL-1 β) inhibitor and chondroitin sulfate (58). However, no DMOAD treatment has been approved by regulatory authorities due to lack of clinical efficacy (58).

Owing to the dearth of therapeutic options for OA, there remains a critical need for new approaches for treating disease and rebuilding tissue. Biomaterials-based strategies may be an option for degenerative musculoskeletal bone and cartilage diseases, as synthetic hydrogels have improved disease score in rabbits with posttraumatic OA (104) as well as in goats and humans with focal cartilage defects (105). Treatment with biologics composed of extracellular matrix (ECM) is a regenerative medicine option for tissue reconstruction.

Unlike synthetic polymeric materials, ECM scaffolds are composed of an intricate mixture of proteins, glycoproteins, and polysaccharides, which can be isolated by chemically and/or mechanically removing cells from various tissue sources. The ECM provides structural support for cells, binds to and sequesters growth factors, and plays important roles in cell adhesion and signaling via integrins (41). These properties make the ECM a biologically active scaffold that influences cell differentiation, proliferation, survival, polarity, and migration (106). ECM scaffolds derived from different tissues have distinct properties, as the structure and function of each tissue is highly specific. For example, while cartilage tissue has a relatively low ratio of cells-to-ECM and high collagen and proteoglycan content, brain tissue contains a much higher ratio of cells-to-ECM, more secreted factors, and little collagen (107, 108). The ECM can also be chemically and physically processed into several biomaterial configurations, including injectable particulates. ECM derived materials manufactured from different tissues, such as urinary bladder and small intestinal submucosa, have applications ranging from burn wound treatment to urinary tract repair (109). Additionally, ECM has been used in a small animal model of post-traumatic OA to reduce cartilage degeneration (47).

In this study, we are using particulate ECM as a biologic and immunomodulatory agent to advance OA therapy and cartilage tissue regeneration. We investigated an ECM biomaterial derived from porcine urinary bladder matrix (UBM), which maintains an intact basement membrane with high amount of collagens III and VII (110), elastic fibers, adhesive proteins, and glycoproteins (110). UBM has been shown to promote regeneration in soft tissue injury through a number of mechanisms. Remodeling UBM was shown to shift the local macrophage response *in vivo* towards a pro-healing, anti-inflammatory phenotype (111), and recruits progenitor cell proliferation and differentiation after traumatic muscle injury in mice (112). UBM similarly promoted muscle repair in patients with volumetric muscle loss in a clinical study (113). UBM has also been applied clinically to chronic non-healing ulcers and has resulted in epithelialization of the ulcers with limited scar tissue formation (114, 115). Additionally, UBM was applied to complicated wounds not responding to conventional therapies with the result of epithelialization and successful skin grafting (116). UBM also facilitates soft tissue reconstruction in traumatic wounds by establishing a neovascularized soft tissue base (117).

The physicochemical and immunomodulatory properties of UBM make it an attractive therapeutic for OA, as OA—previously regarded as a predominantly mechanical disease—is now thought to progress due to excessive inflammation, immune cell infiltration, and cytokine secretion (118, 119) (120). Only one other report has shown the use of ECM in a small animal model of post-traumatic OA, but used human amnion ECM and has not shown evidence of the mechanism by which ECM helped reduce cartilage degeneration or shown functional pain reduction (47). We therefore tested the

effect of UBM on OA disease progression and tissue regeneration in rodents by injecting micronized UBM into a mouse model of post-traumatic OA, and by treating primary human chondrocyte cultures from OA cartilage *in vitro*. The results indicate a positive effect of UBM treatment on cartilage integrity *in vivo*, improved functional outcomes, and enhanced expression of several structural cartilage and anti-inflammatory genes.

Methods

Surgical Procedures: All procedures were approved by the Johns Hopkins University Animal Care and Use Committee (ACUC). OA was induced by anterior cruciate ligament transection (ACLT) (121) in 10-week-old male C57BL/6 mice from Charles River. Two weeks after ACLT, a single 10- μ L injection of either a phosphate-buffered saline (1X PBS, from Life Technologies) vehicle control or micronized UBM (~88% of the particle volume was under 20 μ m and the D50 (median size) was 5.09 μ m) suspended in 1X PBS, pH 7.2, 50 mg/ml, from ACell®, Inc., Columbia, MD) was administered to the joint space of the operated knee via a 30-gauge needle (n=13 animals for 4-week, n=8 animals for 8-week time point). The joint cavity was opened in the sham-group but the ACL was not transected. The study design is depicted in Fig. 1a. UBM particles were made using a Retsch CryoMill from Verder Scientific. A single steel ball (25 mm diameter) resides with the raw UBM sheet material during grinding. The chamber was kept cool via liquid nitrogen. Data on particle size distribution is in supplementary figure 2.

Histological evaluation: After 4 or 8 weeks, animals were sacrificed, and mouse knees were fixed in 4% paraformaldehyde (PFA), decalcified for approximately 2 weeks in 10% EDTA, then dehydrated and embedded in paraffin. Seven- μ m-thick sections were taken throughout the joint and stained for proteoglycans with Safranin-O and Fast Green (Applied biosciences) per manufacturer's instructions. Osteoarthritis research society

international (OARSI) scores are based on blinded histological assessment the medial plateau of the tibia (n=4-7 per group) (122).

Immunohistochemistry: Slides were de-paraffinized and treated with hyaluronidase (0.25% in Tris buffer) before staining for COL2 using Anti-Collagen II antibody (ab34712) from Abcam at 1:300 dilution (in 4% BSA/0.25% Triton X-100) followed by secondary staining with a biotinylated antibody and streptavidin-peroxidase conjugated enzyme using the Histostain-SP IHC kit, AEC, from ThermoFisher (cat. no. 959943) according to the manufacturer's instructions (n=3).

Gene expression analysis: Whole mouse joints were frozen in liquid nitrogen and homogenized using a sterile mortar and pestle (n=3-4). RNA was extracted using TRIzol reagent (Life Technologies) following the manufacturer's protocol. cDNA was synthesized using Superscript III reverse transcriptase (Life Technologies) following the manufacturer's protocol. Real-time RT-PCR was carried out using SYBR Green primers and a StepOnePlus Real-time PCR System (Life Technologies). Relative gene expression was calculated by the $\Delta\Delta C_t$ method. The ΔC_t was calculated using the reference genes $\beta 2$ -microglobulin (*B2m*) and β -actin (*Bact*). $\Delta\Delta C_t$ was calculated relative to the unoperated control group. The mouse specific primers used were the following: *Bact* forward, CCA CCG TGA AAA GAT GAC CC, *Bact* reverse, GTA GAT GGG CAC AGT GTG GG, *B2m* forward, CTC GGT GAC CCT GGT CTT TC, *B2m* reverse, GGA TTT CAA TGT GAG GCG GG, *Acan* forward, CGT TGC AGA CCA GGA GCA AT, *Acan* reverse, CGG TCA TGA AAG TGG CGG TA, *Col2a1* forward, CCT CCG TCT ACT GTC CAC TGA, *Col2a1* reverse, ATT GGA GCC CTG GAT GAG CA, *Mmp13* forward, GTC TTC ATC GCC TGG ACC ATA, *Mmp13* reverse, GGA GCC CTG ATG

TTT CCC AT, *Runx2* forward, GCC GGG AAT GAT GAG AAC TA, *Runx2* reverse, GGT GAA ACT CTT GCC TCG TC, *Il4* forward, ACA GGA GAA GGG ACG CCA T, *Il4* reverse, ACC TTG GAA GCC CTA CAG A, *Il10* forward, TCT CAC CCA GGG AAT TCA AA, *Il10* reverse, AAG TGA TGC CCC AGG CA , *Il6* forward, CCA GGT AGC TAT GGT ACT CCA GAA, *Il6* reverse, GCT ACC AAA CTG GAT ATA ATC AGG A, *Il1b* forward, GTA TGG GCT GGA CTG TTT C, *Il1b* reverse, GCT GTC TGC TCA TTC ACG.

Hind Limb Weight Bearing Assessment: Weight-bearing in mice was measured in the un-operated control animals and compared to ACLT animals receiving PBS control or UBM therapy using an incapitance tester (Columbus Instruments). The percentage weight distributed on the ACLT limb was used as an index of joint discomfort in OA (121). The mice were positioned to stand on their hind paws in an angled box placed above the incapitance tester so that each hind paw rested on a separate force plate. The force (g) exerted by each limb was measured. Three consecutive 3-second readings were taken and averaged to obtain the mean score (123).

Hind Limb Responsiveness: Mice were placed on the hotplate at 55°C. The latency period for hind limb response (jumping or paw-lick) was recorded as response time before surgery and at 2 and 4 weeks after surgery in all animal groups (121). Three readings were taken per mouse and averaged to obtain the mean response time for each time point.

Human Chondrocyte Isolation and Cell Culture: Human chondrocytes were isolated from OA cartilage harvested from cadaveric sources ($n = 3$) from the National Disease

Research Interchange. Cartilage was minced to 1-mm³ pieces, rinsed 3x in 1X PBS, and suspended in 25 mL of collagenase media [DMEM with 5% FBS and 1.67 mg/mL type II collagenase] per every 10 mL of cartilage pieces, then placed on a shaker at 37°C for 16-18 hours. Cells were filtered through a 70-µm cell strainer, spun down at 1000 rpm for 10 minutes, and rinsed 3x with PBS. Chondrocytes were plated in a 6-well plate with ~250,000 cells/well in chondrocyte media (high-glucose DMEM supplemented with 10% FBS, 1% nonessential amino acids, 1% HEPES, 1% sodium pyruvate, 0.2 M L-proline, 25 mg/mL ascorbic acid, and 1% pen/strep). After ~4 hours of attachment, 10 ng/ml of IL-1β was added to the media and allowed to incubate for 16-18 hours before addition of UBM, which then incubated for 24 hours before cell isolation for PCR. ΔΔCt was calculated relative to the untreated control group that received only IL-1β. The following human specific primers were used: *BACT* forward, GCT CCT CCT GAG CGC AAG TAC, *BACT* reverse, GGA CTC GTC ATA CTC CTG CTT GC, *B2M* forward, GAG GCT ATC CAG CGT ACT CCA, *B2M* reverse, CGG CAG GCA TAC TCA TCT TTT, *MMP13* forward, TGG TCC AGG AGA TGA AGA CC, *MMP13* reverse, TCC TCG GAG ACT GGT AAT GG, *ADAMTS5* forward, GAG GCC AAA AAT GGC TAT CA, *ADAMTS5* reverse, GGC AGG ACA CCT GCA TAT TT, *NF-kB* forward, AAC AGA GAG GAT TTC GTT TCC G, *NF-kB* reverse, TTT GAC CTG AGG GTA AGA CTT CT, *TNFα* forward, CCT CTC TCT AAT CAG CCC TCT G, *TNFα* reverse, GAG GAC CTG GGA GTA GAT GAG, *IL6* forward, GGC ACT GGC AGA AAA CAA CC, *IL6* reverse, GCA AGT CTC CTC ATT GAA TCC, *IL1β* forward, GGA CAA GCT GAG GAA GAT GC, *IL1β* reverse, TCG TTA TCC CAT GTG TCG AA

Alamar Blue Assay: Human OA chondrocytes were plated at a density of 10,000 cells/well in a 96-well plate and incubated at 37°C until attachment occurred, after which 10 ng/ml of IL-1 β and varying concentrations of UBM were added to the media and allowed to incubate for 24 hours. Ten μ L of Alamar Blue® reagent (ThermoFisher Scientific) was added directly into each well and the plate was incubated at 37°C for 3 hours protected from light. Absorbance was measured using a microplate reader every hour for 3 hours at a wavelength of 570 nm. Data were normalized to readings at 600 nm. These measurements were used to calculate percent of Alamar Blue reduced compared to control (cells with IL-1 β but no UBM).

UBM particle labeling and confocal microscopy: UBM particles were suspended in bicarbonate buffer (pH=8.3) and labeled with an Alexa Fluor-488 N-hydroxysuccinimide ester conjugate (Thermo Fisher) for 2 hours at room temperature. Excess dye was removed by washing several times with PBS via centrifugation. Fluorescent labeling and dye removal was confirmed by fluorescence measurements with a plate reader (BioTek Synergy 2). Labeled and un-labeled particles were added to human chondrocytes cultured on 1.5 mm thickness coverglass chamber wells (ThermoFisher Scientific) for 24 hours. Cells were then washed with PBS to remove unbound ECM and fixed with 4% paraformaldehyde for 20 minutes at room temperature. Cell membranes and nuclei were counterstained the CellMask Deep Red plasma membrane stain (Thermo) and DAPI, respectively, for 5 min. Entire cell volumes were imaged using a Zeiss LSM 710 confocal microscope with a 63X oil immersion objective and 0.3 μ m slice thickness. Three dimensional cell reconstruction was performed using IMARIS software (Bitplane).

Statistical Analysis: Statistical analysis was performed using a one-way ANOVA with Holm-Sidak multiple comparison correction in GraphPad Prism Software. For *in vivo* work, all groups were compared to each other. For *in vitro* work, each treatment was compared to the control group. $P < 0.05$ was considered significant.

Results

UBM injection reduces OA progression in mice

The ACLT model of post traumatic OA was chosen for its reproducibility and its relevance to human injury; approximately 50% of people of who tear their ACL develop OA within 10-20 years (124). The mouse ACLT model develops OA about 4 weeks after injury (125). ACL-transected mouse knees were injected with UBM particles or saline at 2 weeks post-ACLT and the effects on cartilage integrity and whole-joint inflammation were assessed at 4 and 8 weeks (2 and 6 weeks after therapy, respectively) (Fig. 1a). OARSI scoring, which is indicative of OA severity on a scale of 0 to 5 (0 is no cartilage degeneration, 5 is severe degeneration) revealed a statistically significant decrease in OA severity following UBM treatment group compared to saline controls at both 4 and 8 weeks. UBM particles reduced average disease scores from 3.2 to 1.4 at 4 weeks and from 3.7 to 1.9 at 8 weeks compared to saline alone. (Fig.1b). At 4 weeks, mice treated with the saline control exhibited proteoglycan loss as shown by diminished safranin-o staining (Fig. 1c; arrows) and cartilage lesions (Fig. 1c; stars) on their tibia. Injection of UBM in the synovial cavity decreased the severity of lesions and qualitatively increased the proteoglycan staining compared to the saline control (Fig. 1c). This effect was maintained even at 8 weeks post-injury, indicating a protective effect of UBM treatment on cartilage structure.

UBM therapy decreases expression of inflammatory markers

We next sought to characterize the osteoarthritic microenvironment after UBM treatment. As OA is a whole joint disease involving the cartilage and synovial tissue, inflammatory gene expression was evaluated in whole knee joint tissue using qRT-PCR. Cytokines thought to be involved in the pathophysiology of OA are the pro-inflammatory cytokines IL-1 β , tumor necrosis factor α (TNF- α), and IL-6, which increase the production of matrix metalloproteinase 13 (MMP-13), a collagenase that participates in cartilage degeneration (124). Macrophages are hypothesized to be important in OA and contribute to the expression of these cytokines; M1 polarized macrophages produce the pro-inflammatory cytokines IL-1 β , IL-6, and IFN γ (126), whereas M2 polarized macrophages often produce the anti-inflammatory cytokines IL-10, IL-4, and IL-13.

Gene expression of these inflammatory cytokines as well as cartilage catabolism and anabolism were evaluated in whole mouse joints at 4 and 8 weeks post-ACLT (Fig. 2). At 4 weeks, joints treated with UBM demonstrated significantly increased expression of the structural genes Aggrecan (*Acan*, approximately 9-fold) and collagen 2 α 1 (*Col2a1*, 13-fold) in addition to the anti-inflammatory genes *Il4* (2.6 fold) and *Il10* (5 fold) over un-operated control when compared to the saline control, which did not affect expression (Fig. 2, A and B). Additionally, the 4-week UBM treatment group reduced expression of the inflammatory cytokine *Il1b* compared to saline injections with 1.4 and 2.5-fold changes from unoperated mice, respectively. Conversely, expression of the pro-inflammatory cytokine *Il6* and enzyme *Mmp13* were increased in the saline group as compared to un-operated wild type mice (3 fold and 5-fold, respectively), but not in the

UBM group. Runx2 expression was not affected by any treatment suggesting that there was no chondrocyte hypertrophy. This is consistent with the observed increase in ECM gene expression as chondrocyte hypertrophy is associated with negative cartilage remodeling, including decreased collagen and proteoglycan production and alkaline phosphatase secretion, allowing abnormal calcification of the articular cartilage to occur.

At 8 weeks, joints treated with UBM demonstrated significantly increased expression of the anti-inflammatory gene *Il10* (3.8 fold) compared to the saline control (no change) (Fig. 3). Aggrecan (*Acan*) also exhibited significantly increased expression in the UBM treated group compared to an age-matched normal control (2.2 fold). No other genes were affected by UBM injection, indicating that the anti-inflammatory effect of the UBM had resolved between 4-8 weeks post ACLT (Fig. 3). The maintenance of cartilage integrity observed at 8 weeks post ACLT and the sustained increase in *Il10* and *Acan* expression suggests that the therapeutic effects of UBM may be mediated, at least in part, by these genes.

To validate the finding of increased collagen 2 α 1 expression in UBM-treated mice, histological sections from each treatment group were stained for the collagen 2 α 1 protein (COL2 α 1) (Fig. 4). Cartilage from UBM-treated mice at 4 weeks consistently stained more intensely for COL2 α 1 than the saline control cartilage. The 8-week UBM treatment group stained more intensely than the 8-week saline control despite not expressing significantly higher *Col2a1* (as assayed by qPCR) (Fig. 3). This discrepancy could be due to the fact that collagen protein can be retained long after *Col2a1* gene expression has diminished.

UBM injection reduces pain in OA mice

After the majority of intra-articular cartilage is damaged from OA, severe pain arises from exposed nerve endings that were once protected by the dense cartilage. This is a hallmark of OA and can serve as a clinical endpoint for treatment trials. Thus, we determined if the UBM mediated improvement in cartilage structure (shown in Fig. 1a) correlated with a functional decrease in pain through hotplate and incapacitance testing (Fig. 5) (121). The UBM-treated groups at 4 and 8 weeks exhibited faster response time than saline treated mice with the hotplate test, on par with the healthy sham animals, which indicates decreased motor impairments compared to saline-injected mice (Fig. 5a). UBM-treated animals also demonstrated greater weight-bearing percentage on the operated limb at 4 weeks, indicating less functional impairment than saline-treated mice despite ACLT (Fig. 5b). At 8 weeks, however, weight-bearing percentage was not statistically different between the control (saline) group and UBM-treated animals.

UBM decreased inflammatory marker expression in human OA chondrocytes

Pro-regenerative gene expression within the mouse knee after UBM treatment led us to ask whether there was a biological effect of UBM on human OA chondrocytes. 2D culture is not a perfect model of what occurs in the knee joint; however, *in vitro* chondrocyte culture has been used to elucidate biological effects of therapeutics (123).

To maintain OA conditions *in vitro*, primary human OA chondrocytes were cultured in the presence of IL-1 β for 1 day prior to the addition of varying concentrations of UBM. We assessed the expression of several genes involved in OA progression after 1 day of UBM exposure. Genes tested included the matrix degrading enzyme *MMP13*, the pro-inflammatory stress-related transcription factor *NF- κ B1* (nuclear factor kappa-light-chain-enhancer of activated B cells), the aggrecan degrading enzyme *ADAMTS5* (a

disintegrin and metalloproteinase with thrombospondin motifs 5), and the pro-inflammatory cytokines *TNF α* , *IL6*, and *IL1 β* . As chondrocytes are the cell type synthesizing aggrecan, a major structural component of cartilage, it is relevant to observe expression of *ADAMTS5*, the enzyme that degrades aggrecan. UBM induced a dose-dependent response in most genes tested. The 100 ng/mL and 1000 ng/mL concentrations of UBM produced the most apparent reductions in inflammatory cytokine and matrix-degrading enzyme expression, while the lowest concentrations (1 ng/ml, 10 ng/ml) had no beneficial effects (Fig. 6). The 1 μ g/mL UBM dose lowered *MMP13* compared to the control group (0.5 fold). There was an observed reduction of *NF- κ B1* and *ADAMTS5* expression by UBM treatment (by 0.4 and 0.6-fold, respectively), but did not reach statistical significance ($p=0.054$, 0.07 , respectively). This trend of decreased inflammatory cytokine and matrix-degrading enzyme expression is similar to our findings *in vivo*. Additionally, the alamar blue assay was performed to confirm that UBM treatment is not toxic. There were no significant changes in percent reduction of alamar blue across the tested UBM concentrations.

To determine how UBM may be directly interacting with chondrocytes *in vitro*, confocal imaging was performed 24 hours after adding 1 μ g/ml or 100 ng/ml of fluorescently labeled UBM to chondrocyte media. Imaging revealed that human chondrocytes do not engulf UBM entirely but do appear to contact the surface of most particles (Fig. 6b).

Discussion

ECM biomaterials, such as UBM, are an attractive therapy for OA disease modification due to their regenerative capabilities in animal models and in humans (47, 113). UBM is

used clinically for several different applications including management of trauma wounds (127), chronic non-healing wounds (103), and esophageal reinforcement in gastrectomy (106). Because OA does not yet have a viable treatment, and UBM has shown promise in other musculoskeletal defects and degenerative diseases, the possibility of UBM to treat OA was tested here in a mouse model and in human primary cells. Injection of UBM into the synovial cavity of mice with ACLT-induced OA improved the articular cartilage integrity 4 and 8 weeks after injury and reduced pain compared to saline-treated controls. At 4 weeks, the expression of structural genes (*Acan*, *Col2a1*) and anti-inflammatory cytokines (*IL4*, *IL10*) were significantly increased compared to controls. Accordingly, UBM treatment decreased the expression of the pro-inflammatory cytokine *Il1 β* *in vivo* in mice and the remodeling enzyme *MMP-13* *in vitro* in human OA chondrocytes. While chondrocytes exhibited reduced expression of matrix degrading and pro-inflammatory genes, it is unclear to what extent particles would interact with them directly. Alternatively, the synovium is more permeable to particle passage meaning that synoviocytes may be more likely to encounter particles in synovial fluid; their response to UBM is worthy of further investigation (128).

These results are consistent with the theorized role of the immune response in OA disease progression. Previously, Finnegan *et al.* described a role of IL-10, an important anti-inflammatory cytokine in collagen-induced arthritis. The severity of arthritis in IL-10 knockout (*Il10^{-/-}*) mice was substantially greater than that in wild type or *Il10^{+/-}* (heterozygous) mice, indicating a role for IL-10 in moderating disease severity (129). In a separate study on rabbits with OA, IL-10 cDNA delivered *ex vivo* to rabbit synoviocytes and then injected intra-articularly was able to reduce cartilage breakdown (130). These

reports are consistent with our findings of IL-4 and IL-10 expression accompanied by cartilage protection.

The observed high expression of type II collagen and proteoglycan genes is most likely beneficial in maintaining cartilage integrity (123). Tesche *et al.* found that type II collagen was synthesized by the remaining healthy chondrocytes in OA, but not by the fibroblast-like chondrocytes that produce an abnormal matrix (131, 132). Salminen *et al.* noted that articular chondrocytes are capable of producing type 2A procollagen, but near the margins of cartilage defects, chondrocytes were metabolically inactive and surrounded by a noncollagenous matrix, which probably contributed to the loss of cartilage integrity (133). These findings point to a dynamic in which proteoglycan expression occurs in OA and may actually help maintain cartilage integrity; it is only when collagenases and aggrecanases exceed this repair capability that the cartilage shifts to production of an abnormal matrix, leading to a loss of cartilage integrity resulting in a defect. Because inflammatory cytokines encourage the expression of catabolic enzymes, perhaps control of the inflammation in the knee using biomaterials such as UBM may help shift the balance in the favor of anabolic genes and maintain the cartilage integrity. UBM may additionally work by directly encouraging deposition of chondrocyte-derived matrix; ECM materials are known to induce deposition of host-derived matrix after being degraded by the host (58). Enhanced matrix deposition by UBM was supported in the mouse joints by increased *Col2a1* and *Acan* expression at the 4-week time point. At the 8-week UBM treatment time point, it is plausible that collagen protein was retained well after gene expression had diminished.

In our study, the heightened expression of *Il-10* and *Il-4* suggests that there may be type-2 immune cells (M2 macrophages and Th2 T cells) infiltrating the joint at higher numbers in the UBM-treated animals than in saline controls. M1 macrophages and Th1 T cells are known to lead to type 1, pro-inflammatory immune response (126) while M2 macrophages and Th2 T cells are anti-inflammatory and can lead to matrix deposition(134). Because the dysregulation of these cell types leads to immune-mediated pathologies, it is reasonable that balancing these cell types can help modify OA disease progression (134). Future studies may elucidate how immune cell populations change over the course of OA and how they change with UBM therapy. Additionally, gene expression of these separate cell populations can be examined to identify which immune cell populations are responsible for the increases in IL-4 and IL-10 expression.

In conclusion, injection of UBM in the intra-articular space lessens cartilage degeneration in an ACLT mouse model of OA, and also induces a dose-dependent pro-regenerative, anti-inflammatory gene expression profile in human OA chondrocytes. This therapeutic effect may be due to the reduced inflammation in the joint and maintenance of high expression levels of proteoglycans, which together help to retain normal cartilage and limit tissue degradation. To further validate the use of UBM as an OA therapeutic, additional animal models should be tested (135). Today, there are no FDA-approved disease modifying OA drugs available, making comparisons of UBM to current therapeutic options difficult. However, reduction in OA-associated pain could be compared to NSAIDs, viscosupplements or biological injections such as platelet-rich plasma (PRP) (135, 136).

Acknowledgements

M. Frisk for editing. Okhee Jeon for histology scoring. The Wilmer NEI-NIH funded Imaging Core, the Wilmer Pooled Professor Fund, and Rhonda Grebe for confocal expertise. ACell Inc. for supplying UBM and providing financial support for the study through a Sponsored Research Agreement.

Chapter 2 Figures

Figure 2.1 UBM treated mice show reduced OA progression

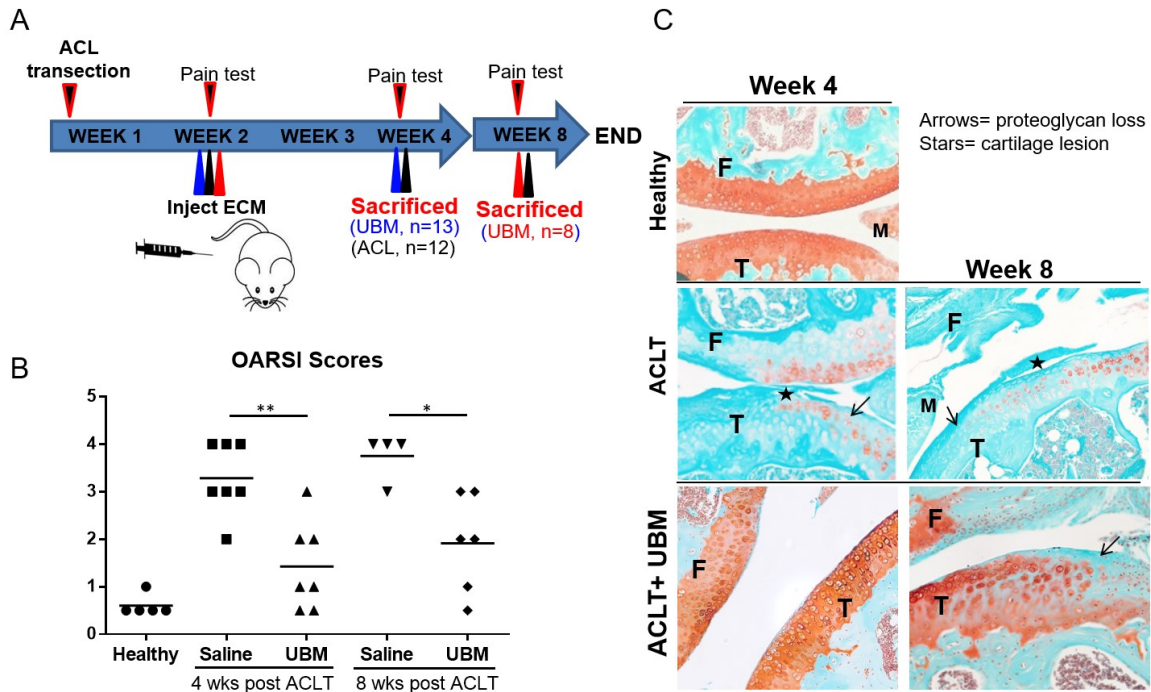


Figure 1: UBM treated mice show reduced OA progression. **A.** Overview of treatment. Mice were injected with 50mg/ml of UBM (10um-20um particles) 2 weeks after ACL transection and euthanized at 4 and 8 weeks post ACL transection. **B.** OARSIS scores from the medial plateau of each animal. **C.** Representative images from each treatment group, Safranin-O stained.

Figure 2.2 UBM injection decreases expression of inflammatory markers

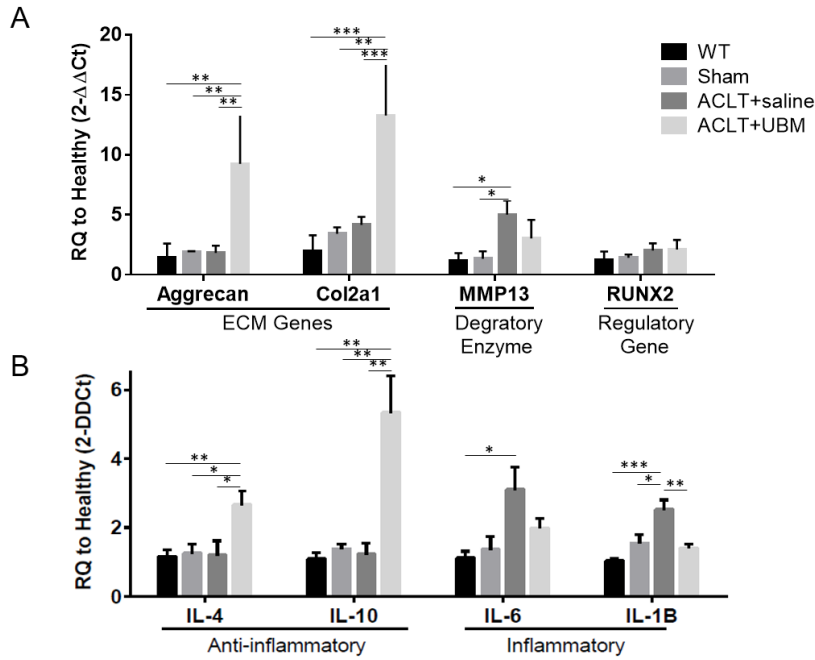


Figure 2. UBM injection decreases expression of inflammatory markers. Quantitative PCR on whole joint samples at 4 weeks post UBM injection. A. Cartilage related genes. UBM treated mice increased Aggrecan (*Acan*) and Collagen 2a1 (*Col2a1*) expression compared to saline treatment. Additionally, expression of Matrixmetalloproteinase 13 (*Mmp13*) and RUNX2 (*Runx2*) are not statistically significantly increased over wild type. B. Immune related genes. UBM treated mice increased IL-4 (*Il4*) and IL-10 (*Il10*) expression and decreased IL-1 β (*Il1b*) expression compared to PBS control mice. Expression of Interleukin-6 (*Il6*) is not statistically significantly increased over wild type.

Figure 2.3 UBM injection decreases expression of inflammatory markers

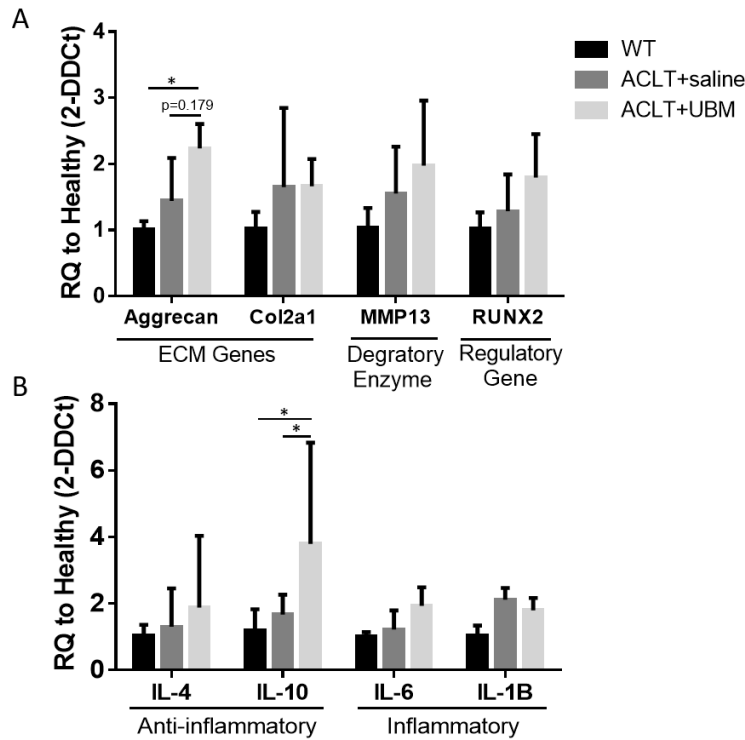


Figure 3. UBM injection decreases expression of inflammatory markers. Quantitative PCR on whole joint samples at 8 weeks post UBM injection. A. Cartilage related genes. UBM treated mice increased Aggrecan (*Acan*) expression compared to WT treatment. B. Immune related genes. UBM treated IL-10 (*Il10*) expression compared to PBS control mice

Figure 2.4 Collagen 2 α 1 Staining

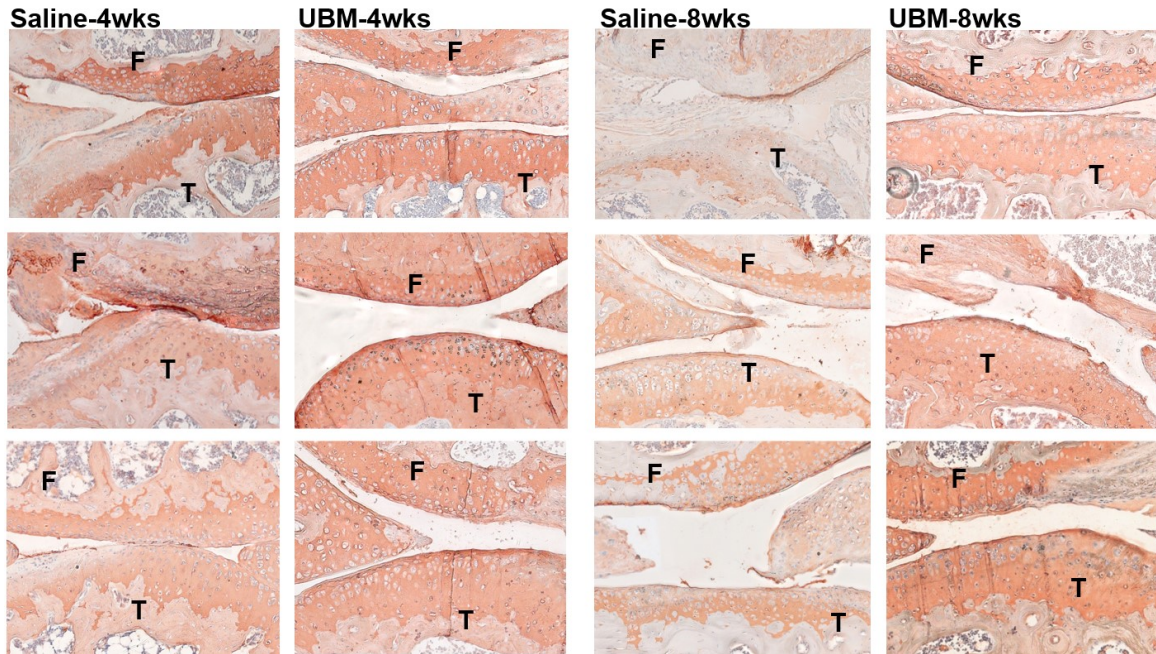


Figure 4. Collagen 2 α 1 Staining. Slides close to the representative image used for OARSI scoring for each joint were stained with col2 α 1 to verify the PCR results of increased *col2 α 1* gene expression. Qualitatively, UBM treated animals at 4 weeks post-surgery have more intense col2 α 1 staining compared to the saline control group. The 8 week UBM group is improved compared to saline, however it is not as intense as at 4 weeks. All slides were counterstained with hematoxylin.

Figure 2.5 UBM treatment reduces pain

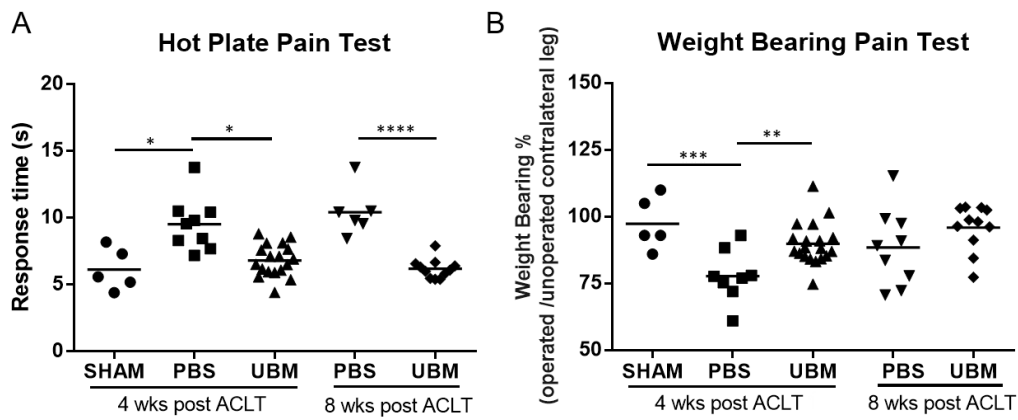


Figure 5: UBM treatment reduces pain. UBM treated mice have reduced pain at 4 weeks compared to PBS control mice. A. UBM treated mice have reduced time on the hotplate compared to PBS control mice, indicating less pain in the operated leg. B. UBM treated mice have increased weight placed on the operated leg as measured by incapacitance testing, also indicating less pain on the operated leg.

Figure 2.6 UBM decreased inflammatory markers in human primary chondrocytes

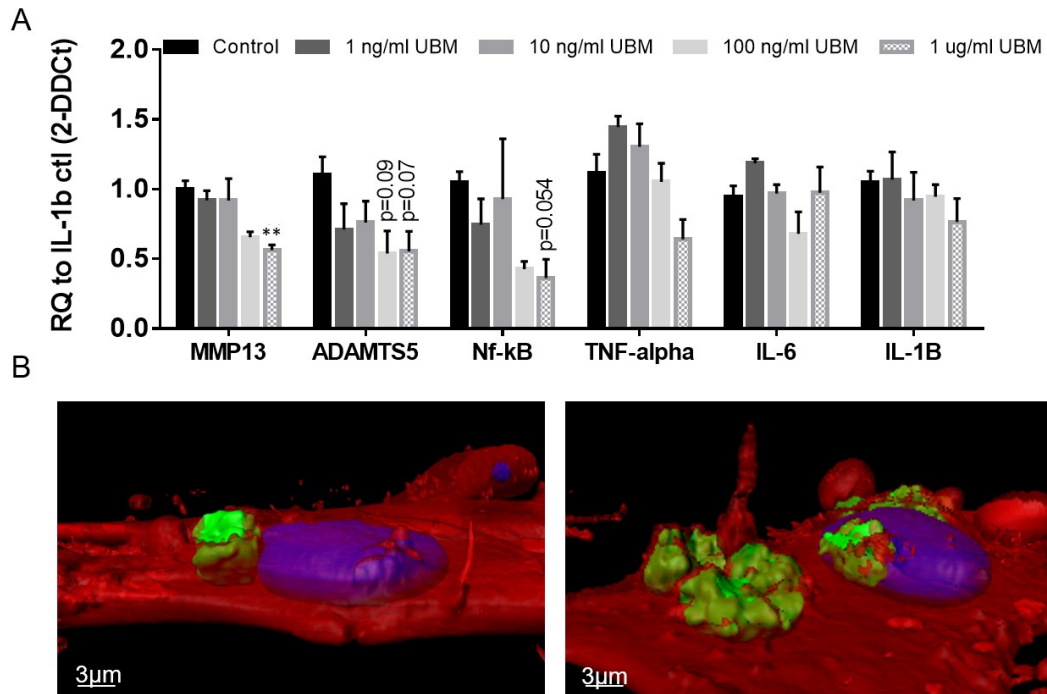
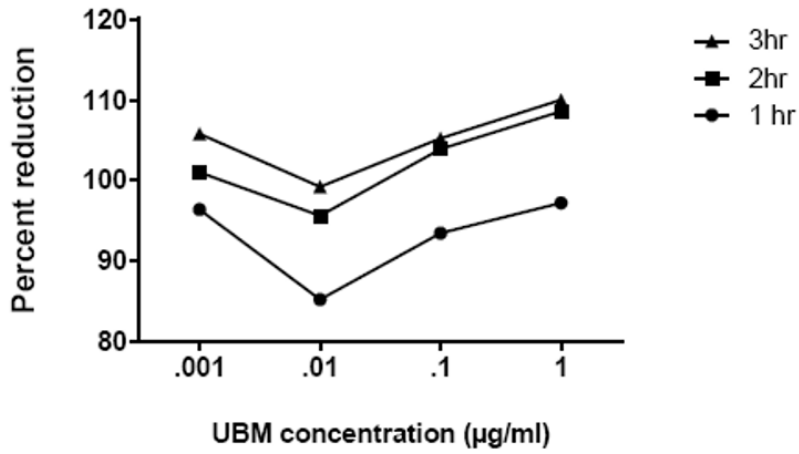


Figure 6: UBM decreased inflammatory markers in human primary chondrocytes A. Gene expression data from *in vitro* human chondrocytes exposed to 10ng/ml of IL-1 β and 1ng/ml-1 μ g/ml of UBM (n=3). B. Confocal imaging of 1ug/ml UBM (left) and 100ug/ml UBM (right) 24 hours after addition into cell culture medium. Red=cell membrane (seen at 50% transparency) , Blue=nucleus, Green=UBM. UBM particles appear to be almost entirely encapsulated by the cell membrane after only 24 hours.

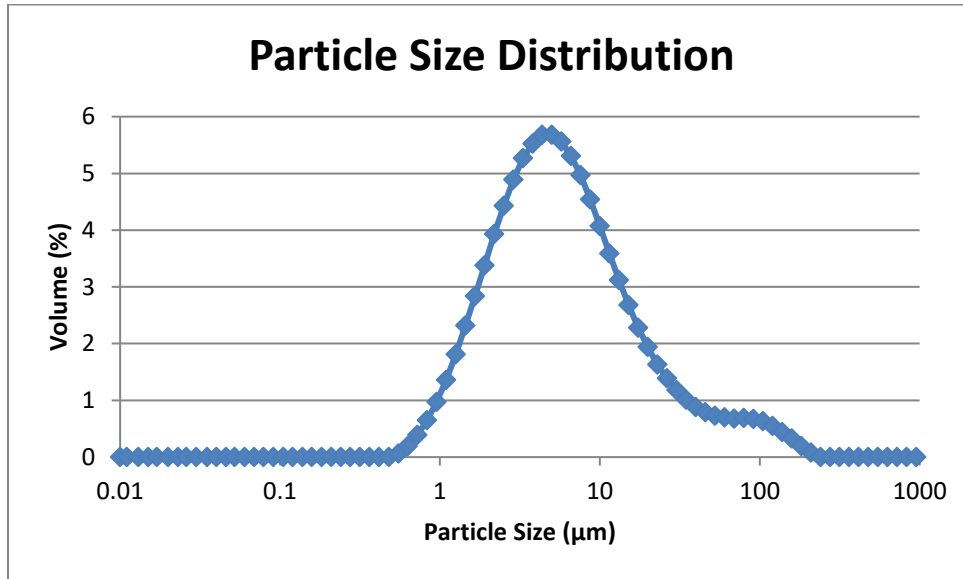
S. Figure 2.1 UBM can reduce chondrocyte toxicity in the presence of IL-1 β



Supplementary figure 1: UBM can reduce chondrocyte toxicity in the presence of IL-1 β .

Alamar blue cell toxicity test. Primary human chondrocytes were cultured in 10ng/mL IL-1 β and each experimental condition for 24 hours before performing the Alamar Blue assay. Absorbance values were taken at 570nm and 600nm 1,2, and 3 hours after addition of alamar blue and percent reduction of alamar blue was calculated based on control cells.

S. Figure 2.2 UBM particle size distribution.



Supplementary figure 2: UBM particle size distribution. Particles were sized using a mastersizer.

**Chapter 3: Optimization and application of HA binding peptide-polymers in
osteoarthritis**

A HYALURONIC ACID BINDING PEPTIDE-POLYMER SYSTEM FOR TREATING OSTEOARTHRITIS

This manuscript has been submitted to Biomaterials and is under review.

Heather J. Faust¹, Sven D. Sommerfeld¹, Sona Rathod¹, Andrew Rittenbach², Sangeeta Ray³, Benjamin M. W. Tsui³, Martin Pomper³, Mario L. Amzel⁴, Anirudha Singh^{1,5,6}, and Jennifer Elisseff^{1*}.

¹Translational Tissue Engineering Center, Wilmer Eye Institute and Department of Biomedical

Engineering, Johns Hopkins University, Baltimore, MD 21287, USA.

²University of Southern California, Information Sciences Institute, CA

³Department of Radiology, Johns Hopkins University, Baltimore, MD 21218, USA

⁴Department of Biophysics and Biophysical chemistry, Johns Hopkins University, Baltimore, MD-21218

⁵Department of Urology, The James Buchanan Brady Urological Institute, The Johns Hopkins School of Medicine, Baltimore, MD-21287

⁶Department of Chemical and Biomolecular Engineering, Johns Hopkins University, Baltimore, MD-21218

*Corresponding author. Tel.: 410-614-6837; fax: 410-614-6840

Abstract

Hyaluronic acid (HA) is found naturally in synovial fluid and is utilized therapeutically to treat osteoarthritis (OA). Here, we employed a peptide-polymer cartilage coating platform to localize HA to the cartilage surface for the purpose of treating post traumatic osteoarthritis. The objective of this study was to increase efficacy of the peptide-polymer platform in reducing OA progression in a mouse model of post-traumatic OA without exogenous HA supplementation. The peptide-polymer is composed of an HA-binding peptide (HABP) conjugated to a heterobifunctional poly (ethylene glycol) (PEG) chain and a collagen binding peptide (COLBP). We created a library of different peptide-polymers and characterized their HA binding properties *in vitro* using quartz crystal microbalance (QCM-D) and isothermal calorimetry (ITC). The peptide polymers were

further tested *in vivo* in an anterior cruciate ligament transection (ACLT) murine model of post traumatic OA. The peptide-polymer with the highest affinity to HA as tested by QCM-D (~4-fold greater binding compared to other peptides tested) and by ITC (~3.8-fold) was HABP2-8-arm PEG-COLBP. Biotin tagging demonstrated that HABP2-8-arm PEG-COLBP localizes to both cartilage defects and synovium. *In vivo*, HABP2-8-arm PEG-COLBP treatment and the clinical HA comparator Orthovisc[®] lowered levels of inflammatory genes including IL-6, IL-1B, and MMP13 compared to saline treated animals and increased aggrecan expression in young mice. HABP2-8-arm PEG-COLBP and Orthovisc[®] also reduced pain as measured by incapacitance and hotplate testing. Cartilage degeneration as measured by OASRI scoring was also reduced by HABP2-8-arm PEG-COLBP and Orthovisc[®]. In aged mice, HABP2-8-arm PEG-COLBP therapeutic efficacy was similar to its efficacy in young mice, but Orthovisc[®] was less efficacious and did not significantly improve OARSII scoring. These results demonstrate that HABP2-8-arm PEG-COLBP is effective at reducing PTOA progression.

Key Words: Osteoarthritis, hyaluronic acid, peptide-polymer, anterior cruciate ligament, cartilage, hyaluronic acid binding peptide

1. Introduction

Osteoarthritis (OA) is a degenerative joint disease that results in both biological and mechanical dysfunction. It is estimated to affect 40% of people over the age of 70 (137). OA is characterized by a progressive loss of cartilage tissue, remodeling of the underlying bone, inflammation of the synovial membrane, and abnormalities in lubrication of the articular joint. Lubrication is facilitated by molecules in the synovial fluid and at the cartilage surface including lubricin and hyaluronic acid (HA). Moreover,

engineered or repair cartilage lacks the typical surface and lubrication properties of normal tissue. Current therapies for OA primarily target symptoms and fail to modify disease progression. Non-steroidal anti-inflammatory drugs (NSAIDs) can reduce pain but do not alter disease progression. Steroids are also effective at relieving pain but cause cartilage damage and chondrotoxicity when used for extended periods of time (138).

While a few potential disease modifying drugs are in clinical testing, the lack of currently available options leaves joint replacement surgery as the only therapeutic choice for treating end stage disease.

One therapeutic approach for managing OA is to supplement the synovial fluid. Synovial fluid is an important constituent of a functional knee joint which acts as a biochemical repository, supplies nutrients to articular cartilage, promotes chondrocyte proliferation and differentiation, and reduces friction at direct cartilage-cartilage surface interactions in the articular joint (139-143). Cartilage lubrication is facilitated by molecules in the synovial fluid and at the cartilage surface including the proteoglycan lubricin and large glycosaminoglycans including hyaluronic acid (HA). High molecular weight (HMW) HA (>1,000 kDa) is the primary contributor to the viscoelasticity of synovial fluid. HMW HA is degraded into proinflammatory low molecular weight (LMW) HA by hyaluronidases in the course of aging and inflammation, including during OA progression, and results in further disease progression. Reduced amounts of HMW HA in synovial fluid lead to decreased synovial fluid viscosity (144-146), which increases friction between articulating cartilage surfaces, leading to increased cartilage deterioration (147).

Introducing HMW HA back into synovial fluid of arthritis patients, known as visco-supplementation, improves joint lubrication and reduces patient pain (148). Visco-

supplementation is a well-established treatment option; however, it has limited longevity and requires frequent, repeated administrations [7]. This challenge has prompted several groups to consider biomaterials-based approaches to augment joint lubrication. Roberts describes the use of HA binding peptides in hydrogels containing HA. These hydrogels enhance retention of HA compared to control gels without HA binding peptide (149). Additionally, there are other investigators pursuing synthetic lubricants for cartilage regeneration. One group employed a lubricating multiblock bottlebrush polymer mimicking lubricin on mica surfaces and showed that it extended wearless friction with the addition of fibronectin. In another study, bottle-brush copolymers were synthesized to mimic the structure and function of lubricin; these polymers reduced friction relative to denuded cartilage plugs (150, 151). Despite the current research aimed to aid in lubrication, supplementing synovial fluid remains a popular approach to treating OA due to the many biological and mechanical properties of increased HA in the synovial fluid, as well as the ease and minimal invasiveness of the procedure.

Supplementing HA in the joint may temporarily increase viscoelasticity, however it also likely has additional biological effects in the articular joint that have not yet been fully elucidated. In any case, HA is not as effective at cartilage lubrication if it is not localized to the cartilage surface (152). Lubricin tethers HA to the joint surface in healthy joints; however, lubricin is reduced after trauma and in OA disease (153, 154). Therefore, we developed a therapy to aid in HA localization and retention to the cartilage surface. We previously developed a biomimetic system in which an HA-binding peptide (HABP) is non-covalently bound to the cartilage surface through a heterobifunctional poly(ethylene glycol) (PEG) chain and a collagen binding peptide (COLBP) (26). The COLBP anchors

the construct to exposed type II collagen in the cartilage, bringing any HA bound by the HABP moiety of the construct close to the cartilage surface. We demonstrated that this technology enhanced HA retention *in vivo* and cartilage lubrication *in vitro* (26). Here, multiple peptide formulations were synthesized and evaluated for HA binding efficacy and OA treatment. HABPs that possess different binding properties, referred to here as HABP1, 2, and 3, were tested. HABP1 and HABP2 are synthetic HABPs found by phage display (155). HABP2 has homology to the hyaluronan mediated motility receptor (RHAMM) and HABP3 has homology to link protein (149, 156). Several formulations were synthesized using these peptides conjugated to linear or 8 arm PEG formulations to determine the optimal formulation of the peptide-polymer conjugate. When implemented in a model of post-traumatic OA, administration of the peptide-polymer binding system alone reduced the expression of inflammatory factors and cartilage degradation.

2. Methods

2.1 Overview of experimental design

Peptide-polymer formulations with different HABPs (HABP1, sequence GAHWQFNALTVR, HABP2, sequence STMMSRSHKTRSHHV, and HABP3, sequence RYPISRPRKRC) and different PEG shapes (linear, 8 arm) were tested to optimize *in vitro* binding to HA and screened *in vivo* for therapeutic efficacy. HABP2-8-arm PEG-COLBP was selected for more in-depth testing of tissue localization *in vivo* against the control groups: HABP2-8-arm PEG, 8-arm PEG-COLBP, and HABP2-8-arm PEG-scrambled COLBP. The therapeutic efficacy of HABP2-8-arm PEG-COLBP was then compared in young and aged mice to the control groups 8-arm PEG-COLBP, HABP2-linear PEG-COLBP, and the clinical HA Orthovisc®. The ranges in peptide concentrations used throughout each animal study are listed here. For the specific

concentrations used in each figure, please refer to the figure legends: HABP1-linear PEG-COLBP (10-20mg/mL), HABP2-linear PEG-COLBP (25-50mg/mL), HABP3-linear PEG-COLBP (50mg/mL), HABP1-8-arm PEG-COLBP (50mg/mL), HABP2-8-arm PEG-COLBP (25mg/mL) and 8-arm PEG-COLBP (25mg/mL). For biotin tagged studies, all peptides were injected at 25mg/mL.

2.2 Peptide-PEG conjugation

HABP2-PEG (3.4 Da)-COLBP, as well as individual peptides HABP1-3 and COLBP, were purchased from Synpeptide (Shanghai, China). For the formulations conjugated to linear PEG, hetero-bifunctional PEG was purchased with NHS on one end and a maleimide group on the other. The amine group on the N terminus of the HABPs reacted with NHS on linear PEG, and the thiol group at the C terminus of COLBP reacted with the maleimide group on linear PEG. For the 8-arm PEG formulations, eight-arm PEG-maleimide (MAL) was purchased from Jenkem (Dallas, Texas). To create 8-arm PEG conjugated to HABP2 and COLBP, cysteine-containing HABP2 and COLBP (SynPeptide) reacted with 8-arm PEG-MAL at a molar ratio of 1:4:4 (8 arm PEG: HABP2: COLBP) in MES buffer (pH 6.0) for 4h followed by a dialysis against water (MWCO ~3400 Da) and lyophilization. For 8-arm PEG-COLBP, the reaction mixture had a ratio of 1:8 (8-arm PEG: COLBP). Peptide sequences can be found in S. Table 1.

2.3 QCM-D (quartz crystal microbalance with dissipation monitoring)

Gold sensor surfaces were coated with biological substrates *in situ* using either HA-thiol (100 µg/ml) or type II collagen fibrils (40 µg/ml). Compositions of HABP (100 µg/ml) were applied at a flow rate of 24 µl/min at 37°C in PBS (n=3) [3].

2.4 ITC (Isothermal Titration Calorimetry)

Twenty kDa Hyaluronic acid was diluted to a concentration of 0.1 mM- 0.4 mM and dialyzed against a buffer containing 100 mM MES pH 7.1. Peptides were diluted to 0.07 mM- 0.2mM in 100 mM MES pH 7.1. ITC experiments were carried out at 26°C with a high-precision VP-ITC titration calorimeter system (Microcal Inc., CA). Ten microliters of the HA solution were added every 400 seconds to the cell containing 1.5 ml of HABP2-8-arm PEG-COLBP. The heat of binding was obtained by integrating the calorimetric signal. The first injections were excluded from the analyses. Data were analyzed using Origin 5.0 (Microcal Software, Inc., Northampton, MA). Details of the analyses are presented in the Results section.

2.5 Surgical Procedures

All procedures were approved by the Animal Care and Use Committee at Johns Hopkins University School of Medicine. A murine model using C57/BL6 male mice was applied. OA was induced by anterior cruciate ligament transection (ACLT) as previously described (121, 157) in adult (10 weeks old) or aged (56 weeks old) mice (n=5-10). Briefly, the sham operation consisted of exposing the knee joint by a medial capsular incision, which cut the patellar tendon, and skin closure with sutures after irrigation with saline. For the ACLT surgery, after opening the joint capsule, the ACL was transected with micro-scissors under a surgical microscope. Two weeks after ACL transection, a single 10 uL intra-articular injection of either saline or specified treatment was administered to the operated knee via a 30-gauge needle. On week 4 post ACLT, the mice were euthanized, and joints were collected for gene expression quantification or histological assessment.

2.6 Histological evaluation

Mouse knees were fixed in 4% PFA, decalcified for 10-14 days in 10% EDTA, dehydrated, and embedded in paraffin. Sections were taken at 7 μ m throughout the joint and stained for proteoglycans with safranin-O and fast green. Osteoarthritis Research Society International (OARSI) scores, which are a measure of cartilage damage, were determined by a blinded scorer and based on a representative image taken from the medial plateau of the tibia unless specified otherwise (n=4-7) (122). OARSI scoring for aged mice was performed on medial and lateral tibial plateaus. The OARSI scores presented are an average of the lateral and medial scores (n=3-5).

2.7 Gene expression analysis

Whole mouse joints were removed and snap frozen in liquid nitrogen and homogenized using a sterile mortar and pestle (n=3-4). RNA was extracted using TRIzol reagent (Life Technologies, Carlsbad, CA) following the manufacturer's protocol. cDNA was synthesized using Superscript III reverse transcriptase (Life Technologies) following the manufacturer's protocol. Real-time PCR was carried out using SYBR Green primers and a StepOnePlus Real-time PCR System (Life Technologies). Relative gene expression was calculated by the $\Delta\Delta$ Ct method. The Δ Ct was calculated using the reference genes β 2 microglobulin and β actin. $\Delta\Delta$ Ct was calculated relative to the un-operated control group. Gene expression fold change values for aged mice were calculated relative to the saline treated ACLT group. Statistical analysis was done with a one-way anova. The mouse specific primers used were the following: *Bact* forward, CCA CCG TGA AAA GAT GAC CC, *Bact* reverse, GTA GAT GGG CAC AGT GTG GG, *B2m* forward, CTC GGT GAC CCT GGT CTT TC, *B2m* reverse, GGA TTT CAA TGT GAG GCG GG, *Acan* forward, CGT TGC AGA CCA GGA GCA AT, *Acan* reverse, CGG TCA TGA

AAG TGG CGG TA, *Col2a1* forward, CCT CCG TCT ACT GTC CAC TGA, *Col2a1* reverse, ATT GGA GCC CTG GAT GAG CA, *Mmp13* forward, GTC TTC ATC GCC TGG ACC ATA, *Mmp13* reverse, GGA GCC CTG ATG TTT CCC AT, *Runx2* forward, GCC GGG AAT GAT GAG AAC TA, *Runx2* reverse, GGT GAA ACT CTT GCC TCG TC, *Il4* forward, ACA GGA GAA GGG ACG CCA T, *Il4* reverse, ACC TTG GAA GCC CTA CAG A, *Il10* forward, TCT CAC CCA GGG AAT TCA AA, *Il10* reverse, AAG TGA TGC CCC AGG CA, *Il6* forward, CCA GGT AGC TAT GGT ACT CCA GAA, *Il6* reverse, GCT ACC AAA CTG GAT ATA ATC AGG A, *IL1b* forward, GTA TGG GCT GGA CTG TTT C, *IL1b* reverse, GCT GTC TGC TCA TTC ACG.

2.8 Incapacitance Assessment

Weight bearing (WB) of mice from the un-operated control, saline control, and treatment groups was measured using an incapacitance tester (Columbus Instruments, Columbus, OH). The percentage weight borne on the ACL transected limb was used as an index of joint discomfort in OA (121). The mice were positioned to stand on their hind paws in an angled box placed above the incapacitance tester so that each hind paw rested on a separate force plate. The force (g) exerted by each limb was measured. Three consecutive three second readings were taken and averaged to obtain the mean score (n=5-10) (123).

2.9 Hotplate Analysis

Mice were placed on the hotplate at 55°C. The latency period for hind limb response (jumping or paw-lick) was recorded as response time before surgery and at 2 and 4 weeks after surgery (n=5-10) (121). A longer response time indicates greater pain in the operated limb.

2.10 Radioactive tagging and imaging studies

The radioactively tagged peptide, ^{111}In -DOTA-PEG-COLBP (MW:2364.31) was custom synthesized. ^{111}In was purchased from Nordion (Ontario, Canada). In a solution of $^{111}\text{InCl}_3$ [51.8 MBq (1.4 mCi)], 11 nmol of PEG-COLBP-DOTA (3.5 μl from a stock of 3.4 mM) and 20 μl 0.2 M sodium acetate buffer (pH 4) were added and incubated at 65°C for 1 h. The resulting ^{111}In -DOTA-PEG-COLBP was incubated with ethylenediaminetetraacetic acid (EDTA) at a final concentration of 10 mM for 5 min to chelate unbound ^{111}In and then subsequently purified on a PBS pre-equilibrated Zeba spin desalting column (Thermo Scientific). Radiochemical purity and stability of ^{111}In -DOTA-PEG-COLBP were tested by instant thin-layer chromatography (ITLC) using EDTA (10 mM) solution as a mobile phase. After purification the overall radiochemical yield and purity was $\geq 98\%$ with specific activity > 3.7 MBq (0.1 mCi)/nmol. The peptide concentration was determined using a NanoDrop spectrophotometer (Thermo Scientific).

Indium-111 tagged PEG-COLBP was injected into mouse knees (n=5) and imaged using a preclinical U-SPECT+ single-photon emission computed (SPECT) system from MILabs (Utrecht, The Netherlands) fitted with a high sensitivity collimator with 0.6 mm resolution. For each mouse, SPECT imaging data of the knee were acquired at the following time points: 5, 10, and 15 minutes, and 1, 3, 6 and 24 hours. The SPECT images were analyzed using AMIDE, a medical image analysis software. The image pixels were correlated to μCi based on a calibration factor. The radioactivity within a region-of-interest over the knee was plotted against time and two separate half-lives were determined: a distribution half-life and an elimination half-life. Elimination half-life corresponds to the kinetics of drug

elimination from the body, and elimination half-life of the PEG-COLBP in the knee (based on uCi content during time period from 3 to 24 hour) is on average 33 h (standard deviation: 20 h).

2.11 Peptide-polymer biotin tagging

Biotin-PEG (2000 Da)-thiol was purchased from Jenkem (Dallas, Texas). The peptides modified with biotin are the following: HABP2-8-arm PEG-COLBP, HABP2-8-arm PEG, 8-arm PEG-COLBP, and HABP2-8-arm PEG-scrambled COLBP. Peptides were modified with biotin by conjugating 8-arm PEG-MAL with thiolated HABP2, thiolated-COLBP and Biotin-PEG-thiol at a ratio of 1:3:3:2 in an MES buffer (pH 6.0). In a similar procedure, a scrambled version containing HABP2-8 arm PEG-scrambled COLBP was obtained. Biotin-labeled 8-arm PEG-COLBP was obtained by reacting 8-arm-PEG-MAL and biotin-PEG-thiol with thiol-COLBP at a ratio of 1:4:4 (8-arm PEG: COLBP: Biotin-PEG), while 8-arm PEG-HABP was obtained by reacting the mixture with thiol-HABP. All peptide-polymer samples were dialyzed against distilled water (MWCO 3400 Da) followed by lyophilization.

2.12 Immunohistochemistry

Biotin tagged peptide was visualized via immunohistochemistry by applying streptavidin-peroxidase conjugated enzyme and AEC chromogen using the Histostain-SP IHC kit, AEC, from ThermoFisher (cat. no. 959943) according to the manufacturer's instructions.

2.12 Statistical analysis

For *in vitro* binding assays, statistical analysis was performed using one-way ANOVA with Tukey's multiple comparison test in GraphPad Prism Software. Each group was compared to each other. For *in vivo* work, statistical analysis was performed using one-way ANOVA with Dunnett's multiple comparison test in GraphPad Prism Software.

Each treatment was compared to the saline control group. $P < 0.05$ was considered significant.

3. Results

3.1 Peptide-polymer reduces cartilage degeneration without HA supplementation

HABP1-linear PEG-COLBP was tested for the ability to reduce OA progression without HA supplementation. The peptide-polymer was injected with and without additional HA and compared to HA only treatment group (S. Fig. 1A). At 4 weeks post ACLT, both HA+ peptide-polymer, as well as peptide-polymer alone, significantly reduced expression of the matrix metalloproteinase MMP13 to approximately healthy levels, in contrast to the saline control (which was increased 5-fold over healthy). HA+ peptide-polymer and peptide-polymer also decreased average expression of IL-6 to healthy levels, however this did not reach statistical significance ($p=0.07$ and $p=0.08$, respectively). The HA only group was similar to the saline group in IL-6 expression. Peptide-polymer reduced TNF α to approximately healthy levels, however this did not reach statistical significance ($p=0.07$). HA did not have any effect on TNF α expression (S. Fig. 2). Meanwhile, treatment with HA, peptide-polymer, and HA+ peptide polymer reduced cartilage degeneration as measured by OARSI scoring (S. Fig. 1B-C). These results demonstrate that HA-binding peptide-polymer is therapeutic even without addition of exogenous HA.

3.2 HABP hyaluronic acid binding characterization

After proof of concept efficacy validation for OA treatment, a library of peptide-polymer formulations was synthesized and screened to determine optimal binding capacity and therapeutic efficacy without exogenous HA supplementation. Three HABPs were combined with linear or 8-arm PEG to create the library of formulations. HABP and

COLBP sequences are listed in S. Table 1 (149, 155, 156, 158, 159). COLBP binding to type II collagen was confirmed with QCM-D (S. Fig. 3).

HA binding to the various HABP formulations was quantified by quartz crystal microbalance with dissipation monitoring (QCM-D). Specifically, HA was thiol-immobilized onto a QCM-D chip surface and different HABP formulations were added. The resulting decrease in frequency is a measure of increased mass on the surface of the chip, and in this experiment, a measure of peptide binding to HA. The HABP constructs were established to bind to immobilized HA (Fig.1A). HABP1 and 2 bound HA with the highest affinity (Δ frequency of ~ 1 and 2.3 Hz, respectively), while HABP3 had no detectable binding (HABP3 not displayed, Δ frequency < 0.5 Hz). As HABP3 had the lowest affinity, it was excluded from further analysis. Binding of HABP1 and HABP2 when conjugated to linear or 8-arm PEG was then evaluated (Fig. 1A). Conjugation to linear PEG reduced the average Δ frequency of HABP1 from 1 to ~ 0.5 Hz but did not significantly impact HABP2 peptide binding to HA (Δ frequency ~ 3 Hz). Conjugation to 8-arm PEG significantly enhanced the binding of HABP2 to HA by approximately four-fold (Δ frequency of 16 Hz), most likely by increasing the avidity of the peptide. However, conjugating HABP1 to 8-arm PEG ablated HA binding, suggesting conjugation interfered with the hydrophobic binding mechanism of HABP proposed by Mummert (155) (Fig. 1a).

Next, the HA binding constant of the peptide-polymer formulation with the greatest binding capacity from the QCMD studies was determined. Isothermal calorimetry (ITC) was used to determine the efficacy of HABP2-8-arm PEG-COLBP binding to HA and was compared to binding of HABP2 alone and conjugated to the linear PEG formulation.

The binding constants were calculated and HABP2-8-arm PEG-COLBP bound HA with the highest affinity ($K_a=5.9E5 \text{ M (+/- 1.06E5)}$), followed by HABP2-linear PEG-COLBP ($K_a=1.53E5 \text{ M (+/- 7.06E3)}$), and lastly HABP2 ($K_a=1.09E5 \text{ M (+/- 5.57E3)}$) (Fig. 1B, for detailed ITC plots see S. Fig. 4).

3.4 Localization of optimized peptide-polymer in vivo

Indium labeled linear PEG-COLBP was injected into the knees of 5 individual mice to determine the lifetime of PEG-COLBP and imaged using a U-SPECT system (0.6 mm resolution). For each mouse, images of the knee were acquired at the following time points: 5, 10, and 15 minutes, 1, 3, 6, and 20 hours (example images are in S. Fig. 5). The elimination half-life, corresponding to the kinetics of drug elimination from the body, was 33hrs for linear PEG-COLBP (+/- 20 hrs) (Fig. 2A).

3.5 HABP2-8 arm PEG-COLBP localizes to degenerated cartilage, synovium, and subchondral bone

The tissue specific retention of the peptide-polymer with optimal HA binding, HABP2-8 arm PEG-COLBP, after OA induction was investigated. Biotin labeled peptide-polymers (defined in Fig. 2), were injected into joints 2 weeks post ACLT and mice were sacrificed 10 minutes, 1 hour, 3 hours, and 24 hours post injection to observe peptide-polymer localization.

At 10 minutes and 1-hour post injection, all peptide-polymer constructs localized to synovium, cartilage defect sites, and bone marrow (S. Fig. 6-7). Peptide-polymer also penetrated healthy cartilage, however it localized to damaged cartilage more strongly than to healthy cartilage. At 3 hours post injection, all peptide-polymers continued to localize to synovium and cartilage defects but exhibited less intense staining of the

synovium (Fig. 2B). At 24 hours post injection, the peptide-polymers exhibited different staining. The only staining observed for 8-arm PEG-COLBP 24 hours post injection was at cartilage defect sites, while 8-arm PEG-HABP only localized to synovium (S. Fig. 8A). Meanwhile, HABP2-8-arm PEG-COLBP localized to cartilage defects and synovium (Fig. 2C), and HABP2-8-arm PEG-scrambled COLBP staining (not shown) was too variable to make a conclusion. Peptide-polymer did not evenly distribute to all defect areas, which may be due to limiting amounts of peptide-polymer. Additionally, a biotin only control was cleared 1-hour post injection, indicating that the observed peptide-polymer localization at 1,3, and 24 hours was not due to non-specific binding of biotin (S. Fig. 8B).

3.6 HABP2-8-arm PEG-COLBP reduces OA progression

Pilot studies confirmed that OA treatment with peptide-polymer with and without HA showed similar results. Therefore, the peptide-polymer was studied alone in the following *in vivo* studies. In a screen of multiple peptide-polymers, most formulations, including HABP1-linear PEG-COLBP, HABP2-linear PEG-COLBP, HABP3-linear PEG-COLBP, and HABP2-8-arm PEG-COLBP, improved cartilage structure after ACLT injury as determined by OARSI scoring (S. Fig. 9A-B). Among these formulations, HABP2-8 arm PEG-COLBP most significantly improved OARSI score compared to saline treatment (OARSI score=0.83).

These *in vivo* results, together with the *in vitro* HA binding results, confirm that HABP2-8-arm PEG-COLBP is the optimal peptide in terms of HA binding and reduction of OA progression. Therefore, HABP2-8-arm PEG-COLBP was studied further for validation of its *in vivo* efficacy and comparison to the clinically used visco-supplement Orthovisc®.

Treatment groups were included to control for (1) the size of the PEG linker (linear vs 8 arm), (2) a peptide-polymer formulation without HABP2 (8-arm PEG-COLBP), and (3) the number of injections. Orthovisc® (OV) was included as a clinical benchmark control for pain reduction (160), and, as it is a high molecular weight HA, it is likely a good control for reducing the pro-inflammatory cytokines IL-6 and IL-1B.

A single injection of the optimal formulation, HABP2-8-arm PEG-COLBP, reduced expression of inflammatory markers (Fig. 3D). HABP2-8-arm PEG-COLBP reduced IL-6 expression from saline levels (~3-fold increased over healthy joints) down to healthy expression. It also reduced IL-1B from saline levels (~2.5-fold increase over healthy) to ~1.1 fold over healthy and it reduced MMP13 from saline levels (~5-fold increase over healthy) to ~1.5 fold over healthy (Fig. 3E). HABP2-8-arm PEG-COLBP also increased aggrecan expression to ~6 fold over healthy joints (Fig. 3D). HABP2-8-arm PEG-COLBP decreased pain as measured by both incapacitance testing and hot plate analysis. It increased weight bearing from ~75% weight bearing on the ACLT leg to almost full recovery (~97% weight bearing on ACLT leg) and reduced hotplate reaction time from saline levels (~8 s) to approximately healthy levels (~6.3 s). HABP2-8-arm PEG-COLBP also reduced cartilage deterioration as measured by OARSI scoring in the post-traumatic mouse OA model (Fig. 3A and B, OARSI avg=1.33). Two injections of HABP2-8-arm PEG-COLBP did not result in an increased therapeutic effect compared to a single injection, and efficacy in terms of gene expression (IL-6, 1.1 fold, IL-1B, 1.4 fold, and MMP13, expressed 1.6 fold over healthy), pain reduction (weight bearing ~97.6% and hot plate reaction time ~6.2s), and cartilage integrity (OARSI avg=1.64) were similar to that of a single injection of HABP2-8-arm PEG-COLBP (S. Fig. 10). Similarly, the other

treatments tested, Orthovisc[®], HABP2-linear PEG-COLBP, and 8-arm PEG-COLBP, also reduced pain as measured by incapacitance and hot plate testing, resulting in weight bearing averages of 91%, 95%, and 94.6%, respectively, and hot plate measures of 6.6s, 7.3s, and 5.8s, respectively (Fig. 4C and S. Fig. 10C). These groups additionally decreased expression of IL-6, IL-1B, and MMP-13 from saline levels to approximately healthy levels but did not significantly increase aggrecan expression (Fig. 3D and S. Fig. 10D-E). Consistent with the observed gene expression and pain reduction conferred by these treatments, similar efficacy in reducing OARSI score was observed in the Orthovisc[®] (OARSI avg= 1.7), HABP2-linear PEG-COLBP, (OARSI avg = 1.9) and the 8-arm PEG-COLBP (OARSI avg =1.58) groups (Fig. 4A-B and S. Fig. 10A-B). OARSI averages of the peptide-polymer treated groups at 4 weeks post ACLT (ranging from ~1.5-2) were also compared to OARSI scores of untreated mice 2 weeks post ACLT (on average ~1.6) to determine the amount of cartilage damage taking place after peptide-polymer injection. The similar OARSI scores suggest that peptide-polymers prevent cartilage degeneration from progressing but do not reverse it (S. Fig. 11).

3.7 HABP2-8-arm PEG-COLBP reduces OA progression in aged mice

The treatments tested in young mice were not significantly different from one another in terms of impact on OA progression with one treatment in the murine PTOA model. To better differentiate treatment group efficacy, HABP2-8-arm PEG-COLBP and control treatments were implemented in aged mice, which already have degeneration and provide a harsher environment for peptide-polymer testing. To mimic upper middle age, HABP2-8-arm PEG-COLBP was tested in 15 month old mice (161).

HABP2-8-arm PEG-COLBP was injected into aged mice and compared to saline, Orthovisc[®], and 8 arm PEG-COLBP. Although no statistically significant changes were observed, only HABP2-8-arm PEG-COLBP treatment decreased average MMP13 expression to ~0.6-fold of the saline group. Similarly, only HABP2-8-arm PEG-COLBP decreased average IL-6 and IL-1B expression (Fig. 4D, each ~0.6-fold of the saline group, not significant). Neither Orthovisc[®] or 8 arm PEG-COLBP altered joint gene expression. Weight bearing was increased from ~75% weight bearing on the ACLT leg to almost full recovery in the HABP2-8-arm PEG-COLBP group (~100%, equal weight on both legs), however hotplate reaction time was similar to ACLT animals (~7.8 s). Similar pain reduction was also observed in the Orthovisc[®] (~90% weight bearing, ~7.5 s hot plate), but 8-arm PEG-COLBP did not reduce pain (~87% weight bearing, 7.5 s hot plate) (Fig. 4C). Only injection of HABP2-8-arm PEG-COLBP significantly reduced cartilage deterioration in the aged post-traumatic mouse OA model (Fig. 4A and B, OARSI avg=1.83, p=0.044). 8-arm PEG-COLBP reduced the average OARSI score to 2 (p=0.07), while the average Orthovisc[®] OARSI score was 2.66.

4. Discussion

Disease modifying therapeutics for OA that could replace or augment HA visco-supplementation are attractive as HA visco-supplementation is controversial. Some reviews claim that the patient benefit of intra-articular HA does not provide clinically relevant therapeutic benefit when compared to saline placebo treatments due to too small of an increase in the magnitude of effect in HA treated groups over placebo (162). Another frequent criticism is the heterogeneity of the effectiveness in pain and functional relief between studies (163). Additionally, HA products have different molecular weights and some are crosslinked; which makes it difficult to assess HA efficacy among different

clinical studies (164). Crosslinked HA has become popular due to its increased longevity, however crosslinking HA sacrifices some of the bio-compatibility of HA (165, 166). Some crosslinked HAs such as Synvisc induce inflammation and exhibit immunogenicity (165). In an extreme case, Synvisc-one caused systemic inflammatory polyarthritis after injection (167). Our HA binding technology could avoid these adverse events by enhancing HA longevity without the need for HA crosslinking. As demonstrated by the *in vivo* data presented, our technology could also be used alone without exogenous HA with comparable benefit to HA supplementation. However, as HA concentrations are reduced in the synovial space following injury, additional HA supplementation may further enhance HA binding technology efficacy in preventing OA progression.

To test the ability of our HA binding technology to reduce OA progression, we employed the anterior cruciate ligament transection (ACLT) model of post traumatic OA. This model was chosen for its reproducibility and its relevance to human injury; approximately 50% of people of who tear their ACL develop OA within 10-20 years (124). When our peptide-polymers were implemented in this mouse model, all groups were efficacious in reducing OA progression. We hypothesized that this could be due in part to the young age of the mice, and that aged mice might be less responsive to treatment, aiding in observation of differences in therapeutic efficacy between treatments. One reason to utilize aged mice for this purpose is because the estimated incidence of symptomatic knee OA diagnosis is highest among adults age 55-64 (168). Mice in the range of 10-15 months are considered middle aged (with 15 months considered upper middle aged). Additionally, there are studies demonstrating that there is impaired regeneration during late middle age compared to youth in humans as well as in mice,

indicating that this is an important factor to account for *in vivo* studies (169-171).

Accordingly, we implemented the peptide-polymers in a harsher, aged mouse model of OA. This enabled observation of different therapeutic effects between groups that were not observed in young mice. In this study, Orthovisc® reduced pain but did not reduce disease progression in the aged mice, which is also observed clinically, supporting the use of this aged mouse model.

The biotin tagged peptide-polymer study demonstrates the ability of peptide-polymer to effectively localize at cartilage lesions. HABP2-8-arm PEG-COLBP localized to both cartilage and synovium 24 hours post injection, however the only staining observed for 8-arm PEG-COLBP 24 hours post injection was at cartilage defect sites, suggesting the specificity of the COLBP for exposed cartilage ECM at cartilage lesions. The presence of HABP2-8-arm PEG at cartilage defects 3 hours post injection suggests that HABP can bind exposed HA in the cartilage. These results suggest that these formulations can be utilized as a delivery mechanism to target therapeutics to areas of cartilage damage or synovial membrane inflammation.

The HA binding technology likely binds and concentrates endogenous HA from the synovial fluid to the cartilage surface to enhance lubrication. It is also possible that HA binding technology modulates some of HA's many biological properties. LMW HA has pro-inflammatory effects while HMW HA has many anti-inflammatory functions (38). Some of the anti-inflammatory properties of HMW HA include inhibiting macrophage phagocytosis, preventing monocyte recognition of tumor cells via blocking CD44, promoting regulatory T cell proliferation via crosslinking the CD44 receptor, and inhibiting angiogenesis (172-174). HA injected intra-articularly can also decrease TNF α .

and IL-8 expression (175). HA binding technology could potentially enhance these anti-inflammatory functions by localizing HA to damaged areas where HMW HA is most needed. LMW HAs (<200kDa) cause macrophages and other cells to produce proinflammatory cytokines through receptors including CD44 and TLR2 (176, 177). HA binding technology could be binding LMW HA and preventing binding of LMW HA to other pro-inflammatory receptors such as TLR2/4. Previous studies have also demonstrated that HABP2 blocks HA signaling through RHAMM, resulting in reduced inflammation and fibrosis in skin wounds (156). Likewise, our study indicates that HA binding technology can modulate the expression of inflammatory genes in the joints of aged mice, unlike the HMW HA Orthovisc® or 8-arm PEG-COLBP groups. Although HMW hyaluronic acid reduces inflammation in many *in vitro* and *in vivo* animal studies, aged animals are rarely used to study therapeutics, limiting the translational relevance of these studies. Aged animals are better predictors of therapeutic outcome in age related diseases, and should be used in more small animal models for screening therapies (178).

5. Conclusion

In summary, we demonstrate that HA binding technology can be implemented after a trauma to slow further degeneration of the cartilage tissue without additional HA supplementation. Additionally, HABP2-8-arm PEG-COLBP could be conjugated to other drugs for targeted delivery to damaged areas of cartilage *in vivo*. Future studies in a larger animal model should be conducted to determine whether the therapeutic ability of HABP2-8-arm PEG-COLBP supplemented with HA will be enhanced over that of HABP2-8-arm PEG-COLBP alone.

Competing interests

The authors declare no competing financial interests.

Acknowledgements

This work was supported by the Defense Health Program, through the Department of Defense Peer Reviewed Orthopaedic Research Program, Translational Research Award under Award No. W81XWH-14-1-0285. Opinions, interpretations, conclusions and recommendations are those of the author and are not necessarily endorsed by the Department of Defense.

We thank Professor Joachim Kohn and Sanjeeva Murthy for kindly allowing use of the QCMD instrument at the New Jersey Center for Biomaterials.

Figures

Chapter 3 Figures

Figure 1. HABP hyaluronic acid binding characterization

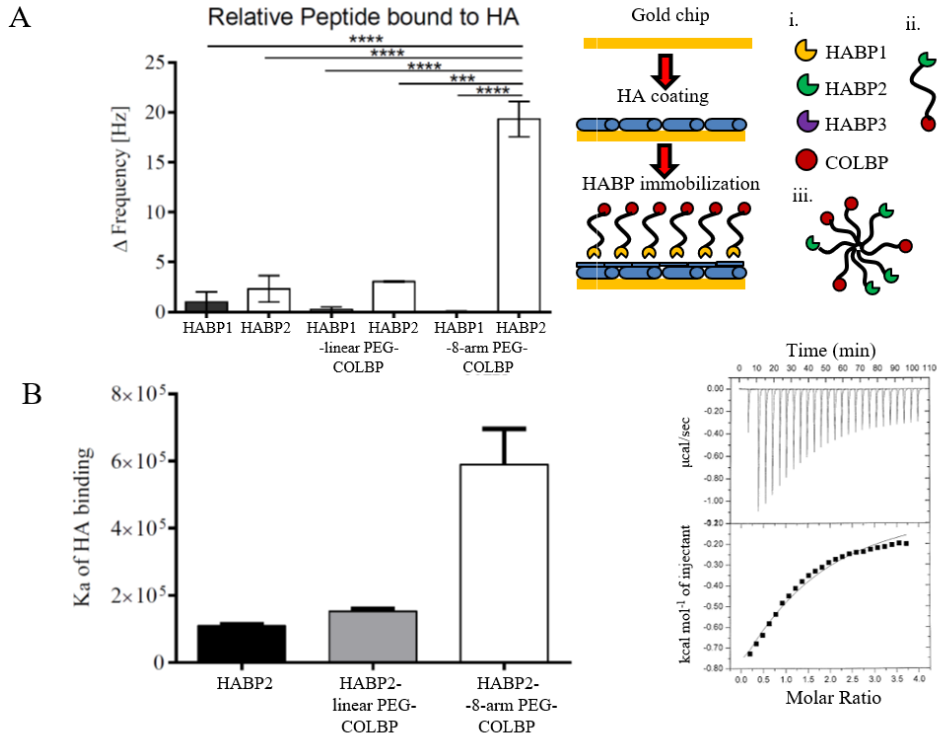


Figure 1. A. QCMD frequencies of peptides binding to thiol-immobilized hyaluronic acid, $n=3$. i. HABP moieties and COLBP moieties available. ii. Cartoon example of peptide conjugated to linear peg. iii. Example of peptide conjugated to 8 arm peg. In sum, binding of HABP1, HABP2, HABP3, HABP1-linear PEG-COLBP, HABP2-linear PEG-COLBP, HABP1-8-arm PEG-COLBP, and HABP2-8-arm PEG-COLBP were determined with QCMD. B. Binding constants of HABP2, HABP2-linear peg-COLBP, and HABP2-8-arm peg-COLBP to HA as determined by ITC. Right: example plot of calorimetric signal (top) and integration (bottom).

Figure 2. Localization of optimized peptide-polymer *in vivo*

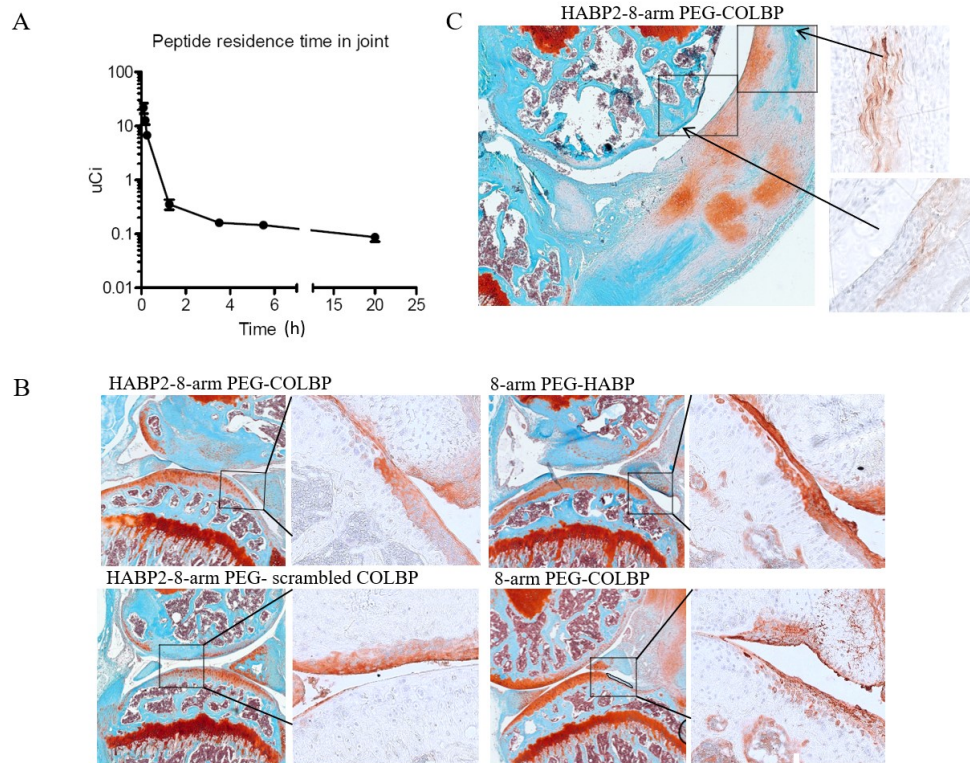


Figure 2. A. Peptide residence time in the joint. All peptide-polymer formulations were injected at 25mg/ml. Radioactively labeled linear PEG-COLBP was injected intra-articularly to determine half-life, n=5. The elimination half-life, corresponding to the kinetics of drug elimination from the body, was 33 h for linear PEG-COLBP (+/- 20 h). B and C. Biotin labeled peptide localization profiling. HABP2-8-arm PEG, 8-arm PEG-COLBP, HABP2-8-arm PEG, and HABP2-8-arm PEG-scrambled COLBP were biotin tagged and compared for tissue localization. Right image is safranin-o staining, left image is IHC (biotin tagged peptide stains brownish-red). B. 3 h post injection. HABP2-8-arm PEG-COLBP localizes to degenerated cartilage, synovium, and subchondral bone. Scrambled COLBP and HABP only (no COLBP) shows some absorption to the degenerated cartilage surface, probably due to interactions with HA in the cartilage. C. 24 hours post injection. Only the full construct retains peptide at cartilage and synovium.

Figure 3. HABP2-8-arm PEG-COLBP reduces OA progression

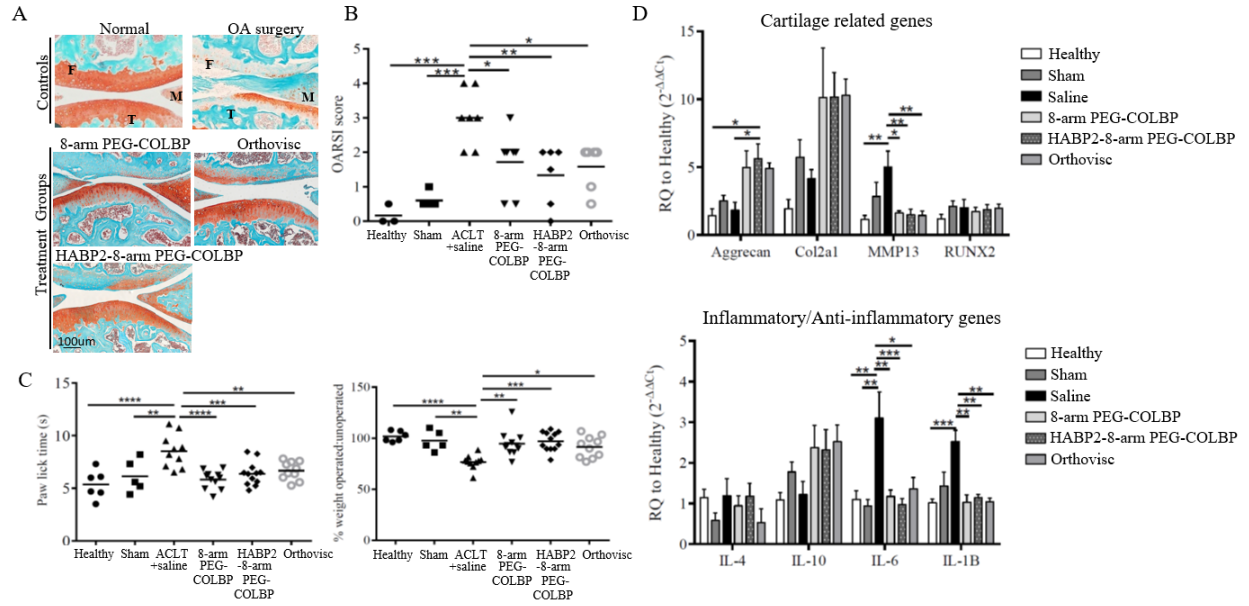


Figure 3. Only one intra-articular injection of each treatment was given unless otherwise specified. Orthovisc[®], HABP2-linear PEG-COLBP, 8-arm PEG-COLBP, HABP2-8-arm PEG-COLBP, and two injections of HABP2-8-arm PEG-COLBP were implemented in this study (for HABP2-linear PEG-COLBP and two injections of HABP2-8-arm PEG-COLBP group results, please see S. Fig. 10). All peptide-polymer formulations were injected at 25mg/ml. A. Representative images from the medial tibial plateau of each treatment group. Safranin-O staining (red) was used to visualize the cartilage proteoglycans. B. OARSI scoring demonstrates reduced cartilage degeneration in most treatment groups, n=6-7. The group with the most significant reduction in OA score was HABP2-8-arm PEG-COLBP, p=0.008. C. Pain testing, n=12. D and E. Whole joint gene expression, n=4.

Figure 4. HABP2-8arm peg-COLBP reduces OA progression in aged mice

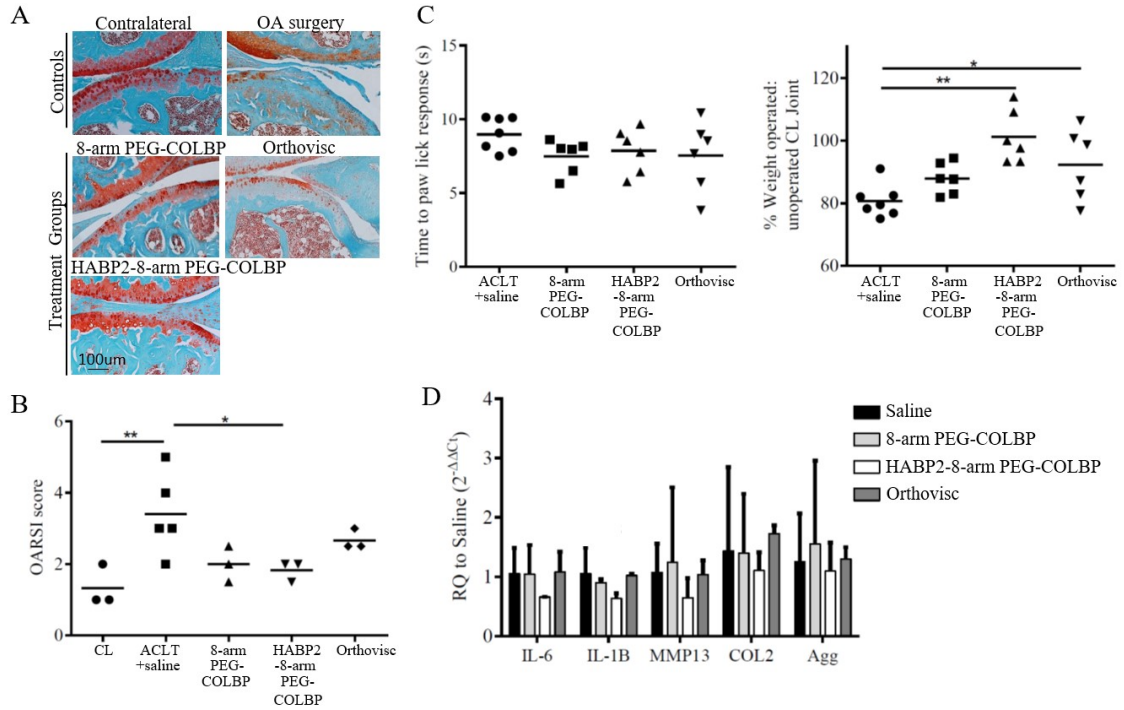
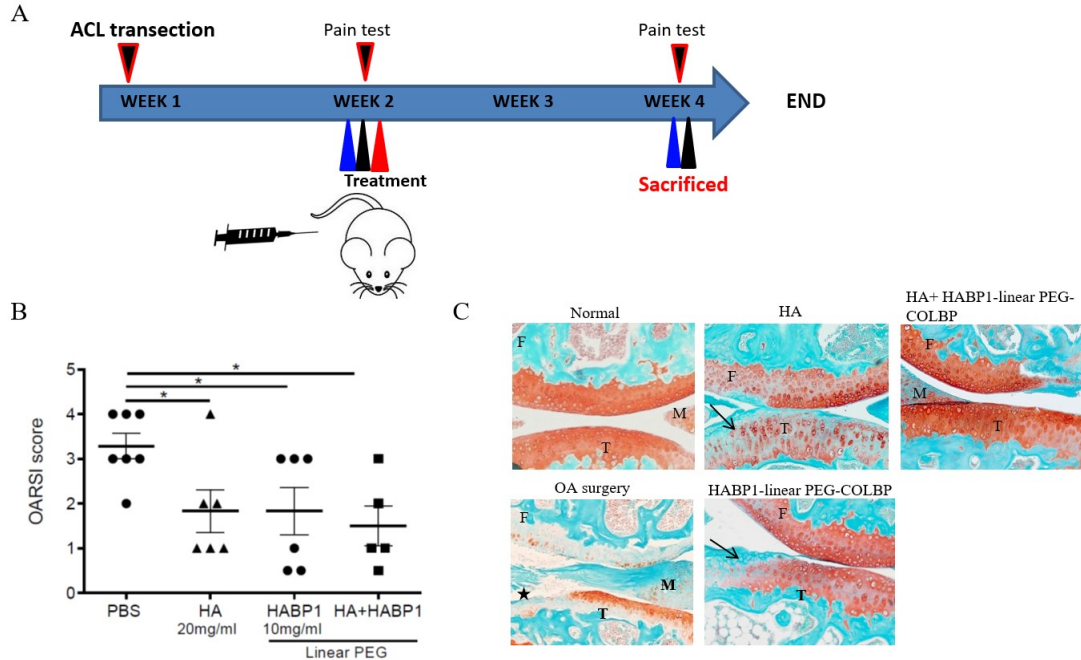


Figure 4. Only one intra-articular injection of each treatment was given unless otherwise specified. HABP2-8-arm PEG-COLBP, 8-arm PEG-COLBP, and Orthovisc® were implemented in aged mice. All peptide-polymer formulations were injected at 25mg/ml. A. Representative images from the medial tibial plateau of each treatment group. Safranin-O staining (red) was used to visualize the cartilage proteoglycans. B. OARSI scoring demonstrates reduced cartilage degeneration with HABP2-8arm peg-COLBP treatment, p=0.044, n=3. C. Pain testing, n=6. Orthovisc® and HABP2-8arm peg-COLBP reduced pain as measured by incapacitance testing, p=0.031 and 0.002, respectively. D Whole joint gene expression, n=3.

Supplementary Table 1. Peptide sequences

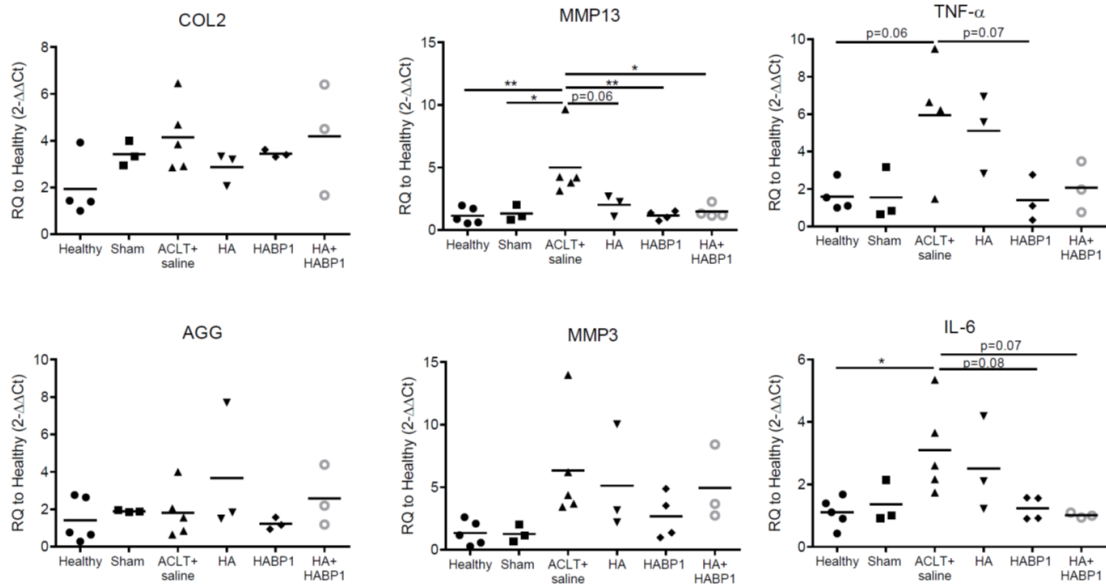
Peptide Name	Sequence
HABP1	GAHWQFNALTVR (Mummert)
HABP2	STMMSRSHKTRSHHV (Tolg)
HABP3	RYPISRPRKRC (Goetinck)
COLBP	WYRGRLC
Scrambled COLBP	YRLGRWC-amide

S. Fig. 1 Peptide-polymer reduces cartilage degeneration without HA supplementation



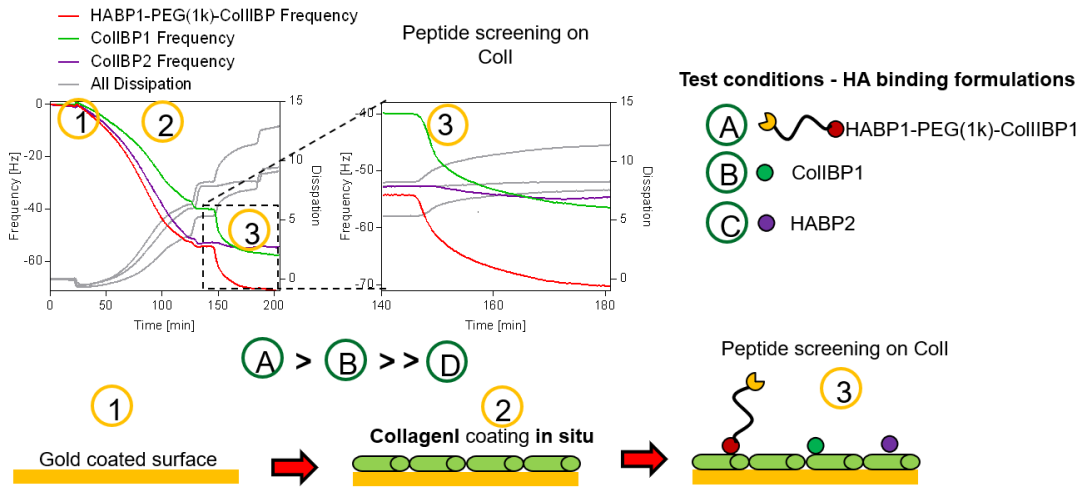
S. Figure 1. A. Mice were ACL transected and treated with either 20mg/mL HA, 10mg/mL HABP1-linear PEG-COLBP (HABP1 in figure), or HA+HABP1-linear PEG-COLBP two weeks post ACLT. B. HABP1-linear PEG-COLBP alone was able to confer a reduction in OA development via OARSI scoring, representative Safranin-O stained images are in C. Arrows=proteoglycan loss Stars=cartilage lesion.

S. Figure 2. Peptide alone can modulate inflammatory cytokine expression



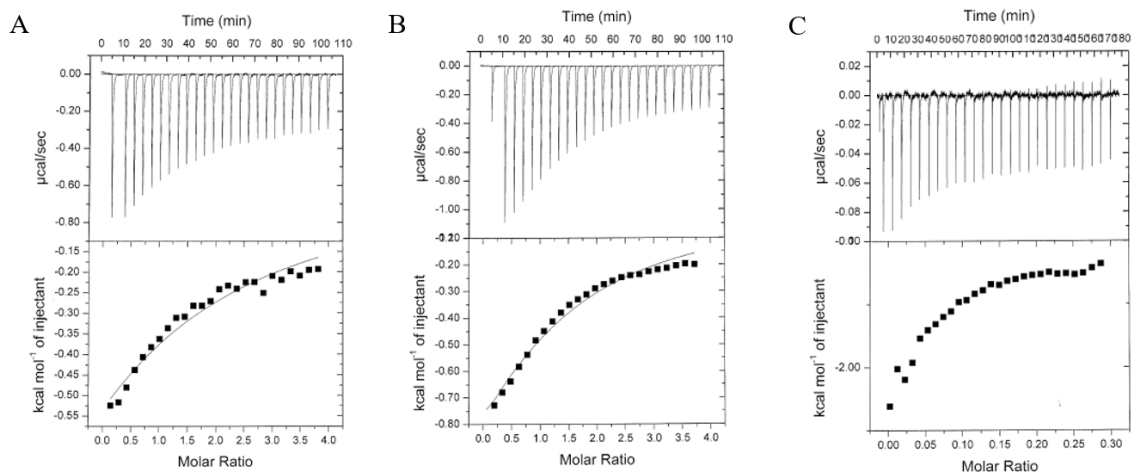
S. Figure 2. HABP1-linear PEG-COLBP (HABP1 in figure) alone reduces MMP13 expression as well as exhibits a lower MMP3, TNFα and IL-6 expression compared to PBS.

S. Figure 3. QCMD frequency and dissipation plots demonstrating COLBP binding to collagen



S. Figure 3. Step 1 is baseline of the gold chip. Step 2 is the baseline after addition Col II. Step 3 is the baseline after addition of specified peptide. Dips in frequency indicate peptide binding to chip surface. The purple line is a negative control; no binding of HABP2 to collagen is observed.

S. Figure 4. Assessment of HABP2 binding to HA with ITC



S. Figure 4. HA was loaded into the injector of the ITC machine and injected into a cell containing HABP2, HABP2-linear PEG-COLBP, or HABP2- 8-arm PEG-COLBP.

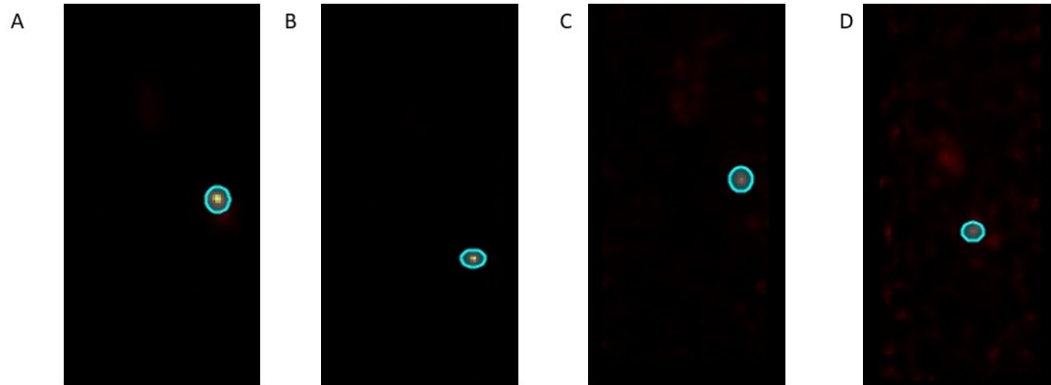
A. 0.4mM HA into 0.2mM HABP2. $K_a=1.09E5$ (+/- 5.57E3), $K_d=9.17E-6$

B. 0.4mM HA into 0.2mM HABP2-linear PEG-COLBP, $K_a=1.53E5$ (+/- 7.06E3),
 $K_d=6.53E-6$

C. 0.1mM HA into 0.07mM HABP2-8-arm PEG-COLBP, $K_a=4.56E5$ (+/- 5.91E4),
 $K_d=2.19E-6$

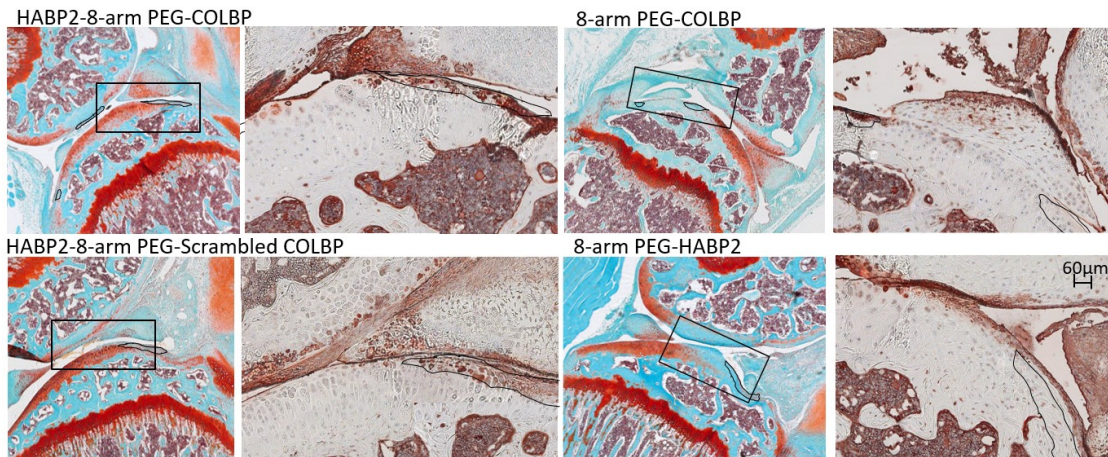
Stoichiometry: 1:10 for HABP2 and HABP2-linear PEG-COLBP, 1:22 for HABP2-8-arm PEG-COLBP

S. Figure 5. Example U-SPECT images after intra-articular injection of ^{111}In labeled PEG-COLBP



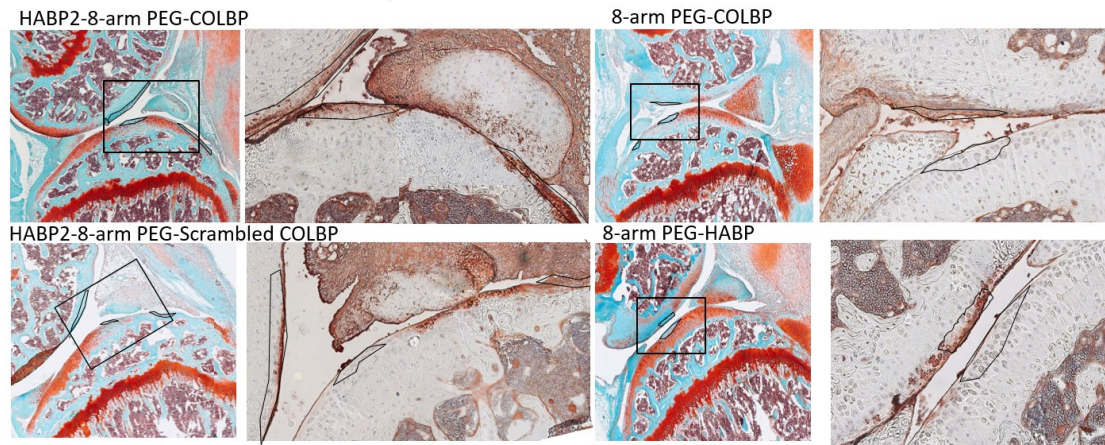
S. Figure 5. Images are rendered in AMIDE. Blue circles represent the ROI taken for analysis of signal intensity at the site of injection (the knee joint). Sagittal views of the 3 dimensional image analyses are shown here. ROI location changes due to the different position of the mice in imaging chamber at each time point. A. 5 minutes post injection. B. 1 h post injection. C. 3 h post injection. D. 20 h post injection.

S. Figure 6. HABP2-8-arm PEG-COLBP localizes to degenerated cartilage, synovium, and subchondral bone



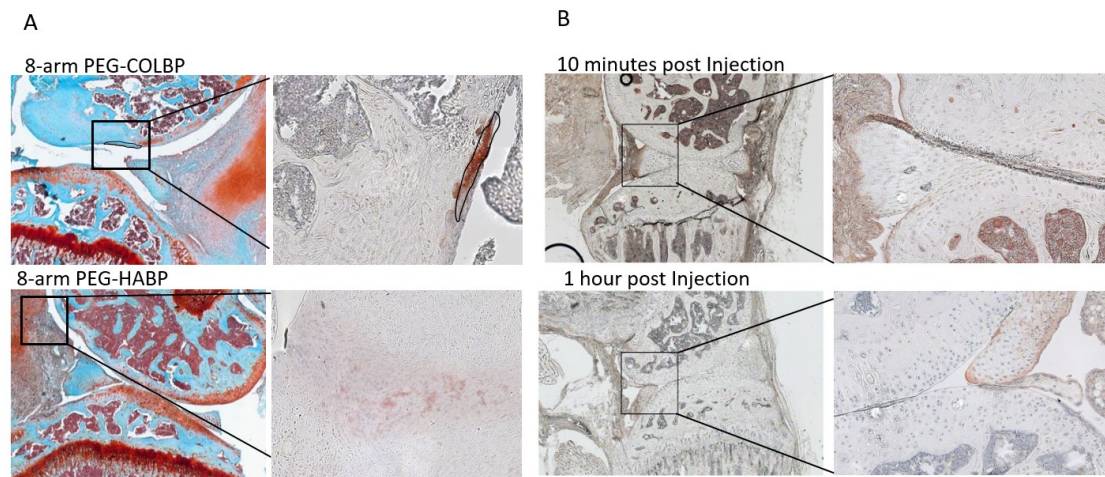
S. Figure 6. HABP2-8-arm PEG-COLBP localizes to degenerated cartilage, synovium, and subchondral bone. HABP2-8-arm PEG, 8-arm PEG-COLBP, HABP2-8-arm PEG, and HABP2-8-arm PEG-scrambled COLBP were biotin tagged and compared. Images above are from knees 10 minutes post injection.

S. Figure 7. HABP2-8-arm PEG-COLBP localizes to degenerated cartilage, synovium, and subchondral bone. 1-hour post injection.



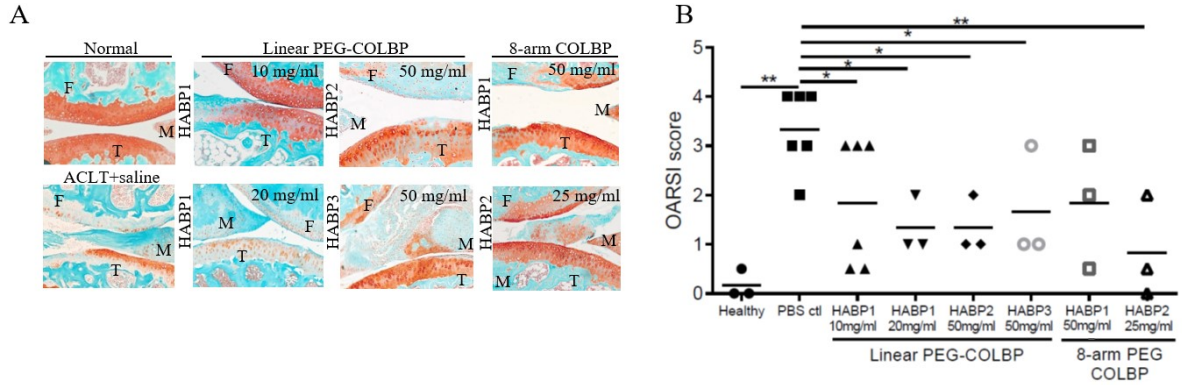
S. Figure 7. HABP2-8-arm PEG-COLBP localizes to degenerated cartilage, synovium, and subchondral bone 1-hour post injection.

S. Figure 8. HABP2-8-arm PEG-COLBP localizes to degenerated cartilage, synovium, and subchondral bone. 24 hours post injection.



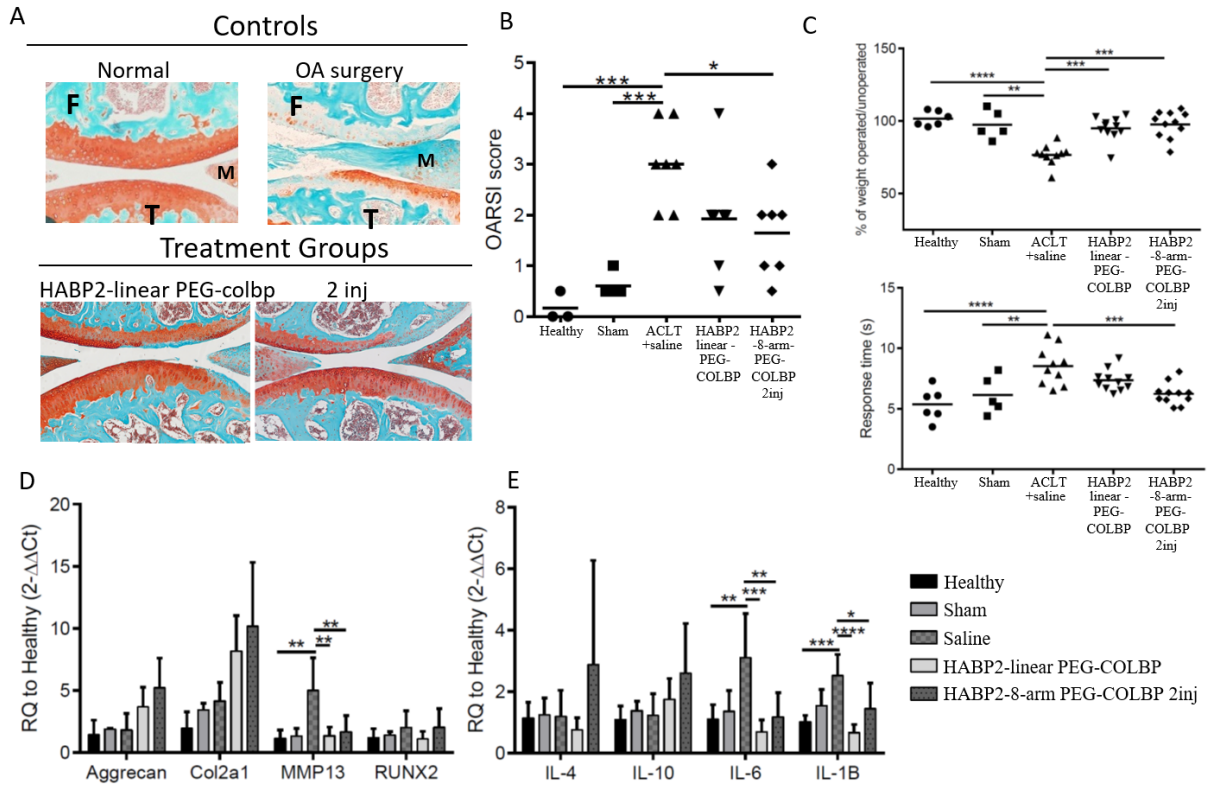
S. Figure 8. HABP2-8-arm PEG-COLBP localizes to degenerated cartilage, synovium, and subchondral bone. A. 24 hours post injection. B. Biotin only control 10 minutes and 1- hour post injection.

S. Figure 9. HABP2-8-arm PEG-COLBP reduces OA progression



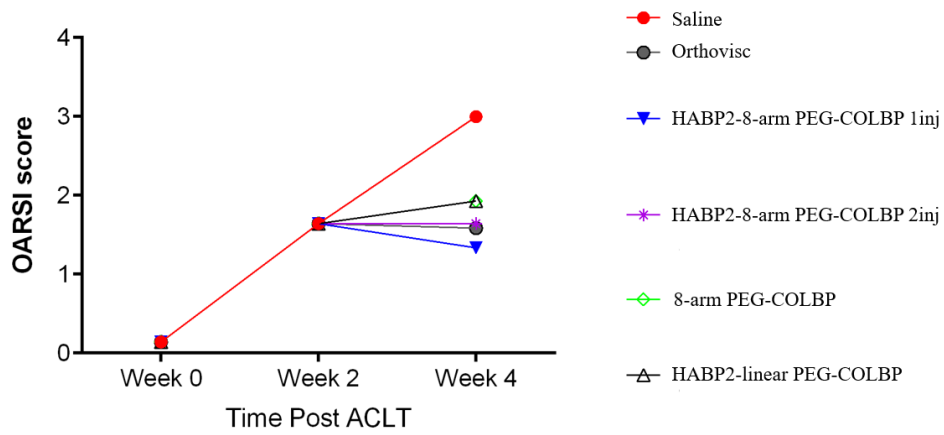
S. Figure 9. The following peptide-polymer formulations were tested for *in vivo* OA reduction: 10 and 20 mg/mL HABP1-linear PEG-COLBP, 50 mg/ml HABP2-linear PEG-COLBP, 50 mg/ml HABP3-linear PEG -COLBP, 50 mg/mL HABP1-8 arm PEG -COLBP, and 25 mg/mL of HABP2-8-arm PEG -COLBP (10 μ L each). Concentrations were based on the maximum solubility of each construct in saline. A. Representative images from the medial tibial plateau of each treatment group. Safranin-O staining (red) was used to visualize the cartilage proteoglycans. B. OARSI scoring demonstrates that HABP2-8arm peg-COLBP treatment most significantly reduces cartilage degeneration.

S. Figure 10. HABP2-8-arm PEG-COLBP reduces OA progression



S. Figure 10. All peptide-polymer formulations were injected at 25mg/ml. A-B. OARSI scores and representative images. Left: representative images from the medial tibial plateau of each treatment group. Safranin-O staining (red) was used to visualize the cartilage proteoglycans. Right: OARSI scoring demonstrates reduced cartilage degeneration in most treatment groups. C. Pain testing. D and E. Whole joint gene expression.

S. Figure 11. Polymer-peptides halts OA progression



S. Figure 11. Week zero is healthy joint OARSI score, 2-week measurements are from 2 week post ACLT joints (no treatment), 4 week scores are of saline treated vs peptide-polymer treatments.

Chapter 4: Th17 and senescent cells in osteoarthritis

Th17 and senescent cells in osteoarthritis

Heather J. Faust^{1*}, Hong Zhang^{1*}, Ada Tam², Franck Housseau², Clifton Bingham³,

Jennifer Elisseff¹

*These authors contributed equally to this work

¹Translational Tissue Engineering Center, Wilmer Eye Institute and Department of Biomedical

Engineering, Johns Hopkins University, Baltimore, MD 21287, USA.

²Sidney Kimmel Cancer Center, Johns Hopkins University, Baltimore, MD 21287, USA.

³Johns Hopkins Arthritis Center, Johns Hopkins University, Baltimore, MD 21287, USA.

Abstract

It has been suggested that IL-17 may play a role in OA because of its observed presence in human OA tissue. However, the cellular sources of IL-17 and its impact on osteoarthritis have not been investigated. In this study, in-depth cell phenotyping revealed that the cell types responsible for IL-17 secretion in OA include $\gamma\delta$ T cells, ILCs, and CD4 T cells. Local inguinal lymph nodes also had altered IL-17 levels. We then investigated the possible link between senescent cells, which are involved in OA pathogenesis, and Th17 cells along with their associated cytokines in osteoarthritis. Senescent cells were found to support Th17 polarization *in vitro* and eliminating senescent cells with IP and IA injections of senolytic in aged mice decreased IL-17 expression and reduced OA progression. Additionally, systemic senolytic treatment increased the CD4/CD8 systemic ratio in aged mice back up to young mouse levels. Anterior cruciate ligament transection (ACLT) in IL-17R $\alpha^{-/-}$ mice also resulted in reduced pain compared to C57BL6 mice, suggesting a role for IL-17 signaling in OA disease.

Introduction

Osteoarthritis (OA) is a painful degenerative disease that destroys joint tissue, with an estimated lifetime risk of about 40% in men and 47% in women (137, 179). A primary cause of OA is joint instability leading to tissue damage, most commonly through tearing the anterior cruciate ligament (180-182). OA is characterized by a progressive loss of cartilage tissue, remodeling of the underlying bone, inflammation of the synovial membrane, and abnormalities in lubrication of the articular joint. Current therapies for OA primarily target symptoms and fail to modify disease progression. Non-steroidal anti-inflammatory drugs (NSAIDs) can reduce pain but do not alter disease progression, and in fact can cause cartilage damage and chondrotoxicity when used for extended periods of time (138). While a few potential disease-modifying drugs are in clinical testing, the lack of currently available options leaves joint replacement surgery as the only therapeutic choice for treating end stage disease.

OA is a multifactorial disease that both the immune system and aging contribute to pathologically. Little is known how these two factors influence the disease progress, however senescent cells appear to accumulate with ageing and are likely a causative factor in OA development (157). Senescence is a cell status wherein the cells are in permanent cell cycle arrest. Senescence is commonly controlled by the p53 pathway and pRB pathway. The p53 mediated DNA damage response activates gene expression of p21, and the pRB pathway triggers nuclear protein p16 response (183). Cells undergoing senescence adapt multiple phenotype changes and acquire a profile termed the senescence-associated secretory phenotype (SASP). Senescent cells (SnCs) influence their resident tissue microenvironment and local immune system through their inflammatory secretome. SnCs are observed in tissue trauma sites and accumulate with

ageing (184). SnCs' complex interactions with tissue and the immune system are reported to multiple disease types. Their phenotype changes based on their activation pathways, local tissue environment, and their phenotype evolves over time (185). Senolysis selectively clears SnCs through activating apoptosis pathways. Previous research indicates senolysis could elongate life span and delay age-related disease (186, 187).

The immune system is also important in the response to tissue damage. Tissue damage initiates a cascade of local and systemic immune events that attract immune cells into the damaged tissue to initiate host defense and tissue repair. The immune system contributes to tissue repair through multiple mechanisms including scavenging debris and dead cells, recruiting and supporting proliferation of tissue progenitor cells, and inducing vascularization (188). The innate immune system is alerted to damaged tissue by the secretion of alarmins (189, 190). Damage associated molecular patterns (DAMPs) attract innate cells (mention neutrophils and monocytes) to the site of injury (190). Antigen presenting cells (APCs) including macrophages and dendritic cells then interact with and process antigen for presentation to T cells, which are part of the adaptive immune system.

These T cells then polarize into a specific subset based on the threat encountered and what cytokines are in the tissue environment. For example, IL-12 helps Th1 polarization while IL-4 promotes Th2 polarization (191). While IL-4 secreted by T_H2 T cells is pro-regenerative, Th1 T cells are pro-inflammatory. In OA, T_H1 cells are sometimes found after disease onset in the synovium (192). These T cells often contain oligoclonal T cell populations with reactivity to chondrocytes and fibroblasts (193). Despite this knowledge, there is no research on the role of T cells in OA progression. A more recently discovered T helper subset, T_H17 T cells, may also be relevant to OA

progression. T_H17 cells produce proinflammatory cytokines including IL-17 and are potential initiators for pathogenesis of fibrosis. Therapies that target IL-17 result in remarkable improvements in psoriatic arthritis, as well as in other forms of spondyloarthritis (SpA) (194-196).

There is also little known about other relevant lymphocytes such as $\gamma\delta$ T cells, despite their role in other forms of arthritis such as psoriatic arthritis. $\gamma\delta$ T cells are different from traditional $\alpha\beta$ T cells because they are activated in an MHC-independent manner and can recognize lipid antigens, contributing to their fast effector response upon stimulation. $\gamma\delta$ T cells are also an early producer of IL-17 in mouse models of inflammatory arthritis (197). IL-17 secreting $\gamma\delta$ T cells are known to play a role in inflammatory arthritis, but their role in osteoarthritis is unknown (197). Another unexplored cell type in OA includes innate lymphoid cells (ILCs), a heterogeneous population of innate cells. Although ILCs are important in host defense, their dysregulation can lead to fibrosis (198). Activated group 3 innate lymphoid cells are enriched in psoriatic arthritis synovial fluid, suggesting that this is a cell type implicated in arthritis progression (199).

Reviewing the literature, beyond the fact that T cells and macrophages are present in the synovium of patients with OA, there is a lack of knowledge of the immune state of the joint during OA disease progression (94, 192, 193). The articular cartilage is considered a tissue with no intrinsic regenerative capacity, which could be in part due to the control of the local immune response (200). Therefore, modulating the immune system within the joint may be a viable approach to improve its defective repair capacity. As senescent cells are known to sit in the joint and secrete pro-inflammatory cytokines,

eliminating senescent cells could potentially improve joint function by restoring healthy local immune cell function. Understanding the immune modulating properties of SnCs will also allow for new potential therapeutic applications for senolytics (201).

Methods

Surgical Procedures: All procedures were approved by the Johns Hopkins University Animal Care and Use Committee (ACUC). OA was induced by anterior cruciate ligament transection (ACLT) (121) in 10-week old or 72-week old male C57BL/6 mice from Charles River. Two weeks after ACLT, a single 10- μ L injection of either a phosphate-buffered saline (1X PBS, from Life Technologies) vehicle control or UBX0101 was administered to the joint space of the operated knee via a 30-gauge needle. The joint cavity was opened in the sham group but the ACL was not transected.

Histological evaluation: After 4 weeks, animals were sacrificed, and mouse knees were fixed in 4% paraformaldehyde (PFA), decalcified for approximately 2 weeks in 10% EDTA, then dehydrated and embedded in paraffin (n=3-5). Seven- μ m-thick sections were taken throughout the joint and stained for proteoglycans with Safranin-O and Fast Green (Applied biosciences) per manufacturer's instructions. Osteoarthritis Research Society International (OARSI) scores are based on blinded histological assessment the medial plateau of the tibia (122).

Immunohistochemistry: Slides were de-paraffinized and treated with hyaluronidase (0.25% in Tris buffer) before staining for IL-23 or IL-17 using Anti IL-17 antibody (ab79056) from Abcam at 1:400 dilution or Anti IL-23 antibody (ab45420) from Abcam at 1:800 dilution (each in 1% BSA/2%NGS/0.05% Tween 20) followed by secondary staining with a biotinylated antibody and streptavidin-peroxidase conjugated enzyme

using the Histostain-SP IHC kit, AEC, from ThermoFisher (cat. no. 959943), according to the manufacturer's instructions.

Immunofluorescence: Slides were de-paraffinized and antigen retrieval was performed in near boiling citrate ARB for 20 minutes on the bench. Slides were blocked in 1.5% BSA, 1.5% normal goat serum, and 0.05% tween 20 for 45 minutes prior to applying primary antibodies. IL-17 staining was performed using rabbit anti IL-17 antibody (ab79056) from Abcam at 1:400 dilution. Rat anti CD4 (eBioscience, clone 4SM95) was used at a 1:200 dilution. Secondary antibodies were applied (anti-rat AF488, anti-rabbit AF594) and followed by DAPI for 5 minutes before mounting.

Gene expression analysis: Whole mouse joints were frozen in liquid nitrogen and homogenized using a sterile mortar and pestle (n=3-4). Inguinal lymph nodes were crushed in a 1.5mL Biomasher tube from Kimble. RNA was extracted using TRIzol reagent (Life Technologies) following the manufacturer's protocol. cDNA was synthesized using Superscript III reverse transcriptase (Life Technologies) following the manufacturer's protocol. Real-time RT-PCR was carried out using SYBR Green primers and a StepOnePlus Real-time PCR System (Life Technologies). Relative gene expression was calculated by the $\Delta\Delta C_t$ method. The ΔC_t was calculated using the reference genes $\beta 2$ -microglobulin (*B2m*) and β -actin (*Bact*). $\Delta\Delta C_t$ was calculated relative to the unoperated control group. The mouse specific primers used were the following: *Bact* forward, CCA CCG TGA AAA GAT GAC CC, *Bact* reverse, GTA GAT GGG CAC AGT GTG GG, *B2m* forward, CTC GGT GAC CCT GGT CTT TC, *B2m* reverse, GGA TTT CAA TGT GAG GCG GG, *Acan* forward, CGT TGC AGA CCA GGA GCA AT, *Acan* reverse, CGG TCA TGA AAG TGG CGG TA, *Col2a1* forward, CCT CCG TCT

ACT GTC CAC TGA, *Col2a1* reverse, ATT GGA GCC CTG GAT GAG CA, *Mmp13* forward, GTC TTC ATC GCC TGG ACC ATA, *Mmp13* reverse, GGA GCC CTG ATG TTT CCC AT, *Runx2* forward, GCC GGG AAT GAT GAG AAC TA, *Runx2* reverse, GGT GAA ACT CTT GCC TCG TC, *Il4* forward, ACA GGA GAA GGG ACG CCA T, *Il4* reverse, ACC TTG GAA GCC CTA CAG A, *Il10* forward, TCT CAC CCA GGG AAT TCA AA, *Il10* reverse, AAG TGA TGC CCC AGG CA, *Il6* forward, CCA GGT AGC TAT GGT ACT CCA GAA, *Il6* reverse, GCT ACC AAA CTG GAT ATA ATC AGG A, *Il1b* forward, GTA TGG GCT GGA CTG TTT C, *Il1b* reverse, GCT GTC TGC TCA TTC ACG. *Il17* expression in lymph nodes was assessed using the following SybrGreen primer: *Il17a* forward, TCAGCGTGTCCAAACACTGAG, *Il17a* reverse, CGCCAAGGGAGTTAAAGACTT.

TaqMan primers were used for detection of IL-17A, IL-17F, and IL-23a in joint tissues.

The IDs are: IL-23a: Mm00518984_m1, IL-17a: Mm00439618_m1, IL-17f:

Mm00521423_m1, B2M: Mm00437762_m1, Bact: Mm04394036_g1

PreAmp: Pre-amplification was performed on cDNA prior to gene expression analysis using TaqMan preamp master mix (Thermo Fisher). IL-17a was preamp'd 14 cycles and IL-17f, IL-23a, GM-CSF, and PTGS2 were preamp'd 10 cycles.

Flow Cytometry: Whole joints and inguinal lymph nodes were harvested at 1 (7 days), 2 (14 days) and 4 (28 days) weeks post-surgery (n=3). Harvested joint tissue was then finely diced and digested for 45 minutes at 37°C in 1.67 Wunsch U/ml Liberase TL (Roche Diagnostics) + 0.2 mg/ml DNase I (Roche Diagnostics, Risch-Rotkreuz, Switzerland) in serum-free RPMI-1640 medium (Gibco) on a shaker at 400 rpm. Digest was filtered through a 70 µm cell strainer (Fisher) then washed twice with 1XPBS. Cells

were stained with the following Myeloid panel: Fixable Viability Dye eFluor®780 (eBioscience), CD45 BV605 (Biolegend, San Diego, CA), CD11b AF700 (Biolegend), CD11c APC (Biolegend), Ly6C PerCP-Cy5.5 (Biolegend), Ly6G Pacific Blue (Biolegend), F4/80 PE-Cy7 (BioLegend), MHCII AF488 (Biolegend), CD86 AmCyan (BioLegend), CD206 PE (BioLegend). After staining cells were fixed and analyzed on a BD LSRII Analyzer (BD Biosciences). LIVE/DEAD® Fixable Aqua Dead Cell Stain negative (live) cells were evaluated based upon percent population of T cells (CD3+), B cells (CD19+), dendritic cells (CD11c+), and macrophages (F4/80+). All analyses were performed in FlowJo Flow Cytometry Analysis Software (Treestar).

The T cell panel displayed in Figure 1 included: Fixable Viability Dye eFluor®780 (eBioscience), CD45 V500 (BD biosciences), CD3 AlexaFluor488 (BioLegend), CD4 PE-Cy7 (BioLegend), CD8 BV711 (BioLegend), NK1.1 BV605 (BioLegend), Thy1.2 Pacific Blue (BioLegend), $\gamma\delta$ TCR PE-CF594 (BD Bioscience), IL4 α PerCP-Cy5.5 (BioLegend), IFN γ APC (Biolegend), IL-17 α AF700 (Biolegend), and IL-17f PE (eBioscience). IL-4 α , IL-17 α , IL-17f, and IFN γ staining followed fixation and permeabilization with BD CytoFix/CytoPerm Kit (BD Biosciences).

Fluorescence activated cell sorting: Innate lymphoid cells were sorted from joints two weeks post ACLT (n=3). Tissue processing is the same as described above for flow cytometry. Only surface staining was performed to keep the cells alive. Fixable Viability Dye eFluor®780 (eBioscience), CD45 V500 (BD biosciences), CD3 AlexaFluor488 (BioLegend), CD4 PE-Cy7 (BioLegend), CD8 BV711 (BioLegend), and Thy1.2 Pacific Blue (BioLegend). Cells were sorted on a BDFACS Aria Fusion SORP for live, CD45+, CD3-, CD4-, CD8- and Thy1.2+ cells defined as innate lymphoid cells. **Hind Limb**

Weight Bearing Assessment: Weight-bearing in mice was measured in the un-operated control animals and compared to ACLT animals receiving PBS control or UBM therapy using an incapitance tester (Columbus Instruments). The percentage weight distributed on the ACLT limb was used as an index of joint discomfort in OA (121). The mice were positioned to stand on their hind paws in an angled box placed above the incapitance tester so that each hind paw rested on a separate force plate. The force (g) exerted by each limb was measured. Three consecutive 3-second readings were taken and averaged to obtain the mean score (123).

Hind Limb Responsiveness: Mice were placed on the hotplate at 55°C. The latency period for hind limb response (jumping or paw-lick) was recorded as response time before surgery and at 2 and 4 weeks after surgery in all animal groups (121). Three readings were taken per mouse and averaged to obtain the mean response time for each time point.

Cell culture and co-culture conditions. NIH 3T3 fibroblasts were cultured for 7 days in fibroblast culture medium. The cells were then irradiated with CIXD Biological Irradiator 10Gy and collected after 7 days. The media the senescent cells (SnCs) were cultured in was collected at the time of cell harvesting and used in the co-culture experiment as “conditioned media” The day the SnCs were harvested, CD4 naïve T cells were isolated from lymph nodes of six-week-old C57/BL6 mice. The CD4 naïve separation kit and MACS column from Miltenyi were used, following the manufacturer’s instructions. T cell purity was assessed by flow cytometry using the following panel: Fixable Viability Dye Aqua (Thermofisher), CD45 V500 (BD biosciences), CD3 AlexaFluor488 (BioLegend), CD4 PE-Cy7 (BioLegend), CD8 BV711 (BioLegend),

CD44 BV605 (BioLegend), and CD62L APC-CY7 (BioLegend). 92.9% of the CD4 T cell population was naïve. T cells and Sncs were seeded in 12 well transwell plates at 500,000 and 300,000 cells/per well, respectively. The media used was IMDM supplemented with 10% FBS, 5% Penn strep and 1% sodium pyruvate. The “Snc” group consisted of T cells+ Sncs; “Snc+IL-2” had the addition of 500 unit/mL IL-2 into the culture medium’ “Snc+IL-2+TGF- β ” also had the addition of 2ng/mL TGF- β ; “CM” consisted of conditioned medium from the Sncs+IL-2+ TGF- β . Control groups consisted of naïve T cells+IL-2 and T cells skewed to Th17 using Th17 Cell Differentiation kit from R&D System. After 3 days in culture, 50% of the media was aliquoted off and fresh media added. After 5 total days in co-culture, T cells were harvested for flow cytometry and PCR analysis (n=3). T cells were stained for Fixable Viability Dye eFluor®780 (eBioscience), CD45 V500 (BD biosciences), CD3 AlexaFluor488 (BioLegend), CD4 PE-Cy7 (BioLegend), CD8 BV711 (BioLegend), IL4 α PerCP-Cy5.5 (BioLegend), IFN γ APC (Biolegend), IL-17 α AF700 (Biolegend), and IL-17f PE (eBioscience). IL-4 α , IL-17 α , IL-17f, and IFN γ staining followed fixation and permeabilization with BD CytoFix/CytoPerm Kit (BD Biosciences).

Statistical Analysis: Statistical analysis was performed using a one-way ANOVA with Holm-Sidak multiple comparison correction in GraphPad Prism Software. For *in vivo* work, all groups were compared to each other. For *in vitro* work, each treatment was compared to the control group. $P < 0.05$ was considered significant.

Results

Immune cells and IL-17 are altered post ACLT

As there is no in-depth phenotyping of the immune cells present in the joint during OA progression, we profiled the myeloid and lymphoid cells in the joint. Of the myeloid cell populations, most F4/80⁺MHCII⁺ macrophages were M2-like, expressing CD206 but no CD86 (S. Fig. 1). There were very few CD206⁺ CD86⁺ macrophages and almost no CD206⁻ CD86⁺ macrophages. The M2-like macrophages were increased in the joint 1 and 2 weeks post ACLT (2.3 and 1.5-fold, respectively), and the CD206⁺ CD86⁺ M2-like macrophages were increased 1-week post ACLT (4.5 fold).

Among the lymphoid cells populations analyzed, most changes were observed 1 week after ACLT. CD8 T cells were increased from approximately 34% of the total CD3 T cell fraction to approximately 43% in sham joints and 50% in ACLT joints. Additionally, $\gamma\delta$ T cells were increased to 5.3% of CD3⁺ cells in ACLT joints over the CL joints (4.3%) and sham joints were increased to 5.9% over sham CL joints (4.6%). Of these $\gamma\delta$ T cells, the IL-17f⁺ fraction was increased from 7.6% in healthy joints to 37.2% in ACLT and 20.6% in sham joints. Additionally, IL-17⁺ CD4 T cells were increased from 3.2% in healthy joints to 9.4% in ACLT and 6.4% in sham joints. Immunofluorescence identified IL-17⁺ cells in the ACLT joint at 1-week post-surgery, whereas healthy joints had little to no IL-17⁺ cells (Fig. 1).

ACLT increased IL-17a gene expression in joints 1, 2, and 4wks post ACLT (4,704, 3,484, and 2,431-fold, respectively) and sham surgery increased IL-17a slowly, peaking at 2 weeks post-surgery and then declining by 4 weeks (3.6 fold at 1 week, 1,502-fold at 2 weeks, and 13.9-fold fold at 4 weeks). IL-17f and IL-23 are moderately upregulated at 1, 2, and 4wks post sham surgery (IL-17f, 2.4, 2.5, 1.8-fold respectively; IL-23, 3.7, 4.2, and 2.7-fold respectively). IL-10 is initially upregulated post sham surgery but diminishes

over time (7.5-fold at 1 week, 5.3-fold at 2 weeks, 2.1-fold at 4 weeks). GM-CSF is initially increased in sham surgery group (5-fold at 1 week) but increases over time in the ACLT group (3.6-fold at 4 weeks). PTGS2, a pro-inflammatory and pain inducing gene, is upregulated in both ACLT groups at 1, 2, and 4wks post-surgery (50, 42, and 3.8-fold) and sham groups (222, 16, 3.7-fold).

As ILCs were altered in the joint post ACLT when assessed by flow cytometry, we sorted the ILCs out of the joint and then assessed for gene expression (Fig. 1c). ILCs appear to have an altered immune profile 2-weeks post ACLT. Nanostring analysis showed changes in cytokine, chemokine, T cell activation, and peptidase activities in the ACLT group. Taqman gene expression on specific factors indicates that RANTES (Ccl5), a T cell chemoattractant, is increased in the ACLT group. Additionally, the IL-17 related cytokines IL-17f and IL-23a are increased in the ACLT group (3.4 and 2-fold, respectively). Other pro-inflammatory cytokines such as IFN γ and IL-1 β are increased as well (1.4 and 1.6-fold, respectively). ILCs are likely involved early on in OA inflammation and recruitment of other immune cells.

As many immune related genes and cytokines were altered in the ACLT joint, the local lymphoid tissue was analyzed for possible changes. Indeed, the gene expression changes observed in the joint are followed by changes in the inguinal lymph nodes. ACLT increased IL-17a gene expression in inguinal lymph nodes 2 and 4wks post ACLT (8.65, 2.75-fold, respectively). IL-17f is initially decreased at 1wk post-surgery in both sham (0.1 fold) and ACLT groups (0.4 fold) but increases over time in the ACLT group (2.2 fold at 4wks post ACLT). IL-23a is also initially downregulated in sham (0.17 fold) and ACLT (0.47 fold) but returns to healthy levels at 2wks (S. Fig. 2). Additionally, IL-17a⁺

T cells are increased in the inguinal lymph nodes 4 weeks post ACLT (S. Fig. 3a) and IL-17a⁺ ILCS are also increased in the ACLT joint 4 weeks post ACLT (S. Fig. 3b).

Clearance of SnCs reduces Th17 related cytokines

SnCs accumulate in joints with trauma and ageing (157). In aged mice, more severe OA-related symptoms develop after ACLT including more severe cartilage erosion and worse pain than in young animals (Fig. 2b, c). SnCs were shown to accumulate with ageing and associate with OA disease development (157). To test how young and aged animals respond differently to trauma, we performed ACLT surgeries on both young (10 week) and aged (72 week) animals. In addition to local intra-articular (IA) injection of senolytic treatments, we added systemic intra-peritoneal (IP) treatments of senolytic to systemically clear SnCs accumulated in aged animals (Fig. 2a). The clearance of SnCs in the joints was confirmed with reduction of the senescent cell marker *Cdkn2a* gene expression (Fig. 2b). Aged animals with combined IA and IP senolytic treatment showed significant decrease in cartilage erosion and pain (Fig. 2b, c). No significant improvement was observed with local only treatment (Fig. 2b, c, d). The OA-related disease outcomes of pain and cartilage erosion were reduced with systemic and local senolytic treatment (Fig. 2c, d). Loss of proteoglycan and cartilage thinning were attenuated in ACLT mice treated with combined senolytics (Fig. 2d).

Whether attenuation of OA-related symptoms by senolysis could be related to local immune cell changes was studied. To study the local joint immune response, gene expression analysis on the signature cytokines of T helper cells was performed. *IL17f*, one of the signature cytokines secreted by Th17, is increased with ACLT, but combined IA and IP senolytic treatment in aged mice decreases *IL-17f* gene expression compared to

vehicle treated joints (Fig. 2e). IA and IP treatment individually reduced the average IL-17f gene expression; however, this was not significant (Fig. 2e).

To confirm that the reduced gene expression of IL-17f in aged mice treated with senolytic is solely induced by the clearance of SnCs, the p16-3MR transgenic mouse strain was utilized, which enables selective killing of p16 positive SnCs by ganciclovir (GCV) through the HSV-TK cassette. In the vehicle group, the mRNA expression of *IL17f* is increased by 30-fold, and treatment with GCV reduces *IL17f* back to healthy levels (Fig. 2f).

Local and systemic immune response correlate with the local joints immune changes

To investigate the impact of ACLT on local lymphoid tissue, IL17 expression was evaluated in the inguinal lymph nodes. The number of IL17a⁺ cells was elevated after induction of OA in mouse joints (1.5 fold over the sham group) and all senolytic treatments reduced the average number of IL-17a⁺ cells, however these changes were not significant (IA+IP similar to sham group, IA half of sham group, IP similar to sham group). The relative gene expression of *IL17a* in the inguinal lymph node treatment groups correlated with the number of IL-17a⁺ cells. The percentage of IL4⁺ CD4T cells (displayed as a percentage of CD45⁺ cells) is decreased in the vehicle group relative to sham group by two-fold and increased with combined local and systemic senolytic treatment (Fig. 3d). The gene expression of *IL4* was increased with systemic and combined treatments by 15-fold compared to vehicle group (Fig. 3e). To evaluate the systemic changes occurring with induction of OA, T cell populations were evaluated in the blood. The frequency of IL17a⁺ CD4 T cells in the blood was elevated with OA by 1.5-fold and reduced with senolytic treatments (not significant) (Fig. 3f). Treatment with

systemic senolytic also increased the CD4/CD8 T cell ratio in the blood to from ~0.6 in the vehicle group to ~1 (Fig. 3g), which falls in the normal 1-2 range of healthy young blood CD4/CD8 ratio.

IL17 expression correlates with senescent cells development

Gene expression analysis was performed on aged joints and inguinal lymph nodes to track senescence associated marker expression of *Cdkn2a* and *Cdkn1a* (Fig. 4a-b). The mRNA level of T cell associated cytokines IL-17a, IL-4, and IFN γ are evaluated in inguinal lymph nodes. IL-17a expression in the inguinal lymph node was found to have a similar trend in expression to *Cdkn2a* and *Cdkn1a* in the joint (Fig.4 a-b). IL-4 had the opposite gene expression profile, while IFN γ increased in ACLT mice gradually over time. Given the apparent correlation between IL-17a and senescent markers, we decided to evaluate if removal of IL17 signaling would attenuate OA development. IL17RAKO mice were used to evaluate this hypothesis. After ACLT, IL17RAKO mice exhibited less pain after four weeks compared to C57BL6 mice and had similar pain levels to the no surgery group (Fig. 4c). Four weeks post-surgery, IL17RAKO mice had less SnC burden compared to wild type, as indicated by 4-fold decrease of *Cdkn2a* expression in the joints (Fig. 4d).

Senescent cells induce Th17 polarization

Senescent cells are known to secrete the pro-inflammatory cytokines IL-6 and IL-1 β , which are cytokines needed for Th17 polarization. To test the theory that senescent cells could polarize T cells to Th17, we co-cultured naïve T cells (5A) with senescent fibroblasts. After five days of culture, the senescent cells induced Th1 and Th17 polarization. However, addition of TGF- β blocked Th1 polarization and enhanced Th17

polarization (Fig. 5B and C). The conditioned media with TGF- β did not enhance Th17 polarization, indicating that senescent cells and TGF- β are needed for strong Th17 phenotype (Fig. 5B). TGF- β is already present in healthy joint synovial fluid, and is increased in OA, suggesting that senescent cells in the joint are more likely to influence T cells to polarize to Th17 over Th1 (202). Th2 T cells also appeared to be downregulated by SnC compared to both naïve and the Th17 control group, however this trend was not significant (Fig. 5C).

Discussion

The role of senescent cells in OA progression has only recently been discovered (157). The role of the immune system, particularly the adaptive immune system, in OA is a relatively uncharted territory. Additionally, no studies to date have shown a relationship between the disease contributing SnCs and T cell polarization, despite the pro-inflammatory cytokines SnCs emit. Determining the relationship between senescence and immune polarization will help inform future OA therapeutic treatment, especially in aging vs trauma induced OA populations, wherein the SnC populations and immune cell balance appear to be physiologically different.

Given the relatively small amount of research on immune cells in OA, we first performed extensive myeloid and lymphoid profiling to identify immune changes in our anterior cruciate ligament transection (ACLT) model of post traumatic OA. This revealed changes in M2-like macrophages, ILCs, $\gamma\delta$ T cells, CD8 T cells, and alterations in the major Th17 cytokines IL-17f and IL-17a. Th17 cells were also altered in the draining inguinal LNs. There were multiple sources of IL-17 identified (T cells, $\gamma\delta$ T cells, ILCs). IL-17 production can be elicited without prior antigen exposure, suggesting that the

development of Th17 cells can occur in non-autoimmune settings like OA. Additionally, whereas naïve $\alpha\beta$ T cells take 5-7 days to develop effector function after antigen priming, $\gamma\delta$ T cells can make IL-17 within 12 hours after stimulation (203, 204). This suggests that IL-17 secreting $\gamma\delta$ T cells could function as a link between innate and adaptive immunity due to their fast cytokine generation time and ability to attract other immune cells. This data provides additional therapeutic targets to the field of OA research.

After identifying IL-17 as a promising therapeutic target, the possible ability of senolytics to modulate IL-17 levels in the joint and draining inguinal LNs, as well as the systemic CD4/CD8 T cell status in the blood, were studied. To test the ability of senolytic to modulate IL-17, a combination of both or either systemic intra-peritoneal and local intra-articular injection of senolytic were administered to young and aged mice. We hypothesized that aged mice might be less responsive to local senolytic treatment due to overall poorer regeneration of aged mice, requiring systemic senolytic treatment to help restore regenerative function (169-171). Aged mice were an important component of this study not only because the estimated incidence of symptomatic knee OA diagnosis is highest among adults age 55-64 (168), but because aged related SnC are likely different from trauma induced SnC.

The ability of combined local and systemic senolytic to reduce IL-17 gene expression and increase IL-4 immunofluorescence signal in aged mice over that of local or systemic treatment alone is very intriguing. The fact that the local lymphoid tissue also has similar trends suggests that the systemic senolytic treatment is supporting the local joint regeneration and immune cell changes. One possible reason the systemic senolytic

treatment has an impact on tissue regeneration may be related to its ability to shift the systemic CD4/CD8 T cell ratio in favor of CD4 T cells. In aged human OA peripheral blood, CD4 T cells are lower than in aged matched controls, and in synovial tissue, there is a shift towards increased CD8 T cells (205). The aged and OA associated skewing of the T cell repertoire to CD8 could possibly result in or reflects a decreased healthy immune response, as CD8 T cells are primarily cytotoxic compared to CD4 T cells, which help generate specific immune responses.

The above observation of modulation of T cell polarization with senolytic treatment *in vivo* was also observed *in vitro*, supporting the idea that SnC influence T cell polarization. Additionally, it is known that inhibition of TGF- β signaling in mesenchymal stem cells of subchondral bone attenuates osteoarthritis. This could reflect a change in T cell polarization from Th17 to Th1 due to loss of the TGF- β signal (as is implied by our *in vitro* results).

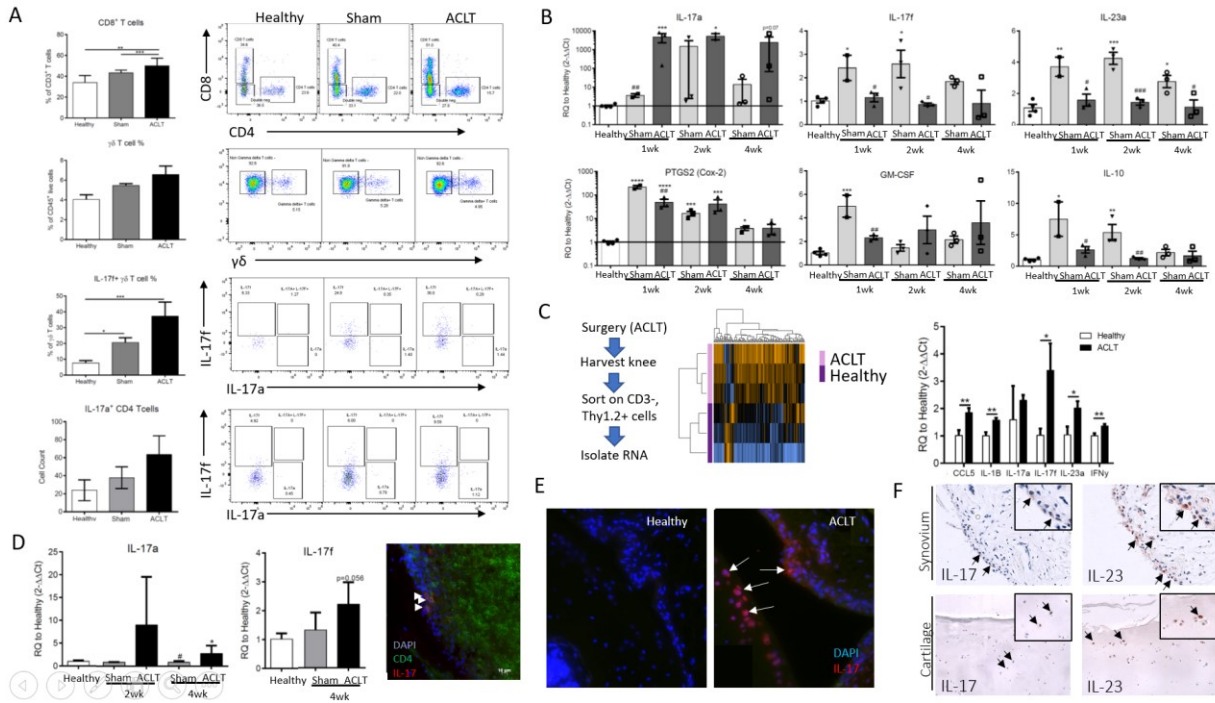
Conclusion

Our study results demonstrate that Th17 signatures are altered in the mouse post-traumatic model of OA and that senolytic treatment can reduce Th17. A direct connection between senescent cells and Th17 polarization was demonstrated in this study. Future studies should examine IL-17 neutralization to determine if direct inhibition of this cytokine reduces OA progression.

Figures

Chapter 4 Figures

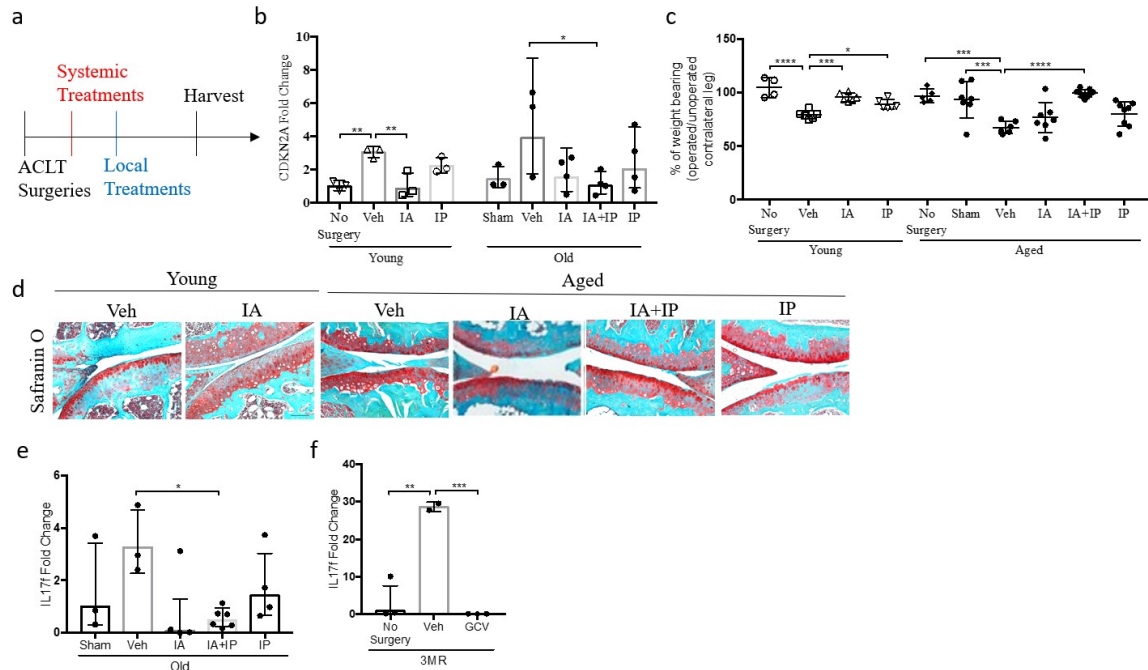
Figure 1. IL-17 is altered post ACLT



A. Flow cytometry revealed early lymphoid changes in the joint 1-week post ACLT. B. Whole joint gene expression. IL-17a gene expression is increased in joints 1, 2, and 4wks post ACLT, and increases in sham joints up until 2 weeks post-surgery and then diminishes. IL-17f and IL-23 are moderately upregulated at 1, 2, and 4wks post sham surgery. IL-10 is initially upregulated post sham surgery but diminishes over time. C. Nanosttring revealed altered gene expression of sorted ILCs from ACLT joints 2wks post ACLT, particularly in IL-17 related cytokines. D. Inguinal lymph node gene expression. IL-17a is increased two and four weeks post ACLT. IL-17f increases over time. Right: immunofluorescence of inguinal lymph node two weeks post ACLT. Th17 cells are observed in the subcapsular sinus. E. Immunofluorescence of a healthy joint (left) and

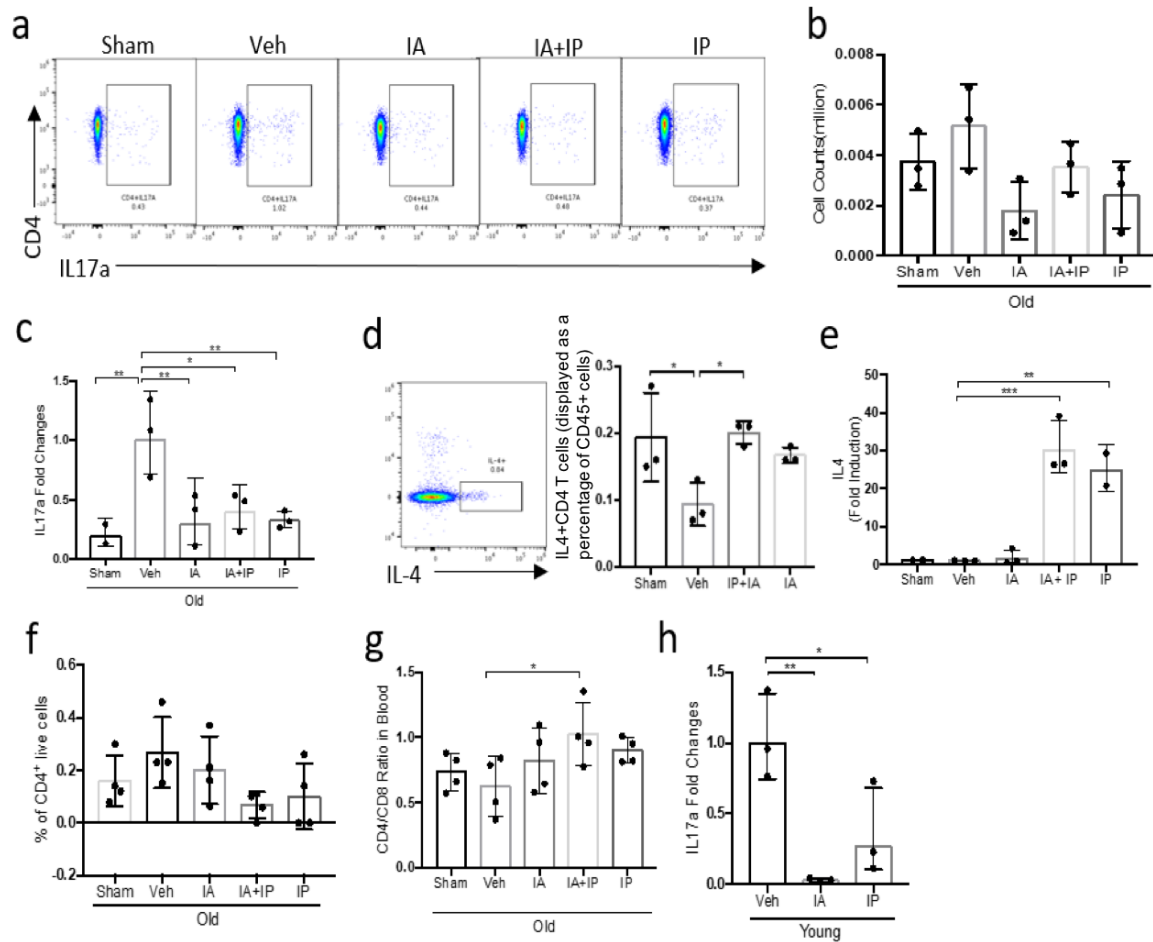
one-week post ACLT joint (right). ACLT joints exhibit IL-17 staining in the synovium and cartilage. F. Immunohistochemistry of human OA synovium and cartilage. Both tissues exhibit IL-17 and IL-23 staining.

Figure 2. Clearance of SnCs attenuates the development of OA and reduces the Th17 related expressions in joints.



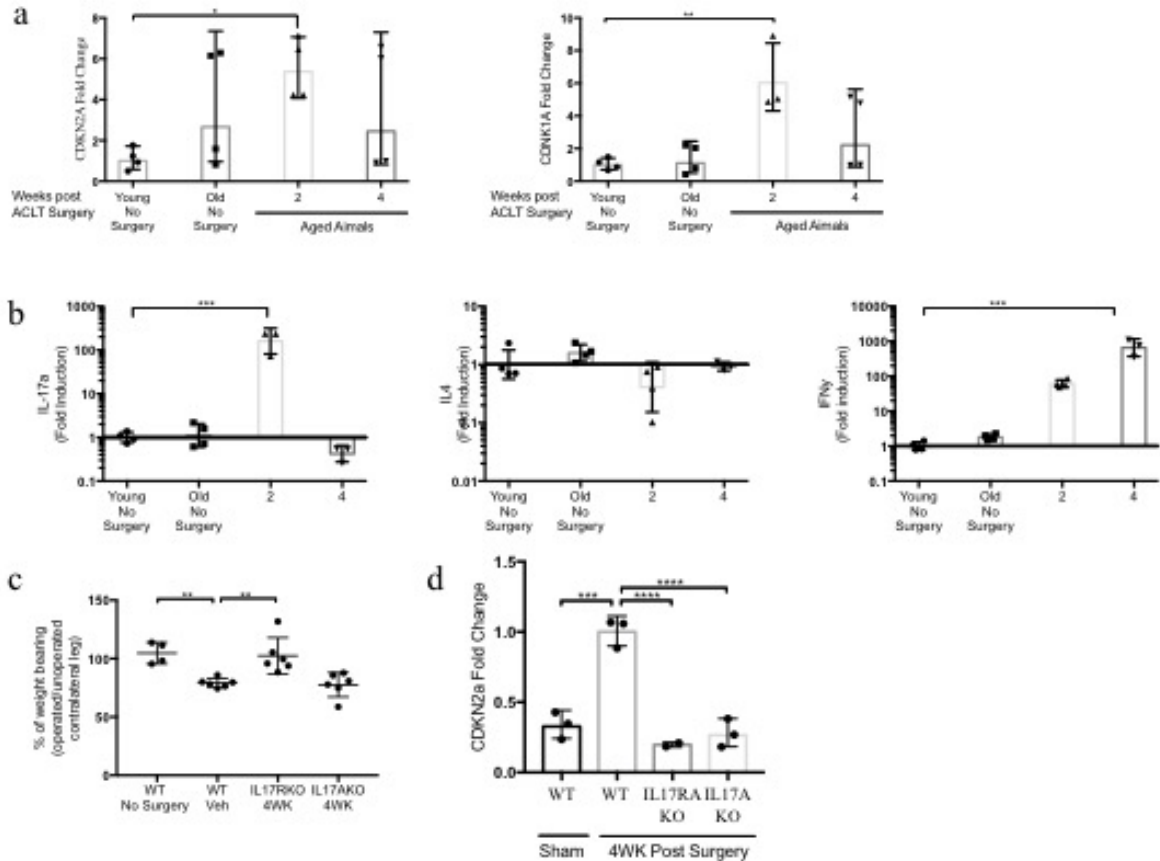
(a) Schematic of the time course for the experiment in b-f. Male C57BL6 mice undergoing ACLT were systemically or locally treated with vehicle (Veh), Nutlin, or ABT263. (b) Quantification of gene expression for *Cdkn2a* in articular joints on day 28 after surgery. (c) The percentage of weight placed on the operated limb versus the contralateral control. (d) Representative images of Safranin O and fast green staining. (e) Quantification of gene expression for *IL17f* in articular joints on day 28 after surgery. (f) Quantification of gene expression for *IL17f* in p16-3MR mice (10 week) articular joints treated on day 28 after surgery.

Figure 3. Local and systemic immune response correlate with the local joints immune changes in aged and young mice



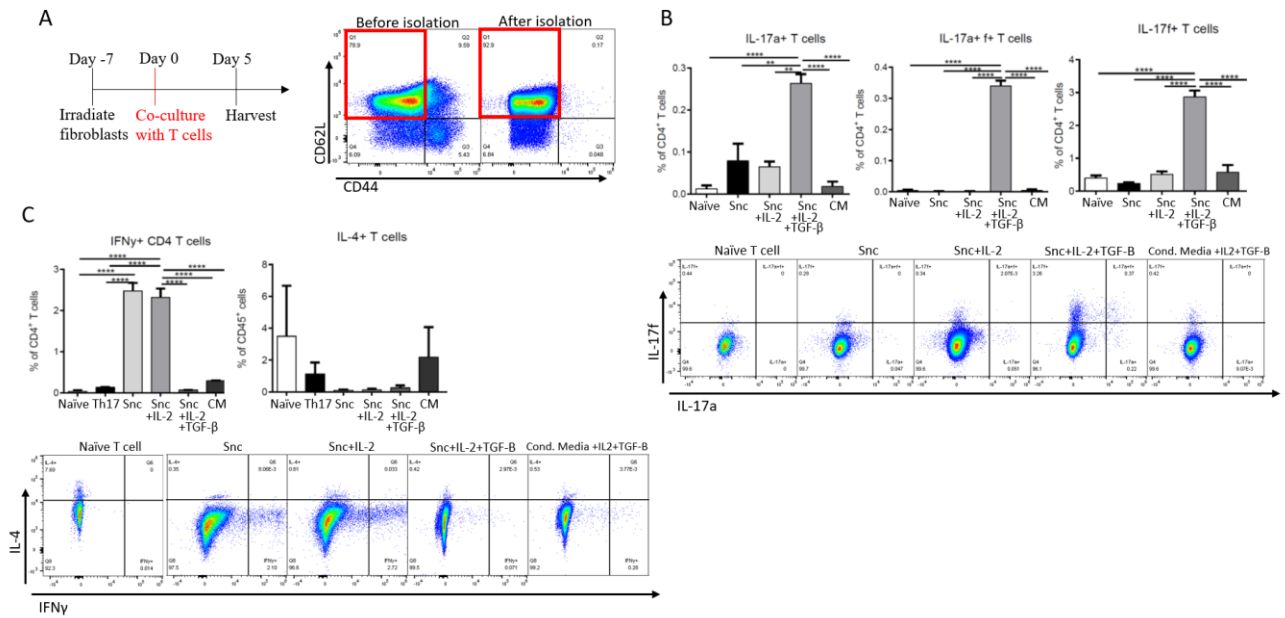
Panels a-g are data from aged mice, panel h is from young mice. (a) Frequency of IL17a⁺ cells in inguinal lymph nodes. Representative data of each group is shown. (b) Cell Number of IL17a⁺ cells in inguinal lymph nodes. (c) Quantification of *IL17a* gene expression in inguinal lymph nodes. (d) Frequency of IL4⁺ cells in inguinal lymph nodes. (e) Quantification of *IL4* gene expression in inguinal lymph nodes. (f) Frequency of IL17a⁺ cells in peripheral blood. (g) CD4/CD8 ratio in peripheral blood. (h) Quantification of *IL17a* gene expression in young animals' inguinal lymph nodes.

Figure 4. IL17 expression parallels senescent cells development, and IL17RAKO mice attenuates the development of pain



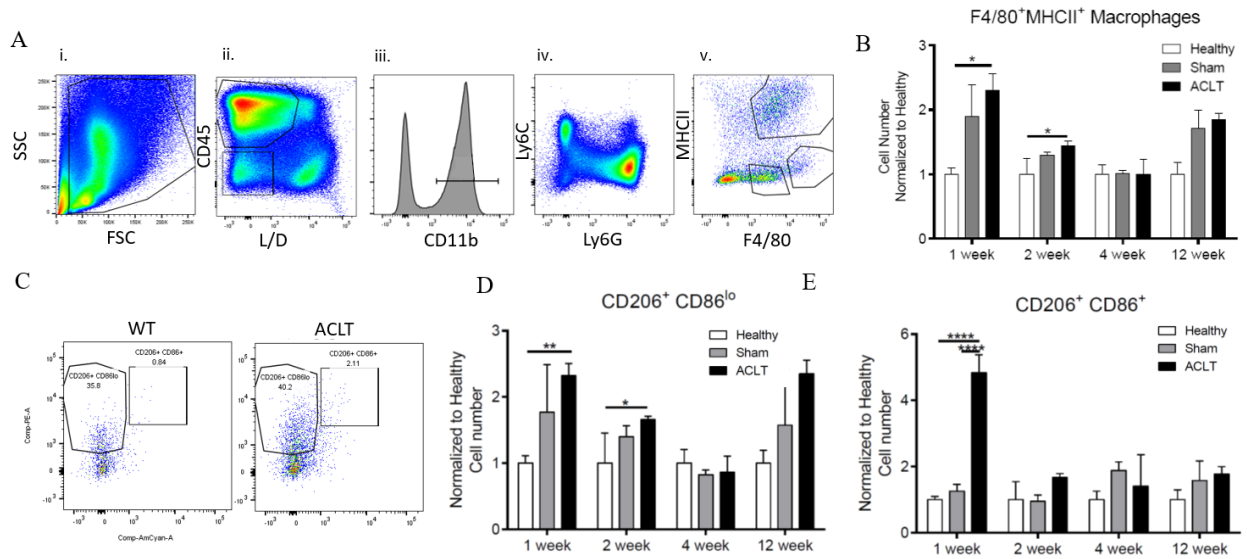
(a) Quantification of *Cdkn2a* and *Cdkn1a* gene expressions in joints of young animals (no surgery) and aged animals (no surgery, 2 week and 4-week post-surgery). (b) Quantification of *IL17a*, *IL4*, and *IFN γ* gene expressions in inguinal lymph nodes of young animals (no surgery) and aged animals (no surgery, 2 week and 4-week post-surgery). (c) The percentage of weight placed on the operated limb versus the contralateral control. (d) Quantification of *Cdkn2a* in articular joints of IL17RAKO, IL17AKO, C57 surgery and sham animals.

Figure 5. Senescent cells induce Th17 polarization



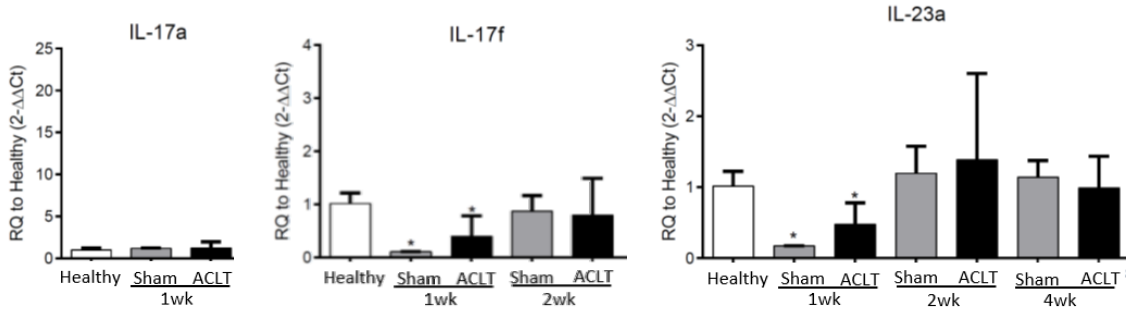
T cell subsets as analyzed by flow cytometry. A. Outline of experiment. Flow plot demonstrates the increased purity of naïve CD4 T cells after isolation. B-C flow cytometry characterizing T cell populations 5 days after co-culture with SnC. Naïve= T cells+IL-2. Other conditions note what was added to the naïve T cells. CM=SnC conditioned media+IL-2+TGF- β . B. Representative flow plot showing IL-17a and IL-17f intracellular cytokine staining. C. Representative flow plot showing IFN γ and IL-4 intracellular cytokine staining.

S. Figure 1. ACLT induces macrophage infiltration



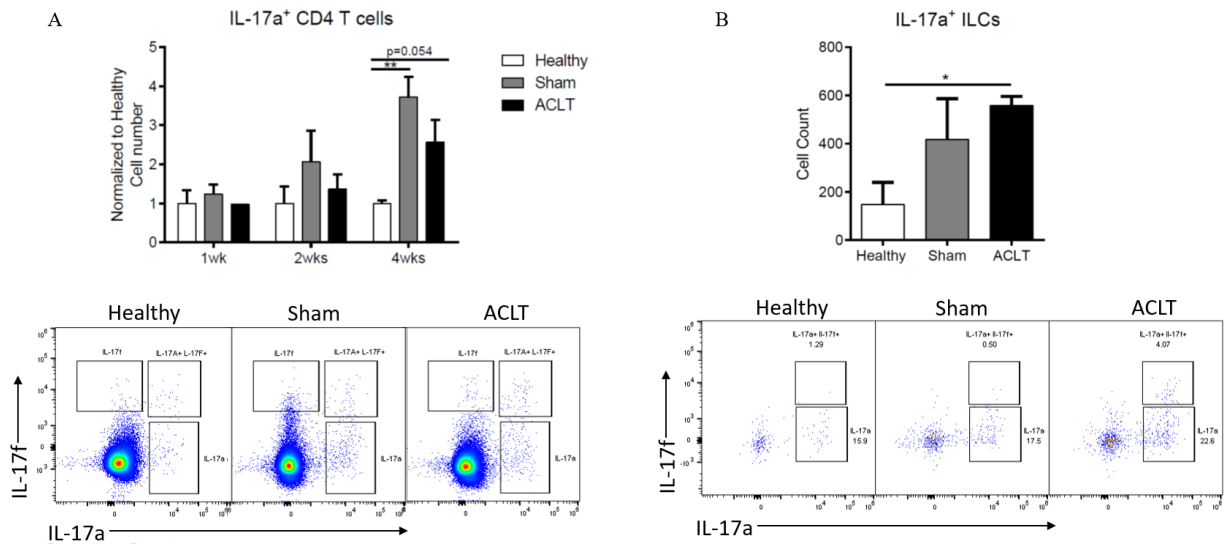
To characterize myeloid cells in whole knee joint post ACLT and sham surgery, joints were processed for flow cytometry analysis and stained with myeloid markers A. Immunophenotyping of macrophages. B. Quantification of the number of F4/80⁺ macrophages in the post-surgery. C. Further immunophenotyping was carried out on the M2 marker CD206 and M1 marker CD86. D. Quantification of the number of CD206⁺ CD86^{LO} macrophages in the knee joint. E. Quantification of the number of CD206⁺ CD86⁺ macrophages in the knee joint.

S.Fig. 2. Inguinal lymph node gene expression



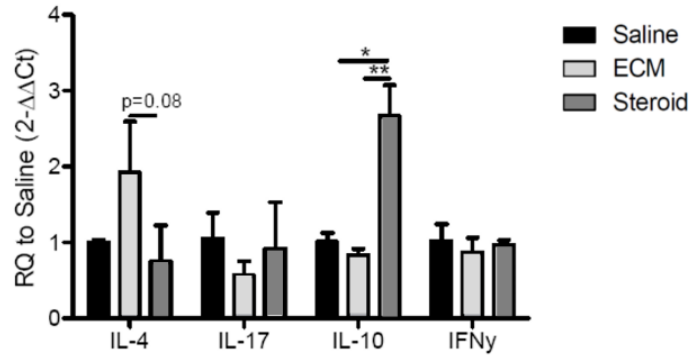
Inguinal lymph node gene expression post ACLT and sham surgery over time.

S. Fig. 3. ACLT alters the local lymphoid tissues



Flow cytometry analysis on the inguinal lymph nodes post-surgery. A. IL-17a⁺ T cells are increased in the inguinal lymph nodes 4 weeks post ACLT. B. IL-17a⁺ ILCs are also increased in the ACLT joint 4 weeks post ACLT.

S. Fig. 4. Therapeutic intervention results in modulation of gene expression in the Inguinal LNs



Gene expression analysis on inguinal lymph nodes harvested 3 days post therapeutic injection.

Steroid treatment increases IL-10 expression.

Chapter 5: Conclusions and Future directions

In the enclosed research, biomaterials such as ECM and hyaluronic acid binding peptide-polymer were implemented to reduce OA progression in a mouse model of post traumatic OA. Our results indicate that urinary bladder matrix (UBM) is a promising biomaterial for OA that should be tested in a larger animal model before clinical testing. As this material is already clinically approved for muscle wound regeneration and healing chronic wounds, it could easily be translated in OA treatment. Additionally, another ECM, AmnioFix® Injectable, a Human Amnion/Chorion Membrane ECM, has been given a designation for use in the treatment of Osteoarthritis (OA) of the knee. This ECM could serve as an example for other ECMs such as UBM to be given designations for OA.

Our results also indicate that hyaluronic acid binding peptide-polymer merits testing in a larger animal model for disease modifying activity alone and with hyaluronic acid supplementation. Hyaluronic acid binding peptide-polymer can potentially replace cross-linked HA injections, which sometimes cause severe inflammatory reactions.

Additionally, the use of hyaluronic acid binding peptide-polymer as a delivery vehicle for other OA disease modifying drugs should be pursued, particularly for drugs that need to localize to the cartilage surface to be efficacious.

During these biomaterials driven studies, aged mice were found to be an improved predictor of therapeutic efficacy over young mice based on therapeutic outcomes tracking more closely with patient outcomes- in the case of Orthovisc®. This work implementing biomaterials led to the deeper dissection of the immune system in OA progression in the hope to identify new adaptive and innate immune cells involved in the disease. This revealed changes in M2-like macrophages, ILCs, $\gamma\delta$ T cells, CD8 T cells, and alterations

in the major Th17 cytokines IL-17f and IL-17a. Th17 cells were also altered in the draining inguinal LNs. There were multiple sources of IL-17 identified (T cells, $\gamma\delta$ T cells, ILCs).

Although we identified IL-17 as a potential player in OA progression, the effect of neutralizing IL-17a and f on OA progression still needs to be performed to assess whether alteration of this cytokine directly impacts disease progression. Additionally, increasing IL-17, either by systemic IP or local IA injection, should be performed in conjunction with ACLT to determine whether IL-17 alone worsens OA disease progression. These experiments will help definitively determine the role of IL-17 in OA progression, which is heavily suggested by the experiments performed as described in chapter 4.

The work in chapter 4 describes global joint immune cell changes including from the subchondral bone, synovium, cartilage and ligaments. All these tissues are involved in OA progression and are known to provide pro-inflammatory signals that aid in OA progression. We located many IL-17⁺ cells among the synovium, inguinal LNs, and sometimes chondrocytes, however the contribution of each of these tissues to OA progression in the context of immune signaling needs to be further dissected. Currently the synovium is thought to control and contribute most of the immune cells and cytokines found in the joint. However, the bone marrow should be considered as a major player as it is the site of B cell production and maturation. Additionally, precursors for T cells, monocytes, and neutrophils are made in the bone marrow (206). The bone marrow is also home to many of these immune cells, including acting as a reservoir for mature, antigen experienced CD4 and CD8 T cells (207). The subchondral bone marrow could act as a reservoir for these cells to migrate in and out of the vascular channels of the bone and

contribute to arthritis progression. Chondrocytes are also often ignored when discussing the immune interface in the joint. However, chondrocytes express many immune related receptors on their surface such as TLR2/4, which may allow them to be more responsive and reactive to cytokine signaling than is currently known. This also brings up the question of whether cartilage is immune privileged. Studies on cartilage immune privilege have been inconclusive. It may simply be the case that the dense cartilage ECM prevents immune cells from interacting with chondrocytes, leading to the appearance of immune privilege in some cases (208-212). However, the cell signaling that chondrocytes participate in suggests that chondrocytes are more diverse than is acknowledged and may actively participate in immune signaling.

In summary, we have optimized and validated the disease modifying biomaterial hyaluronic acid binding peptide-polymer in the post traumatic mouse model of OA as well as defined new immune cell targets for future testing in OA therapy. Future work will include identification of immunomodulatory reagents that will positively modulate these altered cell populations for improvement of OA disease pathogenesis.

References

1. J. S. Temenoff, A. G. Mikos, *Biomaterials* **21**, 431 (Mar, 2000).
2. M. Benjamin, J. R. Ralphs, *Int Rev Cytol* **233**, 1 (2004).
3. W. E. Prentice. (McGraw-Hill Global Education Holdings, LLC., 2014).
4. G. J. van Osch *et al.*, *J Cell Mol Med* **13**, 792 (May, 2009).
5. H. A. Wieland, M. Michaelis, B. J. Kirschbaum, K. A. Rudolphi, *Nat Rev Drug Discov* **4**, 331 (Apr, 2005).
6. P. Sarzi-Puttini *et al.*, *Semin Arthritis Rheum* **35**, 1 (Aug, 2005).
7. C. F. Dillon, E. K. Rasch, Q. Gu, R. Hirsch, *J Rheumatol* **33**, 2271 (Nov, 2006).
8. F. Xie *et al.*, *J Rheumatol* **34**, 165 (Jan, 2007).
9. B. D. Furman, S. A. Olson, F. Guilak, *J Orthop Trauma* **20**, 719 (Nov-Dec, 2006).
10. J. Sokolove, C. M. Lepus, *Ther Adv Musculoskelet Dis* **5**, 77 (Apr, 2013).
11. K. Mithoefer *et al.*, *J Bone Joint Surg Am* **88 Suppl 1 Pt 2**, 294 (Sep, 2006).
12. E. A. Makris, A. H. Gomoll, K. N. Malizos, J. C. Hu, K. A. Athanasiou, *Nat Rev Rheumatol* **11**, 21 (Jan, 2015).
13. L. Hangody *et al.*, *Orthopedics* **21**, 751 (Jul, 1998).
14. L. Hangody, P. Feczko, L. Bartha, G. Bodo, G. Kish, *Clin Orthop Relat Res*, S328 (Oct, 2001).
15. R. Gudas *et al.*, *Am J Sports Med* **40**, 2499 (Nov, 2012).
16. M. Brittberg, *Injury* **39 Suppl 1**, S40 (Apr, 2008).
17. M. Brittberg *et al.*, *N Engl J Med* **331**, 889 (Oct 6, 1994).
18. D. J. Mooney, A. G. Mikos, *Sci Am* **280**, 60 (Apr, 1999).
19. B. Sharma, J. H. Elisseeff, *Ann Biomed Eng* **32**, 148 (Jan, 2004).
20. Y. Peng *et al.*, *J Autoimmun* **29**, 303 (Dec, 2007).
21. J. S. Otis *et al.*, *PLoS One* **9**, e92363 (2014).
22. S. Frantz, K. A. Vincent, O. Feron, R. A. Kelly, *Circ Res* **96**, 15 (Jan 07, 2005).
23. S. F. Badylak, J. E. Valentin, A. K. Ravindra, G. P. McCabe, A. M. Stewart-Akers, *Tissue Eng Part A* **14**, 1835 (Nov, 2008).
24. K. Sadtler *et al.*, *Science* **352**, 366 (Apr 15, 2016).
25. F. J. Blanco, C. Ruiz-Romero, *Ann Rheum Dis* **72**, 631 (May, 2013).
26. A. Singh *et al.*, *Nat Mater* **13**, 988 (Oct, 2014).
27. K. Sadtler, *Nature Reviews*, (2016).
28. X. Banquy, J. Burdynska, D. W. Lee, K. Matyjaszewski, J. Israelachvili, *J Am Chem Soc* **136**, 6199 (Apr 30, 2014).
29. Q. Zhao, *Journal of Cellular Immunotherapy* (2016).
30. C. C. Wyles, M. T. Houdek, A. Behfar, R. J. Sierra, *Stem Cells Cloning* **8**, 117 (2015).
31. J. M. Lamo-Espinosa *et al.*, *J Transl Med* **14**, 246 (Aug 26, 2016).
32. D. Eyre, *Arthritis Res* **4**, 30 (2002).
33. D. R. Eyre, M. A. Weis, J. J. Wu, *Eur Cell Mater* **12**, 57 (2006).
34. J. S. Pieper *et al.*, *Biomaterials* **23**, 3183 (Aug, 2002).
35. S. R. Frenkel, P. E. Di Cesare, *Ann Biomed Eng* **32**, 26 (Jan, 2004).
36. A. Yokoyama *et al.*, *Cell Tissue Res* **322**, 289 (Nov, 2005).
37. M. Akmal *et al.*, *J Bone Joint Surg Br* **87**, 1143 (Aug, 2005).
38. A. C. Petrey, C. A. de la Motte, *Front Immunol* **5**, 101 (2014).
39. M. Litwiniuk, A. Krejner, M. S. Speyrer, A. R. Gauto, T. Grzela, *Wounds* **28**, 78 (Mar, 2016).
40. S. L. Collins *et al.*, *Am J Respir Cell Mol Biol* **45**, 675 (Oct, 2011).

41. Y. Gao *et al.*, *Biomed Res Int* **2014**, 648459 (2014).
42. J. Rosen, *Clinical Medicine Insights: Arthritis and Musculoskeletal Disorders*, (2016).
43. G. N. Homminga, S. K. Bulstra, R. Kuijjer, A. J. van der Linden, *Acta Orthop Scand* **62**, 415 (Oct, 1991).
44. K. E. Benders *et al.*, *Trends Biotechnol* **31**, 169 (Mar, 2013).
45. B. C. Toolan, S. R. Frenkel, D. S. Pereira, H. Alexander, *J Biomed Mater Res* **41**, 244 (Aug, 1998).
46. B. Hawkins, *Wounds* **28**, 152 (May, 2016).
47. N. J. Willett *et al.*, *Arthritis Res Ther* **16**, R47 (2014).
48. M. Pei, J. T. Li, M. Shoukry, Y. Zhang, *Eur Cell Mater* **22**, 333 (Nov 24, 2011).
49. J. A. Hubbell, *Curr Opin Biotechnol* **14**, 551 (Oct, 2003).
50. J. L. Drury, D. J. Mooney, *Biomaterials* **24**, 4337 (Nov, 2003).
51. G. F. Muschler, C. Nakamoto, L. G. Griffith, *J Bone Joint Surg Am* **86-A**, 1541 (Jul, 2004).
52. L. Lu, X. Zhu, R. G. Valenzuela, B. L. Currier, M. J. Yaszemski, *Clin Orthop Relat Res*, S251 (Oct, 2001).
53. H. Liu, E. B. Slamovich, T. J. Webster, *Int J Nanomedicine* **1**, 541 (2006).
54. J. A. Martin, J. A. Buckwalter, *J Bone Joint Surg Am* **85-A Suppl 2**, 106 (2003).
55. W. S. Toh *et al.*, *Acta Orthop*, 1 (Sep 23, 2016).
56. B. Mollon, R. Kandel, J. Chahal, J. Theodoropoulos, *Osteoarthritis Cartilage* **21**, 1824 (Dec, 2013).
57. P. M. van der Kraan, *Biomed Mater Eng* **24**, 75 (2014).
58. J. Martel-Pelletier, L. M. Wildi, J. P. Pelletier, *Bone* **51**, 297 (Aug, 2012).
59. E. N. Blaney Davidson, P. M. van der Kraan, W. B. van den Berg, *Osteoarthritis Cartilage* **15**, 597 (Jun, 2007).
60. J. Martel-Pelletier, *Joint Diseases and Related surgery* **21**, 2 (2010).
61. D. P. Bottaro, A. Liebmann-Vinson, M. A. Heidarani, *Ann N Y Acad Sci* **961**, 143 (Jun, 2002).
62. A. B. Laudy, E. W. Bakker, M. Rekers, M. H. Moen, *Br J Sports Med* **49**, 657 (May, 2015).
63. Y. Zhu *et al.*, *Osteoarthritis Cartilage* **21**, 1627 (Nov, 2013).
64. A. Marmotti *et al.*, *Biomed Res Int* **2015**, 542502 (2015).
65. X. Xie, C. Zhang, R. S. Tuan, *Arthritis Res Ther* **16**, 204 (Feb 25, 2014).
66. H. Fang, F. Beier, *Nat Rev Rheumatol* **10**, 413 (Jul, 2014).
67. A. M. Malfait, C. B. Little, *Arthritis Res Ther* **17**, 225 (Sep 14, 2015).
68. E. Kon, A. Roffi, G. Filardo, G. Tesei, M. Marcacci, *Arthroscopy* **31**, 767 (Apr, 2015).
69. M. Marcacci *et al.*, *Knee Surg Sports Traumatol Arthrosc* **10**, 154 (May, 2002).
70. D. H. Sohn *et al.*, *Clin Orthop Relat Res*, 254 (Jan, 2002).
71. O. Haddo *et al.*, *Knee* **11**, 51 (Feb, 2004).
72. P. D. Benya, J. D. Shaffer, *Cell* **30**, 215 (Aug, 1982).
73. T. Kimura, N. Yasui, S. Ohsawa, K. Ono, *Clin Orthop Relat Res*, 231 (Jun, 1984).
74. D. Saris *et al.*, *Am J Sports Med* **42**, 1384 (Jun, 2014).
75. M. Marcacci *et al.*, *Clin Orthop Relat Res*, 96 (Jun, 2005).
76. D. C. Crawford, T. M. DeBerardino, R. J. Williams, 3rd, *J Bone Joint Surg Am* **94**, 979 (Jun 06, 2012).
77. D. A. Grande *et al.*, *Clin Orthop Relat Res*, S176 (Oct, 1999).
78. Y. Lu *et al.*, *J Orthop Res* **24**, 1261 (Jun, 2006).
79. J. Kramer *et al.*, *Cell Mol Life Sci* **63**, 616 (Mar, 2006).

80. C. D. Hoemann, J. Sun, A. Legare, M. D. McKee, M. D. Buschmann, *Osteoarthritis Cartilage* **13**, 318 (Apr, 2005).
81. C. D. Hoemann *et al.*, *Osteoarthritis Cartilage* **15**, 78 (Jan, 2007).
82. I. M. Khan, S. J. Gilbert, S. K. Singhrao, V. C. Duance, C. W. Archer, *Eur Cell Mater* **16**, 26 (2008).
83. B. Obradovic *et al.*, *J Orthop Res* **19**, 1089 (Nov, 2001).
84. J. van de Breevaart Bravenboer *et al.*, *Arthritis Res Ther* **6**, R469 (2004).
85. S. J. Gilbert *et al.*, *Tissue Eng Part A* **15**, 1739 (Jul, 2009).
86. D. A. Wang *et al.*, *Nat Mater* **6**, 385 (May, 2007).
87. K. B. Metcalf, B. R. Mandelbaum, C. W. McIlwraith, *Cartilage* **4**, 295 (Oct, 2013).
88. C. M. Sermer, *Orthopaedic Proceedings*, (2016).
89. J. Iwasa, L. Engebretsen, Y. Shima, M. Ochi, *Knee Surg Sports Traumatol Arthrosc* **17**, 561 (Jun, 2009).
90. L. Song, D. Baksh, R. S. Tuan, *Cytotherapy* **6**, 596 (2004).
91. C. Y. Wenham, P. G. Conaghan, *Ther Adv Musculoskelet Dis* **2**, 349 (Dec, 2010).
92. P. C. Shen *et al.*, *Osteoarthritis Cartilage* **19**, 728 (Jun, 2011).
93. J. L. Hsieh *et al.*, *Int J Mol Sci* **14**, 19951 (Oct 8, 2013).
94. A. B. Blom *et al.*, *Osteoarthritis Cartilage* **12**, 627 (Aug, 2004).
95. A. Haseeb, T. M. Haqqi, *Clin Immunol* **146**, 185 (Mar, 2013).
96. S. Shiokawa, N. Matsumoto, J. Nishimura, *Ann Rheum Dis* **60**, 802 (Aug, 2001).
97. T. Hayami *et al.*, *Arthritis Rheum* **50**, 1193 (Apr, 2004).
98. C. Janeway, in *Generation of lymphocytes in bone marrow and thymus* G. Science, Ed. (2001).
99. D. R. Haynes *et al.*, *J Bone Joint Surg Br* **79**, 988 (Nov, 1997).
100. T. Huggle, *Rheumatology* **56**, 1461 (2017).
101. B. E. Pippenger *et al.*, *Osteoarthritis Cartilage* **23**, 1865 (Nov, 2015).
102. *MMWR Morb Mortal Wkly Rep* **62**, 869 (Nov 8, 2013).
103. P. M. Sutton, E. S. Holloway, *BMC Med* **11**, 14 (2013).
104. F. Oprenyesz, M. Chausson, V. Maquet, J. E. Dubuc, Y. Henrotin, *Osteoarthritis Cartilage* **21**, 1099 (Aug, 2013).
105. B. Sharma *et al.*, *Sci Transl Med* **5**, 167ra6 (Jan 9, 2013).
106. R. O. Hynes, *Science* **326**, 1216 (Nov 27, 2009).
107. V. Z. Beachley *et al.*, *Nat Methods* **12**, 1197 (Dec, 2015).
108. J. Wilson, T. Hunt, *Molecular biology of the cell : a problems approach*. (Garland Science, New York, ed. 4th, 2002), pp. xxii, 711 p.
109. S. F. Badylak, *Anat Rec B New Anat* **287**, 36 (Nov, 2005).
110. B. Brown, K. Lindberg, J. Reing, D. B. Stolz, S. F. Badylak, *Tissue Eng* **12**, 519 (Mar, 2006).
111. M. T. Wolf *et al.*, *Biomaterials* **35**, 6838 (Aug, 2014).
112. J. Song, *Journal of Tissue Engineering and Regenerative Medicine* **3**, (2014).
113. B. M. Sicari *et al.*, *Sci Transl Med* **6**, 234ra58 (Apr 30, 2014).
114. H. Kimmel, M. Rahn, T. W. Gilbert, *J Am Col Certif Wound Spec* **2**, 55 (Sep, 2010).
115. J. Lecheminant, C. Field, *J Wound Care* **21**, 476 (Oct, 2012).
116. A. Parcells, *Wounds* **26**, 189 (2014).
117. I. Valerio, *Regenerative Medicine* **10**, 611 (2015).
118. M. J. Benito, D. J. Veale, O. FitzGerald, W. B. van den Berg, B. Bresnihan, *Ann Rheum Dis* **64**, 1263 (Sep, 2005).
119. P. A. Revell, V. Mayston, P. Lalor, P. Mapp, *Ann Rheum Dis* **47**, 300 (Apr, 1988).
120. B. J. de Lange-Brokaar *et al.*, *Osteoarthritis Cartilage* **20**, 1484 (Dec, 2012).

121. M. Z. Ruan, R. M. Patel, B. C. Dawson, M. M. Jiang, B. H. Lee, *Osteoarthritis Cartilage* **21**, 1355 (Sep, 2013).
122. S. S. Glasson, M. G. Chambers, W. B. Van Den Berg, C. B. Little, *Osteoarthritis Cartilage* **18 Suppl 3**, S17 (Oct, 2010).
123. M. Z. Ruan *et al.*, *Sci Transl Med* **5**, 176ra34 (Mar 13, 2013).
124. M. Kapoor, J. Martel-Pelletier, D. Lajeunesse, J. P. Pelletier, H. Fahmi, *Nat Rev Rheumatol* **7**, 33 (Jan, 2011).
125. S. Kamekura *et al.*, *Osteoarthritis Cartilage* **13**, 632 (Jul, 2005).
126. C. J. Ferrante, S. J. Leibovich, *Adv Wound Care (New Rochelle)* **1**, 10 (Feb, 2012).
127. R. M. Boehler, J. G. Graham, L. D. Shea, *Biotechniques* **51**, 239 (Oct, 2011).
128. C. D. Evans, *Technical Notes*, (1981).
129. A. Finnegan *et al.*, *Arthritis Res Ther* **5**, R18 (2003).
130. X. Zhang, *Journal of Orthopaedic Research* **22**, (2006).
131. N. Miosge, M. Hartmann, C. Maelicke, R. Herken, *Histochem Cell Biol* **122**, 229 (Sep, 2004).
132. J. G. Tidball, S. A. Villalta, *Am J Physiol Regul Integr Comp Physiol* **298**, R1173 (May, 2010).
133. H. Salminen, E. Vuorio, A. M. Saamanen, *Arthritis Rheum* **44**, 947 (Apr, 2001).
134. F. O. Martinez, S. Gordon, *F1000Prime Rep* **6**, 13 (2014).
135. R. Poole *et al.*, *Osteoarthritis Cartilage* **18 Suppl 3**, S10 (Oct, 2010).
136. B. R. da Costa *et al.*, *Lancet* **387**, 2093 (May 21, 2016).
137. A. M. Valdes, T. D. Spector, *Nat Rev Rheumatol* **7**, 23 (Jan, 2011).
138. C. Wernecke, H. J. Braun, J. L. Dragoo, *Orthop J Sports Med* **3**, 2325967115581163 (May, 2015).
139. B. L. Wong, W. C. Bae, K. R. Gratz, R. L. Sah, *Mol Cell Biomech* **5**, 197 (Sep, 2008).
140. Y. Wang, L. Wei, L. Zeng, D. He, X. Wei, *Knee Surg Sports Traumatol Arthrosc* **21**, 1751 (Aug, 2013).
141. T. M. Tamer, *Interdiscip Toxicol* **6**, 111 (Sep, 2013).
142. A. A. Hegewald *et al.*, *Tissue Cell* **36**, 431 (Dec, 2004).
143. K. Kawasaki, M. Ochi, Y. Uchio, N. Adachi, M. Matsusaki, *J Cell Physiol* **179**, 142 (May, 1999).
144. E. H. Jebens, M. E. Monk-Jones, *J Bone Joint Surg Br* **41-B**, 388 (May, 1959).
145. L. B. Dahl, I. M. Dahl, A. Engstrom-Laurent, K. Granath, *Ann Rheum Dis* **44**, 817 (Dec, 1985).
146. M. Lotz, R. F. Loeser, *Bone* **51**, 241 (Aug, 2012).
147. G. D. Jay *et al.*, *Arthritis Rheum* **56**, 3662 (Nov, 2007).
148. Y. Kusayama *et al.*, *J Exp Orthop* **1**, 16 (Dec, 2014).
149. J. J. Roberts, R. M. Elder, A. J. Neumann, A. Jayaraman, S. J. Bryant, *Biomacromolecules* **15**, 1132 (Apr 14, 2014).
150. R. C. Andresen Eguiluz *et al.*, *Front Bioeng Biotechnol* **5**, 36 (2017).
151. K. J. Samaroo, M. Tan, D. Putnam, L. J. Bonassar, *J Orthop Res* **35**, 548 (Mar, 2017).
152. T. A. Schmidt, N. S. Gastelum, Q. T. Nguyen, B. L. Schumacher, R. L. Sah, *Arthritis Rheum* **56**, 882 (Mar, 2007).
153. J. Seror, L. Zhu, R. Goldberg, A. J. Day, J. Klein, *Nat Commun* **6**, 6497 (Mar 10, 2015).
154. M. A. Szychlinska, R. Leonardi, M. Al-Qahtani, A. Mobasher, G. Musumeci, *Ann Phys Rehabil Med* **59**, 149 (Jun, 2016).

155. M. E. Mummert, M. Mohamadzadeh, D. I. Mummert, N. Mizumoto, A. Takashima, *J Exp Med* **192**, 769 (Sep 18, 2000).
156. C. Tolg *et al.*, *Am J Pathol* **181**, 1250 (Oct, 2012).
157. O. H. Jeon *et al.*, *Nat Med* **23**, 775 (Jun, 2017).
158. B. Yang, B. L. Yang, R. C. Savani, E. A. Turley, *EMBO J* **13**, 286 (Jan 15, 1994).
159. P. F. Goetinck, N. S. Stirpe, P. A. Tsonis, D. Carlone, *J Cell Biol* **105**, 2403 (Nov, 1987).
160. D. Neustadt, J. Caldwell, M. Bell, J. Wade, J. Gimbel, *J Rheumatol* **32**, 1928 (Oct, 2005).
161. K. Flurkey, in *The Mouse in Biomedical Research (Second Edition)* J. G. Fox, Ed. (Academic Press, 2007), vol. III.
162. D. Jevsevar, P. Donnelly, G. A. Brown, D. S. Cummins, *J Bone Joint Surg Am* **97**, 2047 (Dec 16, 2015).
163. J. Arrich *et al.*, *CMAJ* **172**, 1039 (Apr 12, 2005).
164. N. Evaniew, N. Simunovic, J. Karlsson, *Clin Orthop Relat Res* **472**, 2028 (Jul, 2014).
165. M. Ishikawa *et al.*, *Osteoarthritis Cartilage* **22**, 1902 (Nov, 2014).
166. K. D. Brandt, G. N. Smith, Jr., L. S. Simon, *Arthritis Rheum* **43**, 1192 (Jun, 2000).
167. D. Kocak, T. Annaswamy, S. Chong, R. Arora, *Am J Phys Med Rehabil* **97**, 147 (Feb, 2018).
168. E. Losina *et al.*, *Arthritis Care Res (Hoboken)* **65**, 703 (May, 2013).
169. G. Loforese *et al.*, *EMBO Mol Med* **9**, 46 (Jan, 2017).
170. M. H. Yun, *Int J Mol Sci* **16**, 25392 (Oct 23, 2015).
171. W. Kuswanto *et al.*, *Immunity* **44**, 355 (Feb 16, 2016).
172. Y. Suzuki, T. Yamaguchi, *Agents Actions* **38**, 32 (Jan, 1993).
173. B. Mytar, M. Siedlar, M. Woloszyn, V. Colizzi, M. Zembala, *Int J Cancer* **94**, 727 (Dec 1, 2001).
174. P. L. Bollyky *et al.*, *J Immunol* **183**, 2232 (Aug 15, 2009).
175. H. K. Vincent *et al.*, *Open Orthop J* **7**, 378 (2013).
176. C. M. McKee *et al.*, *J Clin Invest* **98**, 2403 (Nov 15, 1996).
177. L. Quero *et al.*, *Arthritis Res Ther* **15**, R94 (Aug 22, 2013).
178. I. Bellantuono, *Drug Discovery Today: Disease Models* **20**, 27 (2014).
179. L. Murphy *et al.*, *Arthritis Rheum* **59**, 1207 (Sep 15, 2008).
180. D. T. Felson, *Osteoarthritis Cartilage* **21**, 10 (Jan, 2013).
181. M. Englund *et al.*, *Arthritis Rheum* **60**, 831 (Mar, 2009).
182. B. E. Oiestad, L. Engebretsen, K. Storheim, M. A. Risberg, *Am J Sports Med* **37**, 1434 (Jul, 2009).
183. J. Campisi, *Cell* **120**, 513 (Feb 25, 2005).
184. J. P. Coppe, P. Y. Desprez, A. Krtolica, J. Campisi, *Annu Rev Pathol* **5**, 99 (2010).
185. B. G. Childs, M. Durik, D. J. Baker, J. M. van Deursen, *Nat Med* **21**, 1424 (Dec, 2015).
186. A. Kampkotter *et al.*, *Comp Biochem Physiol B Biochem Mol Biol* **149**, 314 (Feb, 2008).
187. M. Xu *et al.*, *Nat Med*, (Jul 9, 2018).
188. A. K. Abbas, A. H. Lichtman, S. Pillai, *Basic immunology: functions and disorders of the immune system*. (Elsevier Health Sciences, 2014).
189. P. Matzinger, T. Kamala, *Nat Rev Immunol* **11**, 221 (Mar, 2011).
190. M. E. Bianchi, *J Leukoc Biol* **81**, 1 (Jan, 2007).
191. N. Mikhailkevich *et al.*, *J Immunol* **176**, 1553 (Feb 1, 2006).
192. L. I. Sakkas *et al.*, *Clin Diagn Lab Immunol* **5**, 430 (Jul, 1998).

193. L. I. Sakkas, C. D. Platsoucas, *Arthritis Rheum* **56**, 409 (Feb, 2007).
194. P. J. Mease, *Current Opinion in Rheumatology* **27**, 127 (2015).
195. S. K. Raychaudhuri, A. Saxena, S. P. Raychaudhuri, *Clin Rheumatol* **34**, 1019 (Jun, 2015).
196. S. P. Raychaudhuri, S. K. Raychaudhuri, *Clin Rheumatol* **35**, 1437 (Jun, 2016).
197. C. L. Roark *et al.*, *J Immunol* **179**, 5576 (Oct 15, 2007).
198. S. Horsburgh, S. Todryk, A. Ramming, J. H. W. Distler, S. O'Reilly, *Immunol Lett* **195**, 38 (Mar, 2018).
199. E. F. Leijten *et al.*, *Arthritis Rheumatol* **67**, 2673 (Oct, 2015).
200. A. J. Sophia Fox, A. Bedi, S. A. Rodeo, *Sports Health* **1**, 461 (Nov, 2009).
201. J. Chang *et al.*, *Nat Med* **22**, 78 (Jan, 2016).
202. Q. Jiang, Y. T. Qiu, M. J. Chen, Z. Y. Zhang, C. Yang, *Biomed Rep* **1**, 218 (Mar, 2013).
203. X. Zeng *et al.*, *Immunity* **37**, 524 (Sep 21, 2012).
204. Y. H. Chien, C. Meyer, M. Bonneville, *Annu Rev Immunol* **32**, 121 (2014).
205. J. Pawlowska *et al.*, *Folia Histochem Cytobiol* **47**, 627 (2009).
206. D. K. Fogg *et al.*, *Science* **311**, 83 (Jan 6, 2006).
207. E. Zhao *et al.*, *Cell Mol Immunol* **9**, 11 (Jan, 2012).
208. B. Smith, I. R. Sigal, D. A. Grande, *Immunol Res* **63**, 181 (Dec, 2015).
209. F. Langer, A. E. Gross, *J Bone Joint Surg Am* **56**, 297 (Mar, 1974).
210. P. J. Chesterman, A. U. Smith, *J Bone Joint Surg Br* **50**, 184 (Feb, 1968).
211. P. Jobanputra, V. Corrigan, G. Kingsley, G. Panayi, *Clin Exp Immunol* **90**, 336 (Nov, 1992).
212. H. D. t. Adkisson *et al.*, *Am J Sports Med* **38**, 1324 (Jul, 2010).

Curriculum Vitae

Johns Hopkins University School of Medicine

Heather Jacobs Faust

7/29/2018

EDUCATIONAL HISTORY:

Ph.D. expected 2018

Program in Cellular
and Molecular Medicine

Johns Hopkins
School of Medicine
Mentor: Jennifer Elisseeff

B. S.

2013

Cell Biology and Genetics

University of Maryland
College Park

PROFESSIONAL EXPERIENCE

Johns Hopkins University School of Medicine, Baltimore MD

Aug. 2013-Aug. 2018

PhD research in the lab of Jennifer Elisseeff

Graduate Student

- Identified *in vivo* immunological factors involved in pathophysiology of osteoarthritis.
- Designed and executed flow cytometry panels to profile immune cells in the joint after trauma.
- Developed and screened osteoarthritis treatments using *in vitro* systems and mouse models.
- Designed and executed binding assays to optimize hyaluronic acid binding technology for translational implementation.
- Led investigation of hyaluronic acid binding technology to reduce osteoarthritis progression.
- Initiated and maintained collaborations for radioactivity assays, binding assays, and *in vivo* functional assays to support hyaluronic acid binding technology research.
- Cultured stem cells with ECM from different tissues in a high-throughput 3D culture system to assess the impact of different tissue microenvironments on differentiation.

University of Maryland, College Park

Aug. 2011 – May 2013

Undergraduate research, June Kwak lab

Undergraduate research

- Explored drought stress in *Arabidopsis* regulated by abscisic acid and light signaling networks
- Awarded HHMI Undergraduate Research Fellowship

Clean Green Chesapeake, Baltimore MD

June 2011 – Aug. 2011

Mission: To create sustainable algal biofuels

Intern

- Developed Polymer Membrane chemistry and surface modification for algal attachment, Collaborated with Johns Hopkins University APL
- Optimized growth conditions for multiple algal strains on polymer membranes

Johns Hopkins University Applied Physics Laboratory, Laurel MD

June 2010 – Aug. 2010

- National Security and Technology Department Intern
- Applied chemicals to cell lines; used a flow cytometer to analyze cell signaling cascades
- Internship, Milton Eisenhower Research Center Jan. 2009 – June 2009
- Created Bacteria-Embedded Polymer Membranes

AWARDS AND FUNDING:

- Termis DC Annual conference for Tissue Engineering and Regenerative Medicine International Society, Travel award 2014
- Appleman-Norton Award for Plant Biology 2013
- HHMI Undergraduate Research Fellowship 2012 - 2013
- Maryland Summer Research Scholarship 2012
- Scholarship, John's Hopkins Applied Physics Lab 2009 -2013

PUBLICATIONS:

- **Heather N. Jacobs**, Sona Rathod., Matthew T. Wolf, Jennifer H. Elisseeff. Intra-articular injection of Urinary Bladder Matrix Reduces Osteoarthritis Development. AAPS, 2017. 19:141
- Vince Z Beachley, Matthew T Wolf, Kaitlyn Sadtler, Srikanth S Manda, **Heather Jacobs**,... Drew Pardoll& Jennifer Elisseeff. Tissue matrix arrays for high-throughput screening and systems analysis of cell function. Nat Meth, 2015. 12(12): p. 1197-1204.
- **Jacobs, H.**, Guo, Q., and Elisseeff, J. Cartilage Tissue Engineering, in: Principles of Regenerative Medicine, 3rd Edition, Elsevier, 2017.

POSTERS:

- Jacobs,H.; Singh, A.; Rathod, S.; Sommerfeld, S.; Elisseeff, J.; HYALURONIC ACID BINDING PEPTIDE-POLYMER SYSTEM FOR TREATING OSTEOARTHRITIS. *Poster*. (2016) Osteoarthritis Society International, Amsterdam, Netherlands.
- Jacobs,H.; Rathod, S.; Elisseeff, J.; INTRA-ARTICULAR INJECTION OF URINARY BLADDER MATRIX REDUCES OATEOARTHRITIS DEVELOPMENT. *Poster*. (2016) Osteoarthritis Society International, Amsterdam, Netherlands.
- Jacobs,H.; Singh, A.; Rathod, S.; Sommerfeld, S.; Elisseeff, J.; HYALURONIC ACID BINDING PEPTIDE-POLYMER SYSTEM FOR TREATING OSTEOARTHRITIS. *Poster*. (2015) International Society for Hyaluronan Sciences, Florence Italy.
- Presented poster on “Phospho-flow Cytometry and Cell Signaling” at the University of Maryland’s Scholar’s Academic Showcase May 2011
- Breidenich, J., Potember, R.S., Jacobs, H. "Photosynthetic Hydrogen Production from Bacteria-Embedded Polymer Membranes." Poster presented at American Chemical Society Fall 2009 National Meeting, Washington, D.C., August 16, 2009

PUBLICATIONS SUBMITTED OR IN PREPARATION:

- **Heather J. Faust**, Sven Sommerfeld, Jennifer H. Elisseeff. A Hyaluronic acid binding peptide-polymer system for treating osteoarthritis. *Submitted to Biomaterials*.
- **Heather J. Faust**, Hong Zhang, Clifton Bingham, Jennifer H. Elisseeff. Th17 and senescent cells in osteoarthritis. *In preparation*.

Permission Letters to Reprint or Use Copyrighted Material

Book Chapter Title: " Cartilage Tissue Engineering." Principles of Regenerative Medicine 3rd Edition. Springer International Publishing, 2018.
Publisher: Elsevier

The authors of this chapter have obtained permission to re-print the information contained in chapter 1 through Elsevier

Manuscript title: Intra-articular Injection of Urinary Bladder Matrix Reduces Osteoarthritis Development

Journal: AAPS
Publisher: Springer Nature

The authors of this dissertation have obtained permission to re-print this journal article from Springer Nature (License Number 4350940686473).

All other text and figures are pre-submission or pre-acceptance and not bound by license regulations at this time.